SIGNALING AND MECHANICAL REGULATION OF PODOSOME-TYPE ADHESIONS

Mohd Rafiq, Nisha Bte

Awarding institution:
King's College London

SIGNALING AND MECHANICAL REGULATION OF PODOSOME-TYPE ADHESIONS

NISHA MOHD RAFIQ
(B. Sci. (Hons.), NUS)

A THESIS SUBMITTED FOR THE DEGREE OF DOCTOR OF PHILOSOPHY
NATIONAL UNIVERSITY OF SINGAPORE AND
KING'S COLLEGE LONDON
2016

DECLARATION

I hereby declare that this thesis is my original work and it has been written by me in its entirety. I have duly acknowledged all the sources of information which have been used in the thesis.

This thesis has also not been submitted for any degree in any university previously.

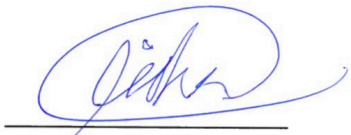

Nisha Mohd Rafiq
11th Aug 2016

ACKNOWLEDGEMENTS

First and foremost, I would like to thank the person who has inspired me the most during my PhD journey, Sasha (Alexander) Bershadsky. He is the definition of class, quality and beauty in science. I am privileged to have been to numerous international conferences, and I have not met anyone better than him with respect to the above qualities. The three research projects in this thesis branched out from our frequent discussions and exchange of ideas. His brilliant approach to science stems out from his attempt to always start with a simple experiment and build it up slowly as it develops. He is a big fan of control experiments. I always have these phrases (which is annoyingly scary) ringing on my head when I'm on the lab bench: "The proper control for this experiment would be…" and "I don't believe this, you should do this control to check…". He made me think of a cell like a person, i.e. to "feel" how the cells would respond to different treatments. This is a key driver to my approach in science these days and surprisingly it works very well when I'm generating explanations to my scientific questions. He taught me (and may these benefit you too) to (i) never rush to a conclusion, (ii) to be open to contradictions no matter how serious they are, (iii) to be optimistic with negative data, (iv) to never over-glorify positive findings and (v) to always be humble but confident when presenting them. He has been like a scientific grandpa to me, to whom I hope to be in touch with till I grow old. Someone reputable once told me, "the goal of a PhD is to find a role model," and I think I am very fortunate to have found one. In fact, he is also very tolerant of my eccentric character. He would patiently listen to all my scientific ideas and stories no matter how ridiculous they sound sometimes, and he has never stopped me from pursuing my interests. While I'm in trouble with work when he is away, he is always available on Skype for a chat. I truly appreciate all the energy and time invested in me throughout the four years. It must be tiring to raise a PhD student like me.

Secondly, I would like to thank Paul Matsudaira for diverting my interest in pursuing MD to science when I was at the crossroad during my undergraduate days. He introduced Sasha and Gareth to me as supervisors. I remember how I was hesitant to meet Sasha but he insisted I emailed him. This insistence is something I appreciate most from Paul, as he made sure I had good mentors. In fact, Paul has always been a pillar of strength and support. He never fails to show up at my TAC meetings. He is always very responsive to all my emails no matter how busy his schedules were. When I was at my lowest point during a phase in my PhD life due to family circumstances, he supported my expenses in UK despite having little knowledge on my scientific progress at that time. He once showed me a pathetic picture of himself in his early days, to boost my morale that no one started easy. I am truly grateful for his unwavering support throughout my undergraduate and PhD years.

Thirdly, I would like to express my gratitude to Gareth Jones, my KCL supervisor. Gareth introduced podosomes to me, and I quickly became very fascinated by these structures. He has been patient and supportive throughout the years, especially during my early days of learning as I was not progressing very well. He emailed me frequently to ensure I was making some progress and was also responsible for pushing our first manuscript out for publication. While I was in KCL, his warm hospitality is something that I will not forget and I appreciate the fact that he allowed me to focus on other projects when things weren't going as planned, which fortunately turned out to be very promising. The joint degree program has been truly challenging and rewarding at the same time, but like Kelly Clarkson's chorus part of a song goes, " what doesn't kill you makes you stronger…."

Next I would like to thank my lab buddy and good friend Beverly, for battling this journey with me. Our constant conversations, conference trips, shopping times and daily scientific discussions are days I will not forget. I am truly fortunate to have a comrade in stride, who is often there to attend to both my personal and scientific

issues. It is truly heartening to have a friend who clicks with you on numerous matters. I have personally learnt a lot from her; her humility and "never-die" spirit are admirable. Both of us went through different sets of difficulties during our PhD years, and the experience has mutually benefited us and made us more appreciative of our supervisors.

I would like to personally thank Misha (Michael) Kozlov, who has directly and indirectly inspired me to consider studying membrane dynamics in the future. His talks and scientific papers have kept me "alive" and passionate about science since late 2014. In fact, the part that I enjoyed most in this thesis is Chapter 4.

I am also grateful for the open-concept laboratory at the Mechanobiology Institute at NUS, which stimulates high-level interactions among different laboratories. Firstly, I would like to thank Robert Lieu and Cheng-Han Yu for serving as great mentors during the course of my PhD. Next, I would like to thank present and past members of the Bershadsky lab, Salma Jalal for being a wonderful and supportive friend; Meenu Bharathi, and Visalatchi for handling my countless purchase orders; Yukako Nishimura for the numerous scientific discussions on our joint project; Hu Shiqiong, Tee Yee Han and Naila Alieva for help in experiments and scientific advices. I would also like to thank Mrinal Shah, Shi Shidong, Edna, Yuan Xin, Luo Weiwei and Xiao Shaowei for the company in the lab. Not forgetting the friendships forged at MBI, I would like to make a shout-out to the following people without which life would not be so colorful: Anitha, TingTing, Pan Meng, Jiawei, Andrea, Celine, Zhongwen, Wah Ing, Catherine, Zijun, Megha, Bakya, Steve, Dee, Liu Xian, Dasan, Anu, Ti Weng, Mingxi, Aneesh, Felix, Naotaka, Darren, Prasuna, Zhihai, Lester, Siti, Jichao, Hongying, Eric, Mallika, Ekta, Karthik, Alok, Nikhil, Megan, Yidan, Sharvari, Yejun, Yiting and Tony.

Furthermore, I would like to thank the "unsung heroes" of MBI: the administrative staff, wet lab, IT and microscopy cores. From the administrative department I would

like to personally thank Sue Ping for being a great friend and listening ear as well as the constant support for my work; Carol for patiently helping me with conference claims and Cynthia Lee who has helped me manage some issues throughout the course of the joint degree program. I would also like to thank Shanta, Ani, Syam, Bernie, Caroline, Siti and Fateha for their company.

In addition, I would like to extend my gratitude to a number of people I have interacted and benefited from during my stint at the Randall division in KCL. In particular, Elizabeth Foxall for the relentless assistance and daily communications to ensure I feel "at home" all the time; Daniel Matthews for teaching me SIM and STORM; James Monypenny and Vineetha Vijayakumar for help in cloning; and the wonderful people who have kept my stay pleasant and memorable, namely, Sweta, Magdalene, Maddy, Yutaka, John, Yan, Jake, Claire, Ah-Lai, Mark, Rosemary, Shailaja, Anneri, Fuad, Karin, Adela, Brooke and Susan. I would also like to thank Helen and Sarah for the administrative support.

Finally I would like to thank my best friend of more than 10 years, Nur Zahirah, who has patiently tolerated all my shortcomings. Our weekly hangouts, travel trips and gossips are things I really appreciate most and will not forget. I hope our beautiful friendship will last even after my dream of having six kids and a lab! I would also like to thank my good friends Chen KangTing, Cheong ShuHui, Samsudin, Najib, Shahirah and Sakinah for the monthly meet-ups, support and encouragements. Furthermore, I would like to thank my violin teacher, Mr Ching for the weekly enjoyable and fun "musical duo" sessions. To my two adorable younger sisters, I think life would be really boring without the both of you, thank you very much for being my closest friends ever since you were born. To my dearest mum, you have been the strongest supporter of all my decisions in life.

This work is dedicated to Mum.

Table of Contents

LIST OF FIGURES

SUMMARY OF THESIS

Podosomes represent a special class of integrin-mediated cell-matrix adhesions formed by migrating and matrix degrading cells. Here, I demonstrated that assembly of podosomes induced in macrophage-like THP1 cells and fibroblasts by different treatments were regulated by the ARF1 GTPase and its GEF ARNO. Down-regulation of ARNO and ARF1 by siRNA, and by pharmacological inhibitors led to a striking reduction in the numbers of podosome-forming cells. ARNO was found to co-localize with the adhesive ring components of podosomes while ARF1 localized to vesicular structures that transiently contact podosome rings. Inhibition of ARF1 led to an increase in RhoA-GTP levels and triggered assembly of myosin-IIA filaments in THP1 cells, whilst the suppression of myosin-IIA rescued podosome formation regardless of ARF1 inhibition. Interestingly, overexpression of constitutively active ARF1 in fibroblasts lacking podosomes was sufficient to induce *bona fide* podosomes lacking adhesion ring components, suggesting that ARF1 can crosstalk and modulate Rho GTPase activity in controlling actin polymerization events.

Secondly, I provide a mechanism to explain the effect of microtubule (MT) disruption on podosome disassembly. Using structured illumination microscopy (SIM), I observed that addition of nocodazole, a microtubule depolymerizing drug, induced an outburst of myosin IIA filament assembly as a consequence of increased RhoA activity in macrophage-like THP1 cells. siRNA knockdown of MT-associated GEF-H1 or inhibition of ROCK by Y-27632 prevented the nocodazole-induced disassembly of podosomes and assembly of myosin II filaments. Prolonged treatment with nocodazole induced formation of sarcomeric-like actomyosin structures and larger focal adhesions typically observed in fibroblast-type cells. I propose a switch mechanism between focal adhesions and podosomes governed by an actomyosin-dependent force generation.

Finally, I showed using high-resolution microscopy that existing podosomes undergo dissolution upon artificial increase in membrane tension by exposure to hypo-osmotic medium and mechanical stretching, while expansion of the membrane to decrease membrane tension by deoxycholate promoted “clustering” of podosomes with shorter connecting actin links than podosomes of control cells. Intriguingly, podosomes exposed to 50% reduction in osmolarity but not deoxycholate-treated ones exhibit reduction in size and fluorescence intensity, but with increased “roundedness” indicated by actin markers. Based on these findings, I hypothesize that podosomes mimic the lamellipodia in response to changes in membrane tension.

Chapter 1 - INTRODUCTION

1.1 - Podosomes: A form of integrin-mediated adhesion

Cells interact with the extracellular matrix (ECM) through a variety of specialized transmembrane proteins known as integrins. They function as specific adhesion receptors that are capable of bridging chemical and mechanical information from the extracellular environment to the intracellular compartment of cells through a complex network of interconnecting adaptors, signaling proteins and cytoskeletal organization (Zaidel-Bar et al. 2007). At a cellular level, this interaction is essential in influencing a cell's response to its microenvironment in terms of its survival, proliferation and migratory abilities (Adams 2001, Geiger, Spatz and Bershadsky 2009). Examples of integrin-mediated adhesions that are capable of interacting and remodeling the extracellular matrix are podosomes and invadopodia, which are formed by monocytic-derived and cancer cells, respectively, for trans-migration and invasion (Calle et al. 2006, Murphy and Courtneidge 2011). Such cell-matrix-contacts are particularly important in a multicellular context, since they can alter tissue organization, differentiation and organ development, hence understanding how integrin-mediated adhesion coordinates the regulation of cell migration and invasiveness through the development of specialized structures is fundamental in both physiological and pathophysiological situations (Block et al. 2008).

Integrins are heterodimeric receptors made up of α and β subunits (Figure 1) that are found in the plasma membrane of cells. Assembly of integrin isoforms in podosomes is cell-type specific. Generally, both β1 and β3 integrins are found in most cell types that form podosomes (Linder 2009, Murphy and Courtneidge 2011) but the recruitment of β2 integrins is seen specifically in dendritic cells and macrophages (Calle et al. 2006). In addition, loss of αvβ3 integrins resulted in a

defective podosome assembly in human and mouse osteoclasts (Nakamura et al. 1999). A study by (Destaing et al. 2010) showed that β1 but not β3 integrin is essential for initial podosome assembly in Src-transformed fibroblasts. Though the exact role of different types of integrin recruitment is unclear, the general consensus is that activation of integrin is essential for the assembly of podosomes(Murphy and Courtneidge 2011).

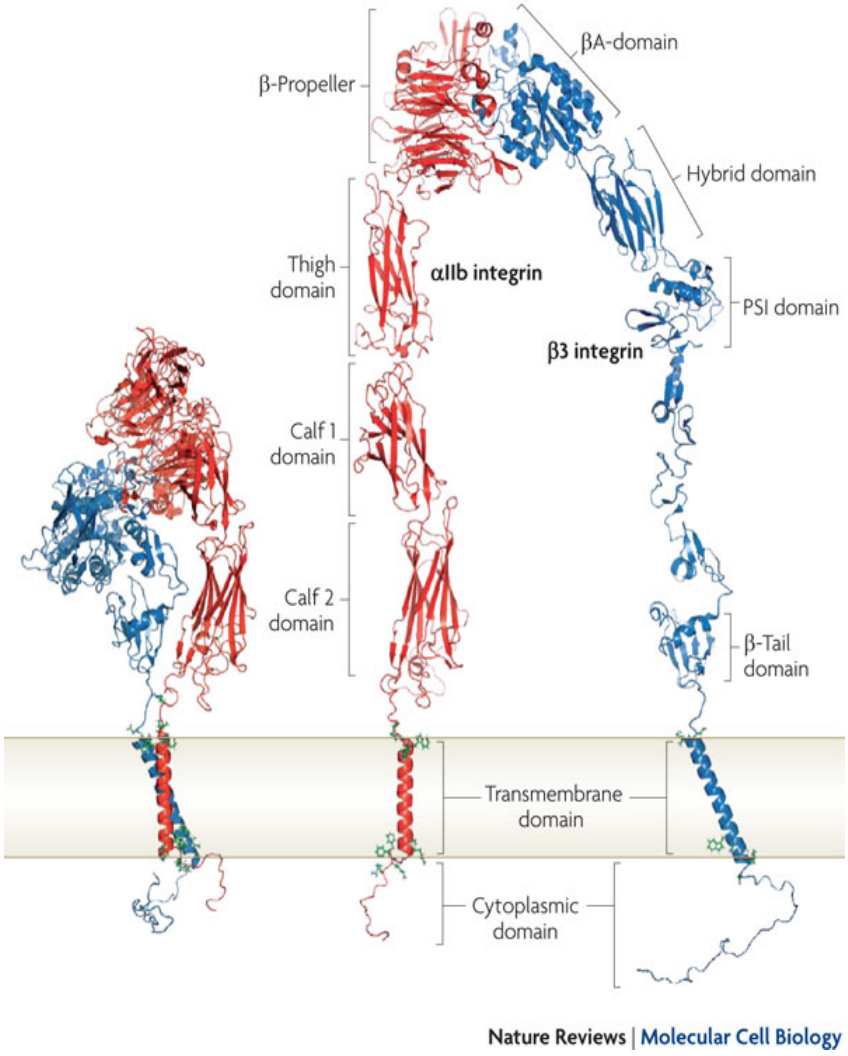

Chapter 1 - Figure 1: The α (red) and β (blue) subunits of an integrin heterodimer.

The βA-domain is capable of interacting with the ECM ligand while the cytoplasmic domain can interact with multiple proteins that can regulate its affinity to the ECM

ligand. The β-integrin tail can interact with talin and kindlins which consequently recruit other proteins that promote adhesion formation and maturation. Figure adapted from Shattil, Kim and Ginsberg (2010).

1.2 - Cell types, function and evidences *in vivo*

Podosomes are constitutively expressed in cells of the monocytic lineage such as macrophages, dendritic cells and osteoclasts (Calle et al. 2006, Murphy and Courtneidge 2011). In culture, immortalized monocytic cell lines can be differentiated into macrophage-like cells through stimulation by transforming growth factor beta (TGFβ) or increasing protein kinase C (PKC) activity by phorbol myristate acetate (PMA). Podosome formation can also be induced in fibroblasts by overexpression of constitutively active Src as well as in TGFβ-stimulated endothelial and smooth muscle cells (Rottiers et al. 2009, Burgstaller and Gimona 2005, Varon et al. 2006, Tarone et al. 1985). More recently, we have shown that non-transformed fibroblasts that typically do not form podosomes develop podosome-like adhesions when spread on fluid RGD-functionalized lipid bilayers that do not allow attached cells to generate a traction force (Yu et al. 2013).

Functionally, podosomes are distinct from other cell-matrix adhesions due to their ability to degrade the ECM via secretion of metalloproteases (Linder and Kopp 2005). The first evidence of a potential connection between podosome and human disease was identified where patients suffering from an X-linked associated disease, Wiskott-Aldrich Syndrome (WAS), exhibit no podosome assembly and have defective chemotaxis in cultured WAS macrophages and dendritic cells (Calle et al. 2004b, Monypenny et al. 2011, Jones et al. 2002). Mutations in the Wiskott-Aldrich Syndrome protein (WASP), a key component for actin nucleation in podosomes, resulted in WASP-null patients. However, it is also important to note that while these WASP-null cells lack podosomes *ex vivo*, it is still not known if the symptoms observed in WAS patients were due to absence of podosomes or other WASP-related functions.

Podosomes have been shown to localize to regions where ECM are lysed (Osiak, Zenner and Linder 2005, Burgstaller and Gimona 2005), but its degradative potential has only been proven recently in dendritic cells through the secretion of matrix metalloproteinases (MMPs)(Gawden-Bone et al. 2010). Furthermore, visualization of podosome have been recently observed in bone marrow-derived macrophages in 3D matrigel (Cougoule et al. 2010) and endothelial cells (Seano et al. 2014) involved in sprouting of new blood vessels through the degradation of the matrix relative to the basement membrane *in vivo* (Figure 2). These podosomes organize into rosette-like structures that resemble podosomes in Src-transformed fibroblast (Tarone et al. 1985). On the other hand, individual podosomes typically observed in cells from the monocytic lineage have yet to be visualized directly, but the protrusive structure formed by blood leukocytes during transendothelial diapedesis has been proposed to be podosome-like in its molecular components and organization (Carman et al. 2007b) but has not been verified.

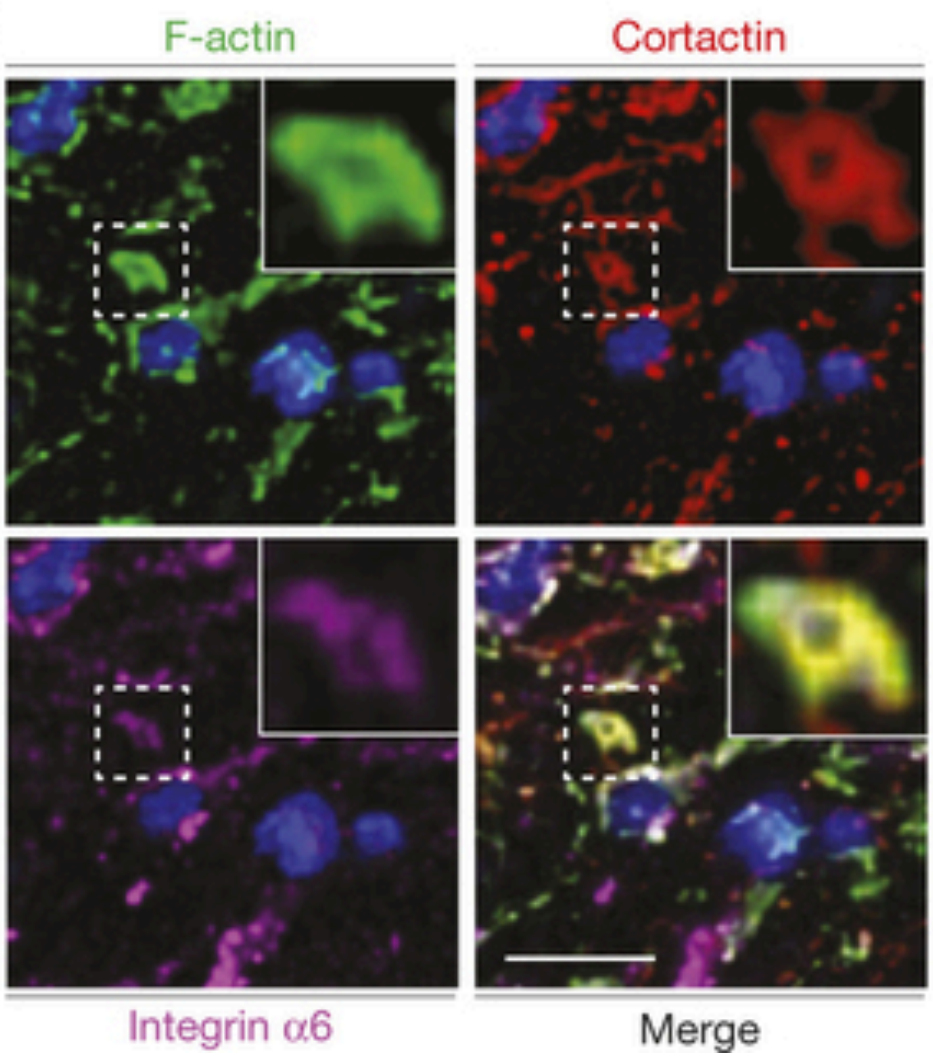

Chapter 1 - Figure 2: Endothelial layer of a VEGF-A-stimulated aortic explant marked by podosomal markers.

Boxed image represent a podosome rosette relative to the basement membrane indicated by F-actin, cortactin and integrin. Figure adapted from Seano et al. (2014).

In addition, a structurally divergent form of podosome termed invadopodia is found exclusively in cancer cells that differ in their dynamics and distribution but are structurally and functionally very similar to podosomes (Linder 2009).

1.3 - Structure and dynamics

In the majority of cell types, podosomes form arrays consisting of numerous individual podosomes connected to each other via f-actin-positive links (Figure 3) (Cox et al. 2012, van den Dries et al. 2013a, Panzer et al. 2016, van den Dries et al. 2013b). The individual dot-like podosomes are found at the ventral surface of cells with a width of approximately 0.5-1 μm and depth length of 1- 2μm (Linder 2007).

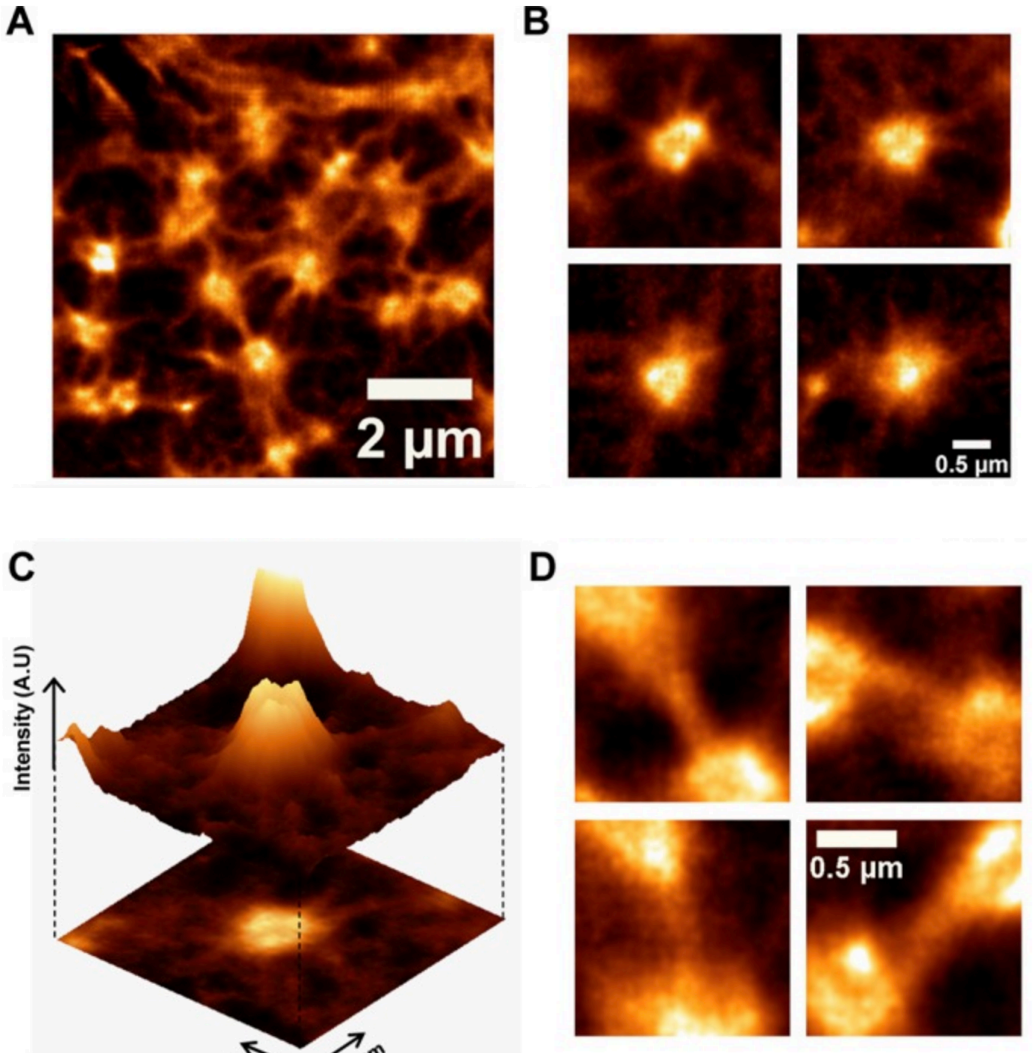

Chapter 1 – Figure 3: STORM images of the central actin core of podosomes.

(A) Phalloidin-stained image of podosomes in dendritic cells visualized by direct stochastic optical reconstruction microscopy (dSTORM) reveal F-actin links

associated between adjacent podosomes. (B) Representative sections (from A) of individual podosomes. (C) 3D reconstruction image in individual podosome while (D) shows the enlarged regions of the F-actin links connecting podosomes. Figure adapted from van den Dries et al. (2013b).

Podosomes can be characterized into two main spatial arrangements, a central actin-rich core and a surrounding ring complex enriched in adhesion-associated proteins (Figure 4). The core consists of branched and unbranched actin filaments with actin regulators such as Wiskott-Aldrich Syndrome protein (WASP), WASP-interacting protein (WIP), Arp2/3 complex, cortactin and cdc42. On the other hand, the ring complex is composed of integrins, to which several focal adhesion-associated proteins such as talin, vinculin and paxillin as well as signaling proteins such as Src kinase and Pyk2 are localized (Linder and Aepfelbacher 2003, Schachtner et al. 2013). Moreover, a super-resolution microscopy technique revealed that the ring complex proteins have distinct localizations and the overall shape of the ring is polygonal (Figure 5) instead of the originally thought circular structure(Cox et al. 2012).

In some cell types such as Src-transformed fibroblasts and growth factor -induced endothelial cells (Rottiers P et al 2009, Seano et al 2014), podosomes are organized in superstructures termed podosome rosettes that are capable of degrading the ECM. In osteoclasts, individual podosomes can fuse to form podosome belt at the cell periphery known as the “sealing zone” for attachment and bone resorption (Destaing et al 2003, Georgess D et al 2014).

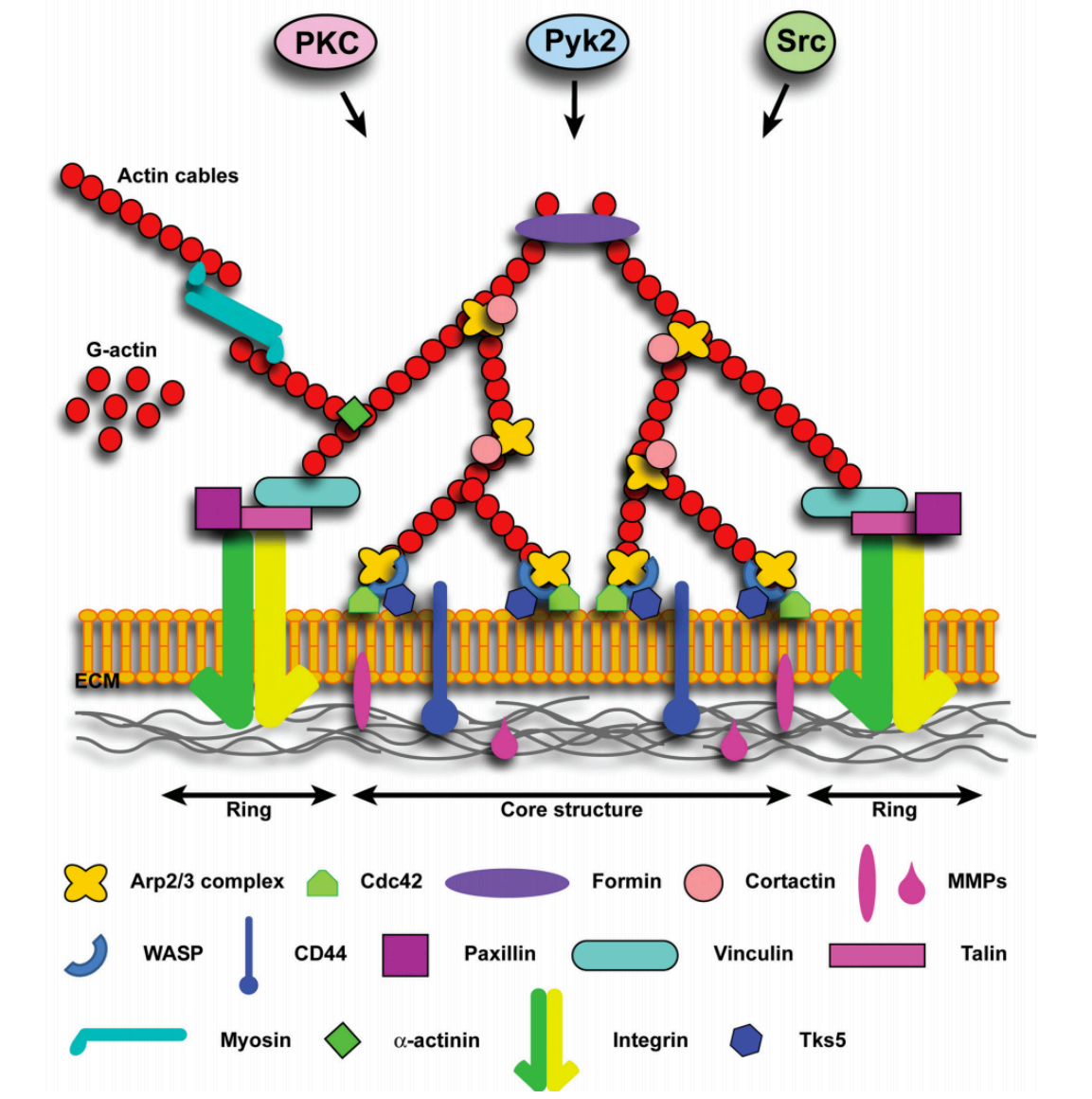

Chapter 1 – Figure 4: Schematic display of proteins associated with the core and ring structure of podosomes.

Figure adapted from Schachtner et al. (2013).

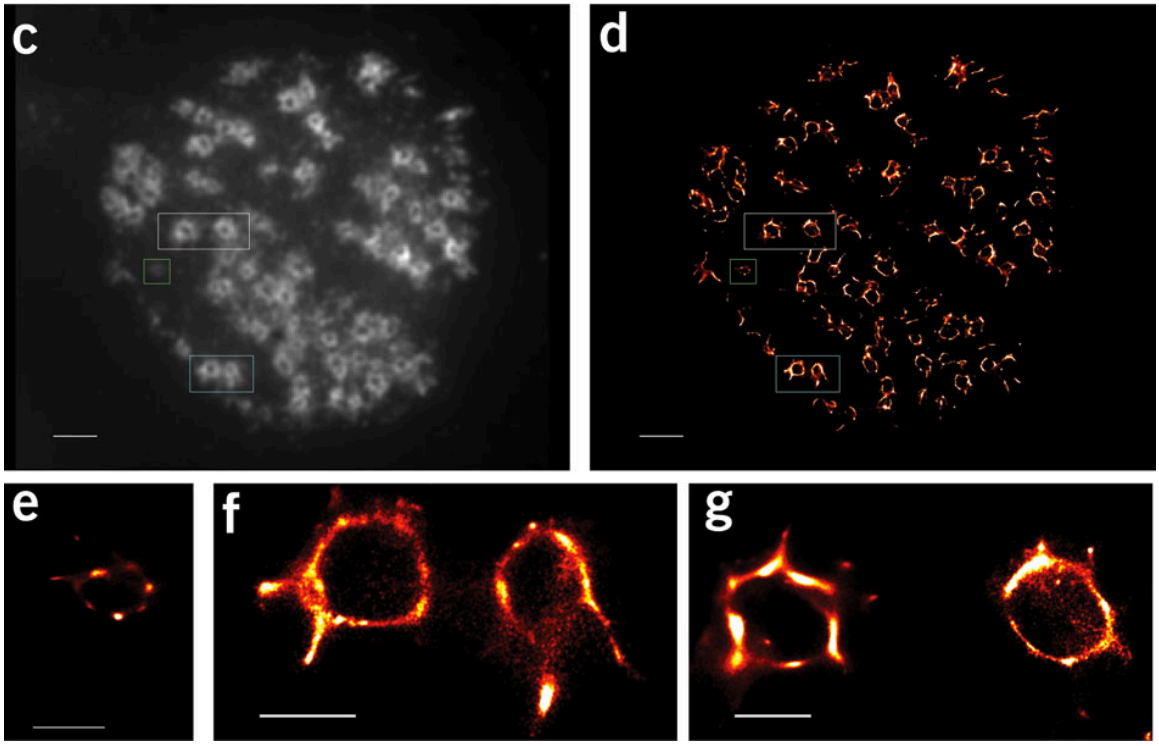

Chapter 1 – Figure 5: 3B superresolution image of podosome ring.
3B analysis (d) of widefield image (c). (e,f,g) represent boxed images in (d) showing polygonal shape of vinculin rings labeled with antibody and Alexa 488 in podosomes of macrophage-like THP1 cell. Figure adapted from Cox et al. (2012).

Unlike focal adhesions, the lifetime of podosomes is much shorter and can range between 2-20 minutes, while the number of podosomes per cell can range from 20 to several hundreds, making it a very dynamic structure (Murphy and Courtneidge 2011).

1.4 - Assembly and maturation

To date, the non-receptor tyrosine kinase Src has been shown to be an important initiator of podosome assembly in Src-transformed fibroblast, osteoclast and macrophage podosomes (Tarone et al. 1985, Soriano et al. 1991, Linder et al.

2000a). Overexpressing active Src induces formation of podosomes in fibroblasts that normally form only focal adhesions, while inhibiting Src in macrophages that constitutively form podosomes disrupts podosome assembly. ((Tarone et al. 1985, Linder et al. 2000). However, little is known of the mechanism by which Src is activated to regulate podosome formation. Nevertheless, there are small numbers of important proteins (Foxall et al. 2016) that have been shown to be key markers of podosomes that are not seen in focal adhesions, namely, WASP, WASP-interacting protein (WIP) and Tks5 (tyrosine kinase substrate with five SH3 domains, Src substrate)(Murphy and Courtneidge 2011) that will be discussed in further detail in this section.

Currently, there are two explanations as to how podosome assembly can be initiated. The first model argues that local activation of integrins can lead to actin nucleation in an Arp2/3-dependent manner. Actin-related protein 2/3 (Arp2/3) complex mediates actin nucleation from the sides of pre-existing actin filaments generating branched network of filaments (Schoumacher et al. 2010). Actin nucleation is believed to be Arp2/3 complex-dependent in podosomes where WASP, which is absent in focal adhesions, is a potent activator of Arp2/3 (Linder 2009, Murphy and Courtneidge 2011, Calle et al. 2006, Jones et al. 2002). This process is regulated by the RhoGTPase, Cdc42, which activates WASP. The conserved verpolin-cofilin-homology and acidic-rich (VCA) domain at the c-terminal region of WASP can bind directly to monomeric actin and the Arp2/3 complex to initiate actin polymerization at the podosome core. That Cdc42-WASP-Arp2/3 complex activation is key to podosome assembly was demonstrated by microinjection of constitutively inactive Cdc42 has been shown to reduce podosome formation significantly, while WASP-deficient paitent-derived macrophages and dendritic cells lack podosomes (Burns et al. 2001, Linder et al. 2000a).

It is still not clear how integrin activation and Cdc42 localization are connected for podosome to form their core-ring complex. In the case of invadopodia (structurally

similar to podosome), Tks5 can interact with PtdIns(3,4)P_2 on the plasma membrane through its Phox homology (PX) domain and serve as a scaffold that recruits cortactin, which is another protein that is capable of interacting with actin-regulatory proteins such as N-WASP and Arp2/3 to initiate actin polymerization (Oser et al. 2009). Even though cortactin has been shown to play an essential role in invadopodia assembly, its role in podosome formation is not so clear-cut, since the cortactin homologue HS-1 (hematopoietic lineage cell-specific protein 1) is needed for the polarized distribution of podosomes but not its assembly during cell migration (Dehring et al. 2011). Interestingly, while cortactin is dispensable for podosome assembly, its recruitment is important for stabilization and subsequent substitution of WASP after its release.

A second model that has been proposed for podosome assembly is the initial assembly of CD44 in the plasma membrane at the putative podosome core prior to integrin-matrix interaction. This model was first demonstrated in osteoclasts (Chabadel et al. 2007), since actin polymerization at the podosome core is often observed prior to integrin-enrichment at the podosome ring. CD44 is a cell surface glycoprotein receptor that interacts with glycosaminoglycan constituent of the ECM as well as a variety of other ligands such as collagen (Cichy and Pure 2003). Recently, Luxenburg et al. (2012)showed that cortactin and paxillin were first recruited into podosomes followed by delayed enrichment of β3 integrins at the podosome ring of osteaclasts.

As actin polymerizes, various scaffolding and adaptor proteins continue to be recruited as the podosome matures. This includes focal adhesion proteins such as talin, vinculin and zyxin, which display intensity increments as measure by fluorescent tags as the podosome grows. Additionally, podosomes are comprised of a large pool of regulators -protein kinases, cross-linkers and adaptor proteins, as shown below in Figure 6.

The specific roles and temporal localizations of most of these proteins in regulating podosome growth, stability and dissolution have yet to be elucidated. For example, Src has been shown to be important in stimulating actin nucleation in osteoclast podosomes, yet podosomes observed in Src-null cells showed a longer lifespan than those in wild-type cells, indicating that Src is also needed for the disassembly of podosomes (Destaing et al. 2008). In another study, the focal adhesion kinase (FAK), which resides in the ring region of podosomes, was shown to be essential in forming podosome rosettes typically observed in Src-transformed fibroblasts, but is not required for individual podosome formation (Pan, Chen and Chen 2011).

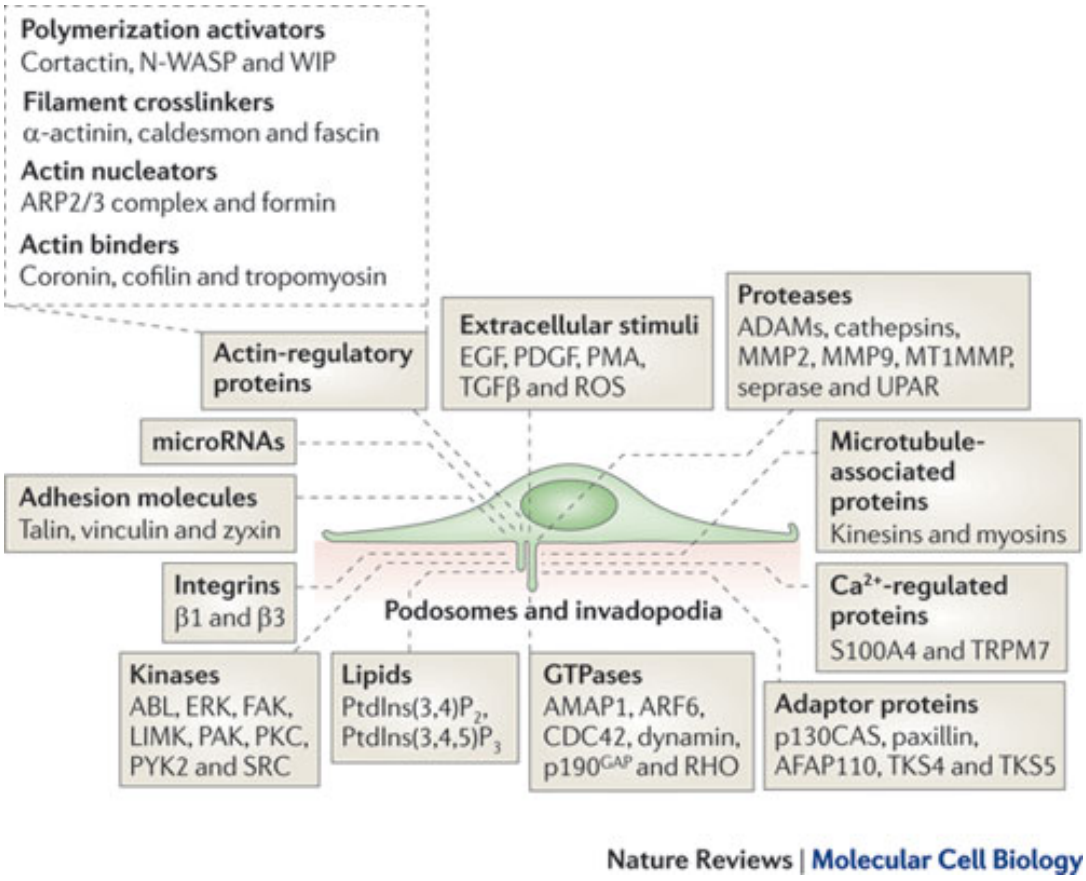

Chapter 1 – Figure 6: Adhesion regulators and components of the podosomes.
Each proteins play different or overlapping roles in regulating the initial growth, maturation and disassembly of podosomes. Figure adapted from Murphy and

Courtneidge (2011).

With regard to function, the localization of matrix metalloproteinases (MMPs) has been shown to be an indicator of podosome maturity (Murphy and Courtneidge 2011). Notably, the presence of TKS5, cortactin and subsequent recruitment of TKS4 is necessary for focal activation of MMPs to degrade the ECM (Poincloux, Lizarraga and Chavrier 2009, Buschman et al. 2009). The process of MMP delivery to the site of podosome is still a subject of active discussion, and has been proposed to be microtubule-dependent through endocytic recycling or intracellular store mobilization via a Rab8-dependent secretory pathway(Wiesner, El Azzouzi and Linder 2013, Murphy and Courtneidge 2011).

1.5 - Small GTPases I: Rho family

Most Rho proteins cycle between the active and inactive state through GTP binding and hydrolysis catalyzed by the guanine nucleotide exchange factor (GEFs) and GTPase-activating proteins, respectively (Hodge and Ridley 2016). In addition, Rho proteins can bind to guanine nucleotide dissociation inhibitors (GDIs) that sequester Rho binding to the plasma membrane (Ridley 2001, Dovas et al. 2011, Hodge and Ridley 2016). There are three key Rho GTPases; RhoA, Rac and Cdc42 that are widely known to control actin polymerization during cell migration and adhesion turnover (Etienne-Manneville and Hall 2002, Bershadsky, Balaban and Geiger 2003) in a spatiotemporal-dependent manner. The regulated activity of Rho GTPases is essential for efficient and directed cell migration (Ridley et al. 2003). In a simplified general model, RhoA activation induces stress fiber formation and focal adhesion maturation, while active Rac1 is often localized to the leading edge of a cell for lamellipodia formation, Cdc42 is localized to protrusions at the leading edge, filopodia and podosome-type adhesions (Ridley 2001, Geiger et al 2009, Murphy and Courtneidge 2011).

Actin polymerization at podosomes is primarily mediated by the Arp2/3 complex activated by Wiskott–Aldrich Syndrome protein (WASP)(Machesky and Insall 1998, Linder et al. 1999, Burns et al. 2001). In turn, WASP activation depends largely upon the activity of the small G protein Cdc42 and can be regulated by WASP-interacting protein (WIP)(Abdul-Manan et al. 1999a, Calle et al. 2004a, Monypenny et al. 2011, Schachtner et al. 2013, Vijayakumar et al. 2015). Indeed, microinjection of dominant negative Cdc42 has been shown to significantly impair podosome formation in human dendritic cells (Burns et al. 2001). Similarly, podosome formation is impaired in cells microinjected with dominant negative Rac1 (Burns et al. 2001), as well as in Rac1- and especially Rac2-depleted cells (Wheeler et al. 2006) though the downstream pathways are yet to be elucidated. Conversely, RhoA activity, which typically promotes assembly of stress fibers and focal adhesions, has been generally described to be low in podosome-forming cells (Pan et al. 2011, Yu et al. 2013) and microinjection of active RhoA impaired podosome formation (Burns et al. 2001).

1.6 - Small GTPases II: ARF family

While the role of Rho family GTPases in podosome formation is relatively well-documented, the function of the ARF family of small G proteins is essentially unknown, even though it is known that these proteins participate in crosstalk with Rho family GTPases and regulate actin polymerization (Myers and Casanova 2008, Heuvingh et al. 2007, Kumari and Mayor 2008, Cao et al. 2005, Dubois et al. 2005, Humphreys et al. 2012a, Humphreys et al. 2012b, Koronakis et al. 2011, Rocca et al. 2013).

To date, there are six known mammalian ARF GTPases (ARF1-6). ARF1 is the most abundant of the ARFs, primarily localized to the Golgi apparatus, while ARF6 is the principal ARF thought to regulate membrane dynamics at the cell surface (Donaldson and Jackson 2011). ARF1's Golgi-related functions include recruitment of coatomer complexes such as COPI (Pepperkok et al. 2000, Beck et al. 2009),

clathrin adaptor proteins (AP1, AP3 and AP4) and γ-ear-containing, ADP-ribosylation factor-binding proteins (GGAs) for vesicle biogenesis and transport (Dell'Angelica et al. 2000, Puertollano et al. 2001, Bonifacino and Lippincott-Schwartz 2003, Carvajal-Gonzalez et al. 2015). At the plasma membrane, ARF1 has been directly attributed to endocytosis of GPI-anchored proteins through modulation of Cdc42 activity (Kumari and Mayor 2008). ARF1 has also been implicated in PI3K-dependent pathways during epidermal growth factor dependent cell migration (Boulay et al. 2008) as well as Fcγ receptor-mediated phagocytosis in macrophages (Beemiller, Hoppe and Swanson 2006). More recently, it was reported that formation of "ventral actin structures" induced by PMA in HeLa cells and Beas-2b cells was inhibited upon depletion of ARF1 by siRNA (Caviston, Cohen and Donaldson 2014). These PMA-treated cells also showed an increase in measured active ARF levels indicating that PMA, an activator of Protein Kinase C, can either directly or indirectly modulate the activity of ARF GTPases to promote actin reorganization at the ventral surface of the cells. Furthermore, the recruitment of certain adhesion components such as paxillin was shown to require dynamic GTP/GDP turnover of ARF1 (Liu et al., 2002; Liu et al., 2005). Nevertheless, the direct role of ARF1 in adhesion formation has not been described previously.

1.7 - Role of microtubules

Microtubules are dynamic, hollow and polar tube-like polymers with an average diameter of approximately 25 nm (Beese, Stubbs and Cohen 1987, de Pablo et al. 2003). They are comprised of alternating α and β subunit heterodimers arranged next to each other in a linear protofilament, to which the α and β subunits cap the negative and positive ends, respectively (de Pablo et al. 2003, Chretien and Wade 1991). These individual protofilaments combine to form a 13-protofilament tubular structure. Microtubules play important roles in intracellular vesicle transport and cell division and provide structural integrity to the cell especially during processes such as cell migration (Nogales 2000). Furthermore, microtubules have been

proposed to regulate focal adhesion dynamics (Bershadsky et al. 1996) through sequestration of guanine nucleotide exchange factors, which in turn can regulate local Rho/Rac GTPase activity (Krendel, Zenke and Bokoch 2002, Chang et al. 2008, Rooney et al. 2010).

The relationship between microtubules and podosomes was first established by (Linder et al. 2000a) in macrophages. Disruption of microtubules by a microtubule-depolymerizing drug, nocodazole, led to immediate disassembly of podosomes and the same group subsequently suggested that kinesins, which are microtubule-based motor proteins, might be involved in the regulation of podosome dynamics and transport of metalloproteases to the sites of podosome-matrix degradation (Wiesner et al. 2010, Cornfine et al. 2011, Kopp et al. 2006). On the other hand, the effect of a microtubule-stabilizing drug, taxol is still debatable, as there are mixed reports on its effect on podosome assembly (Ang et al. 2012, Purev et al. 2009). In a separate study, (Evans et al. 2003) suggested that both nocodazole and taxol had no effect on the dissolution of individual podosomes but regulates podosome fusion/fission characteristics in macrophages.

While the direct interaction and function of microtubules in podosome assembly is not clear, it has been proposed that the Golgi network might be involved in the polarized trafficking of molecular components to podosome sites (Gimona et al. 2008). In this thesis, I provide data and a mechanism as to how microtubules may regulate podosome formation in macrophage-like cells (see Chapter 3 for details).

1.8 - Actomyosin network and force generation

Actin filaments and myosins (i.e. myosin II) co-assemble into an actomyosin network necessary for the generation of contractile fibers in both muscle and non-muscle cells. Among the known myosin isoforms, myosin II form bipolar filaments that bind and slide pass adjacent actin filaments by catalyzing the ATP in their head

domains. The synchronized 'sliding' action of myosin II filaments on actin allows the contraction of actomyosin filaments, capable of generating force (Volkmann and Hanein 2000, Vicente-Manzanares et al. 2009).

There are significant differences in the way skeletal muscle and non-muscle cells organize their contractile bundles. In muscle cells, myosin II assembles into numerous thick filaments with ends connected to titin and arranged between actin filaments that are bound to a perpendicularly oriented Z disc in a sarcomere unit. Muscle contraction is primarily regulated by calcium release and troponin. On the other hand, non-muscle cells assemble a similar but smaller and less structured contractile bundle that can develop into stress fibers (Figure 7) that are connected to adhesion structures such as focal adhesions, with different set of accessory proteins (e.g. α-actinin and filamin). Their binding to actin is regulated by phosphorylation of the helical rod domain for the head domain to interact with actin. Likewise, the head domain is responsible for the ATP-dependent motor activity for contraction of the assembled filaments (Cai and Sheetz 2009, Vicente-Manzanares et al. 2009).

Most cells of mesenchymal origin typically interact with the extracellular matrix through formation of focal adhesions. Similar to podosomes, focal adhesions comprise of integrins and its associated proteins (e.g. talin, vinculin), which in turn connects to the intracellular actin cytoskeleton to generate force on the substrate. Non-muscle myosin II (NMII) is a major component involved in the actin bundling and force generation for adhesion stabilization during cell motility (Choi et al. 2008).

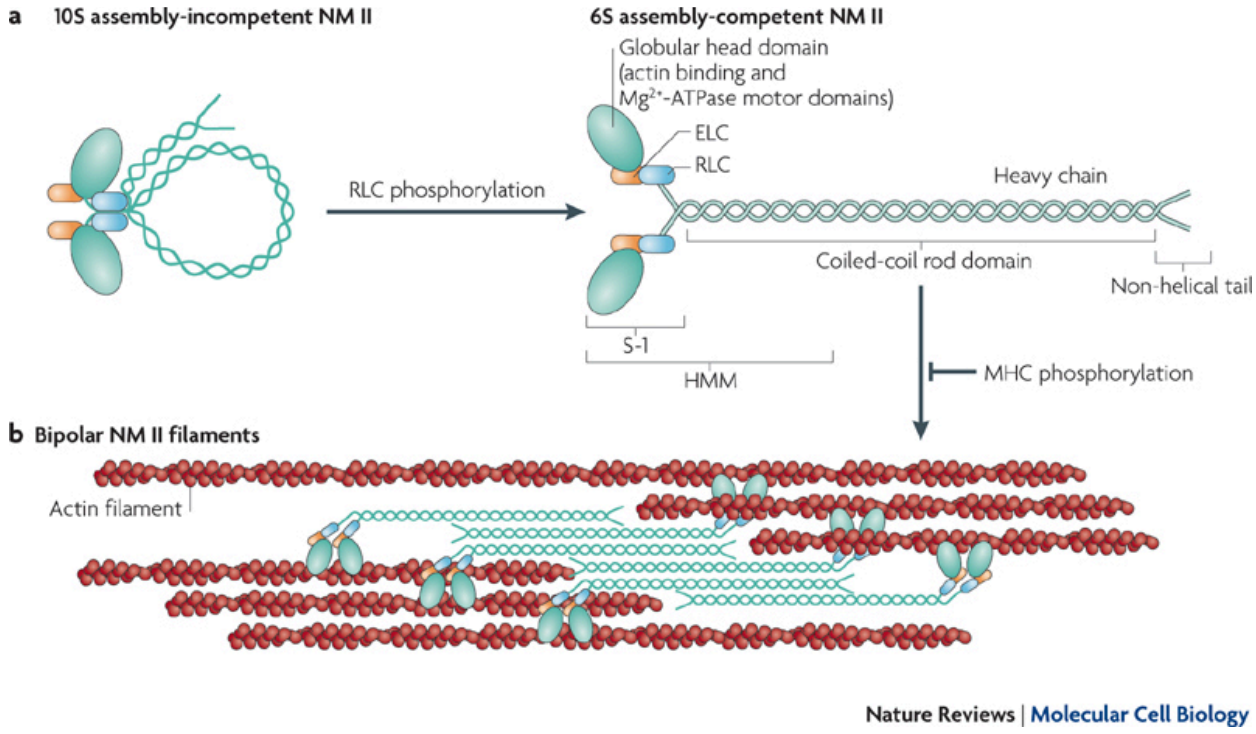

Chapter 1 – Figure 7: Structure and regulation of non-muscle myosin II.
(a) Non-muscle myosin II remains in its auto-inhibited conformation but (b) exposes its coiled-coil rod domain upon phosphorylation of the light chain to (c) form bipolar filaments that can interact with actin filaments. Figure adapted from Vicente-Manzanares et al. (2009).

While myosin II associates with actin and regulate FA maturation, the role of myosin II in podosome dynamics is less clear. Myosin IIA has been shown to localize to the cortical F-actin microfilaments connecting groups of podosomes and actomyosin contractility has been proposed to drive the oscillatory behavior (Figure 8) of podosomes during protrusion activity (van den Dries et al. 2013a, Labernadie et al. 2014). However, perturbation by small-molecule inhibitors of myosin II (Y-27632 or blebbistatin) or knockdown of myosin IIA did not inhibit the formation and recruitment of either the core or ring components of podosomes. In fact, actin polymerization at the podosome core seems to be important for generating tension at the ring to recruit tension-sensitive proteins such as vinculin and zyxin, while

myosin II counterbalances the actin growth to maintain the protrusion size (van den Dries et al. 2013a). Furthermore, the combined roles of actin polymerization and actomyosin contractility regulate the protrusive force that is dependent on the substrate stiffness (Labernadie et al. 2014). While the function of myosin II in podosomes has been associated with protrusiveness, the exact localization and arrangement of myosin II within individual podosomes and how it regulates oscillation are not clear and deserve future investigations.

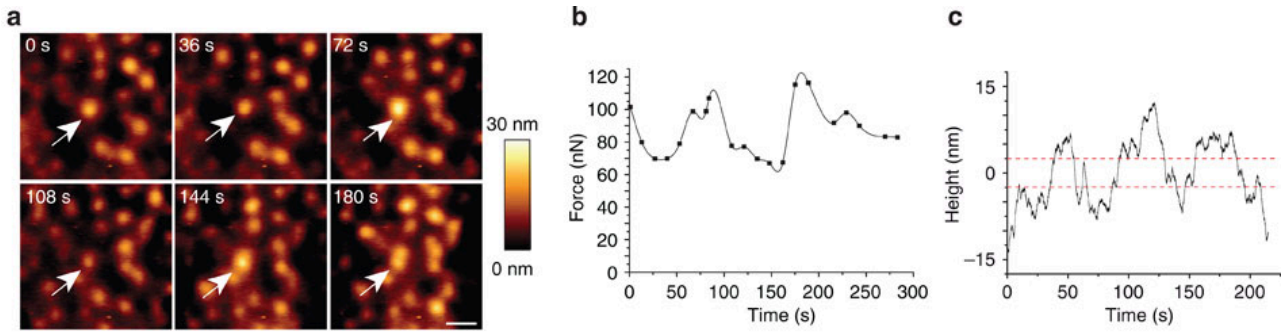

Chapter 1 – Figure 8: Oscillatory behaviour of podosomes depends on myosin II.

(a) Time-lapse images of podosomes in macrophages using atomic force microscopy (AFM) with the correseponding (b) force and (c) height protrusion measurements on a Formvar sheet. Figure adapted from Labernadie et al. (2014).

1.9 –Specific aims

While podosomes are widely known to be dependent on regulation by the Rho GTPases (e.g. Cdc42), I discovered a novel role for the ARF family of GTPases. In particular, the ARF1 GTPase and its GEF ARNO were found to be critical regulators of podosomes dynamics in macrophage-like THP1 cells, Src-transformed fibroblasts and fibroblasts on fluid lipid bilayer (Chapter 2). I further show that the constitutively active ARF1 can induce formation of *bona fide* podosomes in fibroblasts. In Chapter 3, I propose a mechanism for the microtubule-induced disassembly of podosomes. I demonstrate that microtubule disruption by nocodazole induced release of MT-associated GEF-H1 and activated a RhoA/ROCK/Myosin II –dependent pathway, which antagonized podosome formation in macrophage-like THP1 cells. Inhibition of GEF-H1 or ROCK prevented the nocodazole-induced disassembly of podosomes. Lastly in Chapter 4, I provide evidences that podosomes are sensitive to changes in membrane tension using several methods such as exposure to osmotic shock and detergent treatments, as well as mechanically stretching the cells. I found that formation of podosomes was favored at high membrane tension but perturbed at low tension in macrophage-like THP1 cells. I conclude by providing some hypotheses on the potential connection of membrane tension and previously reported localizations of membrane curvature-inducing proteins at podosomes for future investigations.

Chapter 2 - Podosome assembly is controlled by the GTPase ARF1 and its nucleotide exchange factor ARNO (Rafiq et al *J Cell Biol* 2017)

2.1 - Abstract

Podosomes represent a class of integrin-mediated cell-matrix adhesions formed by migrating and matrix-degrading cells. Here, we demonstrate that in macrophage-like THP1 cells and in fibroblasts stimulated to produce podosomes, down-regulation of G protein ARF1 or the ARF1-GEF ARNO by siRNAs or by pharmacological inhibitors led to striking podosome elimination. Concomitantly, treatments inducing podosome formation increased the level of GTP-bound ARF1. ARNO was found to co-localize with the adhesive rings of podosomes while ARF1 was localized to vesicular structures transiently contacting podosome rings. Inhibition of ARF1 led to an increase in RhoA-GTP levels and triggered assembly of myosin-IIA filaments in THP1 cells, whilst the suppression of myosin-IIA rescued podosome formation regardless of ARF1 inhibition. Finally, expression of constitutively active ARF1 in fibroblasts induced formation of putative podosome precursors: actin-rich puncta coinciding with matrix degradation sites and containing proteins of the podosome core but not of the adhesive ring. Thus, ARNO-ARF1 regulates formation of podosomes by inhibition of RhoA/myosin-II and promotion of actin core assembly.

2.2 - Introduction

Podosomes are a distinctive form of integrin-mediated cell-matrix adhesion typical of monocyte-derived cells but under some circumstances are produced by cells of other lineages. They usually appear as micron-sized radially symmetrical protrusions containing central actin cores (height about ~2 μm) rooted in the cytoplasm surrounded by matrix-associated "adhesive rings"(~1 μm diameter) enriched in integrins and plaque proteins such as talin, paxillin, vinculin and Tks5 (Calle et al. 2006, Murphy and Courtneidge 2011, Cox and Jones 2013, Meddens, van den Dries and Cambi 2014, Labernadie et al. 2014, Seano et al. 2014, Wiesner et al. 2010). In the majority of cell types, podosomes form arrays consisting of numerous individual podosomes connected to each other via a mesh of F-actin-containing links containing myosin-II (Cox et al. 2012, Dries et al. 2013, Panzer et al. 2016). Individual podosome-like structures formed by invasive cancer cells are more stable, protrusive and larger in size than normal podosomes and are often termed invadopodia (Gimona et al. 2008, Murphy and Courtneidge 2011). Podosomes participate in the processes of cell migration and invasion as well as degradation of extracellular matrix via secretion of matrix metalloproteinases (Gawden-Bone et al. 2010, Wiesner et al. 2010, Linder and Wiesner 2015, El Azzouzi, Wiesner and Linder 2016).

Cells of monocytic origin (for example cultured macrophage-like THP1 cells) form numerous podosomes upon stimulation with transforming growth factor beta (TGFβ) or increasing protein kinase C (PKC) activity by phorbol esters (e.g. PMA). Moreover, upon appropriate stimulation, even podosome-lacking cells can be forced to form podosome-like structures. In particular, expression of constitutively active Src in fibroblasts triggers formation of high-order adhesion structures termed podosome "rosettes", which are capable of degrading the ECM (Tarone et al. 1985). More recently, we have shown that non-transformed fibroblasts that typically do not form podosomes develop podosome-like adhesions under conditions where a

cell cannot apply strong traction force to nascent integrin clusters, such as spreading on fluid RGD-functionalized lipid bilayers, where stress fibres fail to assemble (Yu et al. 2013).

A key process in podosome formation is a local polymerization of actin cores primarily mediated by Arp2/3 complex activated by Wiskott–Aldrich Syndrome protein (WASP)(Machesky and Insall 1998, Linder et al. 1999, Burns et al. 2001). In turn, WASP activation depends largely upon the activity of the small G protein Cdc42 and can be regulated by WASP-interacting protein (WIP)(Abdul-Manan et al. 1999b, Calle et al. 2004a, Monypenny et al. 2011, Schachtner et al. 2013, Vijayakumar et al. 2015). Indeed, microinjection of dominant negative Cdc42 has been shown to significantly impair podosome formation in human dendritic cells (Burns et al. 2001). Similarly, podosome formation is impaired in cells microinjected with dominant negative Rac1 (Burns et al. 2001), as well as in Rac1- and especially Rac2-depleted cells (Wheeler et al. 2006) though the downstream pathways are not yet elucidated. Conversely, active RhoA, which typically promotes assembly of stress fibres and focal adhesions, has been generally described to be low in podosome-forming cells (Pan et al. 2011, Yu et al. 2013) and microinjection of active RhoA impairs podosome formation (Burns et al. 2001).

While the role of Rho family GTPases in podosome formation is relatively well-documented, the function of ARF family of G proteins is essentially unknown. Even though these proteins are considered mainly as regulators of membrane traffic, some evidence exists that they also participate in a variety of processes related to regulation of the actin cytoskeleton and involved in a crosstalk with the G proteins of the Rho family. In particular, ARF1, the most abundant ARF family member, known to recruit the coatomer complexes for vesicle budding in the Golgi (Donaldson and Jackson 2011), was shown to be required for clathrin-independent endocytosis (CLIC-GEEC)(Kumari and Mayor 2008), as well as for formation of “ventral actin structures” in some cell types (Caviston et al. 2014). Thus ARF1 is a

potentially interesting candidate for function as a podosome regulator since it could control fundamental systems involved in podosome formation, actin cytoskeleton and the plasma membrane.

In this study, we demonstrate that regardless of particular stimuli, ARF1 is required for inducing podosome formation in different cell types. Moreover, these stimuli, via an ARF exchange factor ARNO, increase the fraction of GTP-bound ARF1 in cells. ARNO localizes to the adhesive ring of podosomes, and its inhibition interferes with podosome assembly. We demonstrate that the ARNO-ARF1 pathway regulates podosomes by inhibition of RhoA- and ROCK-dependent formation of myosin-II filaments, which antagonizes podosome integrity. In addition, constitutively active ARF1 induces formation of actin-rich puncta co-localizing with matrix degradation sites and containing podosome core markers. Our data strongly suggest a direct role for ARF1 in podosome-type adhesions, and further extends the increasing number of roles for ARF1 at the plasma membrane.

2.3 - Results

2.3.1 - Depletion of endogenous ARF1 interferes with podosome formation

Stimulation by either transforming growth factor-beta 1 (TGFβ1) or the protein kinase C activator, phorbol ester 12-myristate 13-acetate (PMA), has been previously used as a model system to study podosome formation and dynamics in several cell types (Varon et al. 2006, Tatin et al. 2006, Monypenny et al. 2011, Burger et al. 2011). Consistent with numerous previous studies, we define podosomes as F-actin-rich spots with a diameter of about 0.5 μm surrounded by an approximately ring-shaped vinculin-rich zone. We consider a cell as "podosome-forming" if it had more than 10 morphologically identifiable podosomes.

In this study, 85 ± 4.7% (mean ± SD, n =3 independent experiments) of cells of the human monocytic cell line, THP1, plated on fibronectin-coated substrata in the presence of TGFβ1, formed podosomes after 24 hours, with 55 ± 3.2 (mean ± SEM, n=212 cells) podosomes per cell. The corresponding numbers for PMA-stimulated cells were 88 ± 5.5% and 140 ± 19.5 (n=80 cells), respectively. For cells plated on fibronectin in the absence of any additional stimuli, the percentage of podosome-forming cells was only 15 ± 4.7% (n =3 independent experiments) and even among these cells the average number of podosomes did not exceed 22± 8.7 (n= 58 cells).

To investigate the role of ARF1 in podosome dynamics, we depleted ARF1 in TGFβ1-treated THP1 cells by siRNA. Immediately prior to plating, cells were electroporated with the ARF1 or control siRNAs and then seeded onto fibronectin in the presence of TGFβ1. We observed that maximum silencing (>95%) was achieved by 48 hours (Figure 1A).

Depletion of ARF1 led to dramatic decrease of podosome number in TGFβ1-treated cells (Figure 1B,C). Both the number of podosomes per cell and percentage of

podosome-forming cells significantly dropped upon ARF1 depletion (Figure 1D-F). Whilst the mean number of podosomes per cell and percentage of podosome-forming cells in cells transfected with control siRNA did not differ from aforementioned control numbers, the cells transfected with ARF1 siRNA had on average only 8 ± 1.7 (n= 96 cells) podosomes per cell. Total intensity of F-actin-containing non-podosomal structures at the ventral surface of the cells became somewhat higher in ARF1-depleted cells (Figure 1B and C, left panels). At the same time, the vinculin-containing non-podosomal structures at the cell periphery that can be classified as small focal adhesions were not apparently affected (Figure 1B and C, right panels). Depletion of ARF1 by siRNA did not affect the integrity of the Golgi apparatus as visualized by *cis*-Golgi markers GM130/GRASP65 (Figure 1B and C) in agreement with previous publications (Volpicelli-Daley et al. 2005, Szul et al. 2007, Nakai et al. 2013).

The effect of ARF1 siRNA on podosome number was specific since it could be fully reversed by expression of exogenous bovine HA-ARF1 insensitive to human ARF1 siRNA (Figure 1D-F). Interestingly, exogenous HA-ARF1 was often localized in the spots adjacent to the podosomes of transfected cells (Figure 1D'). See below for a detailed analysis of localization dynamics. Significantly, we found that loss of podosome induction due to ARF1 depletion was not exclusive to TGFβ1 stimulation, since after PMA stimulation (Supplementary Figure S1A-I), ARF1 depleted cells demonstrated a significant decrease in both the number of podosomes and the percentage of podosome-forming cells as compared to control cells (Supplementary Figure S1A, D, F, G).

In contrast to ARF1, depletion of ARF6 by siRNA with a silencing efficiency of >95% (Supplementary Figure S1J) did not affect podosome induction in TGFβ1-treated THP1 cells (Supplementary Figure S2K). Both the average number of podosomes per cell and the percentage of cells forming more than 10 podosomes were not significantly different from control siRNA-treated cells (Figure 1E and 1F). Taken

together, these data indicate a specific role for ARF1 in podosome induction in stimulated THP1 cells.

We also examined the effect of expression of dominant negative and constitutively active mutants of ARF1 on adhesion of THP1 cells in the presence of TGFβ1. The dominant negative mutant, CFP-ARF1 (T31N), led to a significant decrease of cell adhesion to fibronectin under these conditions (control: 71 ± 5.5%, ARF1 T31N: 4 ± 0.3%) and the few adherent cells observed did not form podosomes (data not shown). This behaviour resembles a "non-adhesive phenotype", described previously in the culture of normal human dendritic cells (Burns et al. 2004). Unexpectedly, the expression of a constitutively active mutant of ARF1, CFP-ARF1 (Q71L), also interfered with cell adhesion and completely prevented podosome formation. Thus, sustained high activity of ARF1 is also damaging for cell adhesion and podosome formation in THP1 cells. Overexpression of wild-type ARF1 or constitutively active ARF1 in unstimulated THP1 cells did not induce any apparent phenotypic changes. These cells remain poorly attached to the fibronectin and do not form podosomes.

2.3.2 - ARF1-containing vesicles transiently contact podosomes

We used fluorescently-tagged ARF1 to further elucidate the localization and dynamics of ARF1 in TGFβ1-stimulated THP-1 cells. Expression of GFP-ARF1 showed a predominant Golgi localization (Figure 1D) in agreement with previous publications (Lippincott-Schwartz et al. 1989, Sciaky et al. 1997). However, in addition to the Golgi localization, we found numerous irregular puncta throughout the cell, some of which were apparently associated with podosomes (Figure 1D' and Figure 2A).

We employed total internal reflection fluorescence (TIRF) microscopy to explore the spatiotemporal dynamics of ARF1 puncta at the plasma membrane. GFP-ARF1 puncta displayed temporal localization at regions of podosome assemblies and made transient periodic contacts with the adhesive rings of podosomes, as marked by mCherry-vinculin in THP1 cells (Figure 2B, 2B' and Supplementary movie 1). Up to 80% of podosomes appeared to be in contact with ARF1-containing puncta during 5-minute periods of observation (Figure 2C) with an average dwell time of 10 ± 1.6 seconds (mean ± SEM, Figure 2D). In contrast, CFP-ARF6 does not form puncta-like structures in THP1 cells and no preferential localization of CFP-ARF6 to regions of podosome assembly was found (Supplementary Figure S1L). We further characterized the GFP-ARF1 associated puncta by determining if their mobility was dependent on a cytoskeletal network. We found that GFP-ARF1 patches appeared to be travelling on microtubule tracks identified by labeling with mCherry-ensconsin (Figure 2E,F and Supplementary movie 2). To elucidate the nature of the ARF1 puncta, we co-express GFP-ARF1 with several markers of vesicular traffic carriers, Rab6, Rab7, Rab8 and Rab11 (Supplementary Figure S2A-D). Amongst those, Rab11 (Welz, Wellbourne-Wood and Kerkhoff 2014) demonstrated significant co-localization (Supplementary Figure S2E) with ARF1 suggesting that ARF1-containing puncta have a vesicular nature.

2.3.3 - Inhibition of ARF1 activity interferes with formation of podosomes induced by diverse stimuli

To study the immediate effect of ARF1 inhibition on podosome formation, we used two inhibitors known to suppress ARF1 activity. Brefeldin A (BFA) promotes formation of complexes between GDP-bound ARF1 and Sec7 domains of ARF1 nucleotide exchange factors GBF1, BIG1 and BIG2, and prevents completion of the nucleotide exchange reaction (D'Souza-Schorey and Chavrier 2006), while secinH3 inhibits activity of another group of ARF exchange factors, cytohesins (1-4), by

binding to their Sec7 domain, without formation of a complex with ARF1 (Casanova 2007).

Using a G-LISA assay for the measurement of ARF1-GTP levels, we demonstrate that TGFβ1 or PMA treatment of THP1 cells enhances the fraction of active, GTP-bound ARF1, while both secinH3 and BFA significantly reduced it (Figure 3A, Supplementary Figure S1C). Both secinH3 and BFA treatment induced rapid disassembly of all podosomes in about 30-40 minutes (Figure 3B-D, graphs 3E, F and Supplementary movie 3). In the case of secinH3, this process was accompanied by a burst of lamellipodial activity (Figure 3B), the integrity of the Golgi apparatus, as well as localization of ARF1 to Golgi and to vesicular structures in the cytoplasm was not affected (Figure 3B, 3C). Unlike secinH3 treatment, disruption of podosomes with BFA was accompanied by loss of ARF1 localization at the Golgi and at cytoplasmic vesicular structures (Figure 3D) as well as structural disintegration of the Golgi apparatus, in agreement with numerous previous studies (Lippincott-Schwartz et al. 1989, Donaldson, Honda and Weigert 2005). Thus, comparison between the SecinH3 and BFA effects confirmed that active ARF1 is required for podosome integrity and this function of ARF1 does not depend on its role in Golgi stabilization. A second confirmation of independence of podosomes from Golgi traffic can be inferred from experiments with knockdown of COPB1, a subunit of the COPI coatomer protein complex required for retrograde transport from *trans*-Golgi to *cis*-Golgi and endoplasmic reticulum (Beck et al. 2009). We found that COPB1 knockdown or its inhibition generated only minor effects on podosome integrity (Supplementary Figure S3A-E). Finally, disruption of podosomes with secinH3 or BFA still proceeded (albeit in a slower rate) in TGFβ1-stimulated THP1 cells expressing constitutively active Cdc42 (GFP-Cdc42 Q61L), a potent podosome-inducing signalling protein (Supplementary Figure S3H). Moreover, treatment of cells with BFA or SecinH3 as well as knockdown of ARNO or ARF1 did not change the level of Cdc42-GTP in TGFβ-stimulated THP1 cells (Supplementary Figure S3I and J).

Visualization of podosomes using structured-illumination microscopy (SIM) revealed a central F-actin core surrounded by patches enriched in adhesion proteins (talin and vinculin) as well as the thin F-actin-rich links connecting neighboring podosomes (Supplementary Figure S4A, boxed image S4A' and Supplementary movie 4) in agreement with previous studies (Cox et al. 2012, Dries et al. 2013). Treatment with secinH3 led to the rapid disappearance of the connecting links and gradual concurrent disassembly of both the actin cores and surrounding adhesive rings (Supplementary Figure S4B, C and Supplementary movie 5).

In view of the high podosome turnover rate (Dries et al. 2013), gradual disruption of podosomes upon addition of secinH3 suggests that inactivation of ARF1 changes the balance between podosome assembly and disassembly rather than completely block the assembly processes. The process of disassembly often proceeds through podosome fission and is accompanied by an apparent increase of podosome mobility in the plane of the plasma membrane (Supplementary Figure S4D-F).

We next studied the effect of inhibition of ARF1 on podosome-like structures formed by fibroblast-type cells. Under standard culture conditions, mouse embryonic fibroblasts (MEFs) generally form focal adhesions, which appeared to be resistant to treatment with either BFA (Bershadsky and Futerman 1994) or SecinH3 (Supplementary Figure S5A). It was recently shown that fibroblasts plated on a fluid substratum (supported RGD-functionalized lipid bilayer), under conditions where they cannot exert traction forces, by default formed podosome-like adhesion structures (Yu et al. 2013). We showed that the level of GTP-ARF1 increased in MEF plated on supported lipid bilayers (Figure 3G). Similarly to "classic" podosomes, podosome-like structures formed by MEFs plated on the lipid bilayer underwent rapid disassembly upon treatment with either BFA or SecinH3 (Figure 3H, I).

A well-known method of induction of podosome-like structures in fibroblast-like cells is ectopic expression of constitutively active Src. In agreement with published results (Tarone et al. 1985), expression of Src Y527F in MEFs led to the formation of prominent rosettes formed as a result of fusion of numerous podosome-like structures (Supplementary Figure S5B and C). Treatment of such cells with either BFA or SecinH3 resulted in the gradual disassembly of these rosettes and a decrease in the number of rosette-positive cells (Supplementary Figure S5B and C).

Altogether, these data demonstrate that ARF1 activity is required for formation/maintenance of podosome-like structure irrespective of upstream stimuli (TGFβ1, PMA, active Src or fluid substratum). We conclude that a role for ARF1 in podosome dynamics is independent of early signalling pathways that lead to initiation of cellular differentiation to a podosome-generating phenotype.

2.3.4 - ARNO GEF activates ARF1 to drive podosome formation

The mammalian ARF GTPases are activated by 15 different GEFs categorized in five classes. Among these, only 7 GEFs can activate ARF1: 3 BFA-sensitive (GBF1, BIG1, BIG2) and 4 SecinH3-sensitive (cytohesins 1-4) (D'Souza-Schorey and Chavrier 2006, Donaldson and Jackson 2011). Both BFA- and SecinH3-sensitive GEFs share a common conserved SEC7 domain that promotes GDP release and subsequent GTP binding to ARF1. SecinH3-sensitive GEFs have in addition a pleckstrin homology (PH) domain that enables them to interact with phosphoinositides at the plasma membrane (Santy et al. 1999, DiNitto et al. 2007).

We examined the effect of inhibition of a number of ARF1 GEFs on the process of podosome formation (Supplementary Figure S3B, D-G). We found that expression of dominant negative mutants of two BFA-sensitive GEFs, HA-BIG1 (E793K) and HA-BIG2 (E738K) did not prevent formation of podosomes in THP1 cells treated with TGFβ1 (Supplementary Figure S3F and G, lower panel). Conversely podosomes

formation was not affected by overexpression of wild-type HA-BIG1 or HA-BIG2 (Supplementary Figure S3F and G, upper panel). Furthermore, both the wild-type HA-BIG1 and HA-BIG2 showed predominant Golgi localization (Supplementary Figure S3F and G) and no podosome localization, consistent with previous reports (Citterio et al. 2006, Ishizaki et al. 2008). To inhibit the activity of the third BFA-sensitive GEF, GBF1, we used a small-molecule inhibitor, Golgicide A (Saenz et al. 2009). We found only partial dissolution of podosomes in THP1 cells treated with TGFβ1 after application of Golgicide A in a concentration that induced visible fragmentation of the Golgi complex (Supplementary Figure S3B, D and E). Thus, in spite of profound inhibitory effect of BFA on podosome formation, selective inhibition of the BFA-sensitive GEFs produced only minor effect on podosomes.

In contrast, knockdown of one of the SecinH3-sensitive GEFs, ARNO (cytohesin-2), significantly affected podosome formation in TGFβ1- (Figure 4A-D) or PMA-activated THP1 cells (Supplementary Figure S1B, E, H, I). Knockdown of ARNO led to a significant decrease in the number of podosomes per cell as well as the percentage of cells having more than 10 podosomes (Figure 4C and 4D). Additionally we found that ARNO knockdown reduced ARF1 activity in THP1 cells stimulated by TGFβ1 (Figure 4E). Moreover, a dominant negative mutant of ARNO (E156K) also suppressed podosome formation/maintenance (Figure 4F and 4G). The effect of ARNO knockdown on podosomes was specific since knockdown of another secinH3-sensitive GEF, cytohesin-1 did not inhibit podosome formation in stimulated THP1 cells (Figure 4B). Neither ARNO nor cytohesin-1 knockdown produced any significant effect on Golgi integrity (Figure 4B).

Next, we investigated the localization of ARNO and cytohesin-1 in TGFβ1-treated THP1 cells by expressing GFP-fusion construct of these GEFs. ARNO was found to localize to the rings surrounding the actin cores of podosomes (Figure 5A). Similarly, GFP-ARNO localized to the rim around the actin core of podosome rosettes (Figure 5B). Moreover, podosome-like structures formed by normal

fibroblasts plated on RGD-functionalized lipid bilayers also contain ARNO in the rings surrounding the actin cores (Figure 5C). Live imaging of GFP-ARNO in all these situations revealed that ARNO localization at the podosome ring was stable and spanned the entire lifetime of a podosome (Figure 5D,D' and Supplementary movie 6). Unlike ARNO, Cytohesin-1 showed diffuse localization over the plasma membrane and was not enriched at podosomes (Figure 5E).

2.3.5 - Inhibition of ARF1 triggers podosome disassembly via activation of Rho and myosin-IIA

In search of downstream factors that mediate podosome disruption upon ARF1 inhibition we checked the activity of three major Rho family G proteins in TGFβ1-treated THP1 cells. We found that the fraction of RhoA-GTP significantly increased upon inhibition of ARF1 by SecinH3 (Figure 6A), while activities of both Rac1 and Cdc42 did not change (Figure 6B and C). RhoA and Rho-associated kinase (ROCK) are master regulators of myosin-IIA-driven cell contractility, since ROCK-mediated activation of myosin regulatory light chain (MRLC) phosphorylation promotes assembly of myosin-II filaments as well as myosin-II motor activity (Vicente-Manzanares et al. 2009). Indeed, we have demonstrated that inhibition of ARF1 by SecinH3 promoted assembly of the myosin-II filaments visualized by live imaging of GFP-MRLC using SIM (Figure 6D and Supplementary movie 7). Simultaneous visualization of podosomes and myosin-II filaments revealed that podosome disappearance occurred in those cell regions enriched in myosin-II filaments (Figure 6D), suggesting that podosome disassembly is triggered by local activation of myosin-II-driven contractility. Indeed, treatment of ARF1-inhibited cells lacking a majority of podosomes with an inhibitor of ROCK, Y-27632, led to a burst of podosome formation concurrent with the disappearance of myosin-II filaments (Figure 6E and Supplementary movie 8). To confirm that inhibition of ARF1 led to podosome disruption via activation of myosin-II filament assembly, we performed siRNA-mediated myosin-IIA heavy chain (MYH9) knockdown, which completely

blocked formation of myosin-IIA filaments as visualized by antibody to NM-MHCIIA (Figure 6F-H). Myosin-II knockdown by itself did not affect podosome integrity (Figure 6F, I, K and L). While treatment of THP1 cells transfected with control siRNA by SecinH3 led to pronounced disassembly of podosomes (Figure 6G, K and L), the same treatment on myosin-IIA knockdown cells did not disrupt podosomes (Figure 6J, K and L).

2.3.6 - Constitutively active ARF1 induces actin-rich puncta in fibroblasts

To test if constitutively active ARF1 could induce formation of podosome-like adhesions in a more general context, we expressed constitutively active ARF1, CFP-ARF1 (Q71L), in cells that normally do not form podosomes, such as mouse embryonic fibroblasts (MEFs). Overexpression of constitutively active but not wild type ARF1 induced formation of numerous actin-rich puncta localized to the ventral surface of these cells, in the same focal plane as focal adhesions (Figure 7A and B). Similar to mature podosomes, the actin-rich puncta induced by constitutively active ARF1 (CFP-ARF1 Q71L) were transiently associated with CFP-ARF1 (Q71L)-containing vesicles (Figure 7B'). Formation of these puncta was accompanied by some reduction in the number of stress fibres and focal adhesions, but even total disassembly of these structures upon expression of dominant negative RhoA (GFP-RhoA T19N) was not sufficient to induce actin-containing puncta (Figure 7C). At the same time, constitutively active ARF1 efficiently triggered formation of such puncta in cells also expressing dominant negative RhoA (Figure 7D). Similarly, inhibition of Rho activity by cell-permeable C3 transferase (2 μg/ml) did not by itself induce formation of the actin puncta and did not interfere with the induction of these puncta by constitutively active ARF1 (Supplementary Figure S5D and E).

Proteins typically associated with podosome cores in different cell types (WIP, N-WASP, cortactin, Arp3, dynamin-2) were found in the actin-rich puncta

(Supplementary Figure S5F-J). At the same time, protein components of the podosome "ring", such as vinculin (not shown) and paxillin (Supplementary Figure S5K), were not found to be associated with active ARF1-induced actin puncta suggesting incomplete podosome formation. ARF1-induced actin puncta were not related to clathrin-depended endocytic activity since they did not co-localize with clathrin-coated pits (Supplementary Figure S5L).

Unlike native podosomes, the puncta induced by constitutively active ARF1 were motile. While podosomes of THP1 cells (Supplementary Figure S4D, right insets), as well as podosome-like structures in fibroblasts plated on fluid substrate (Yu et al. 2013), are essentially stationary with respect to the substratum, the positions of puncta induced by active ARF1 are oscillating with an average velocity of 0.88 ± 0.28 μm/s (± SD). Thus constitutively active ARF1 induced formation of actin-rich puncta in proximity to the ventral cell membrane that can be considered as incompletely anchored podosome-like structures and possibly podosome precursors.

In spite of the difference between authentic podosomes and the actin-rich puncta induced by constitutively active ARF1, the puncta mimic one important podosome function namely, matrix metalloproteinase (MMP)-dependent ability to degrade the matrix. Indeed, the positions of actin puncta induced in the fibroblasts by constitutively active ARF1 (Q71L) coincided with the sites of matrix degradation - dark areas on the substratum covered with fluorescently-labeled gelatin (Figure 7G, G'). Formation of such dark areas could be prevented by treatment with 25 μM of MMP inhibitor GM6001 (Figure 7H,H'), and therefore depended on the exocytosis of MMPs by cells. Thus, our experiments showed that actin puncta induced in fibroblasts by constitutively active ARF1 trigger local matrix degradation by facilitating exocytosis of MMPs independent of podosome ring assembly.

2.4 - Figures

Figure 1

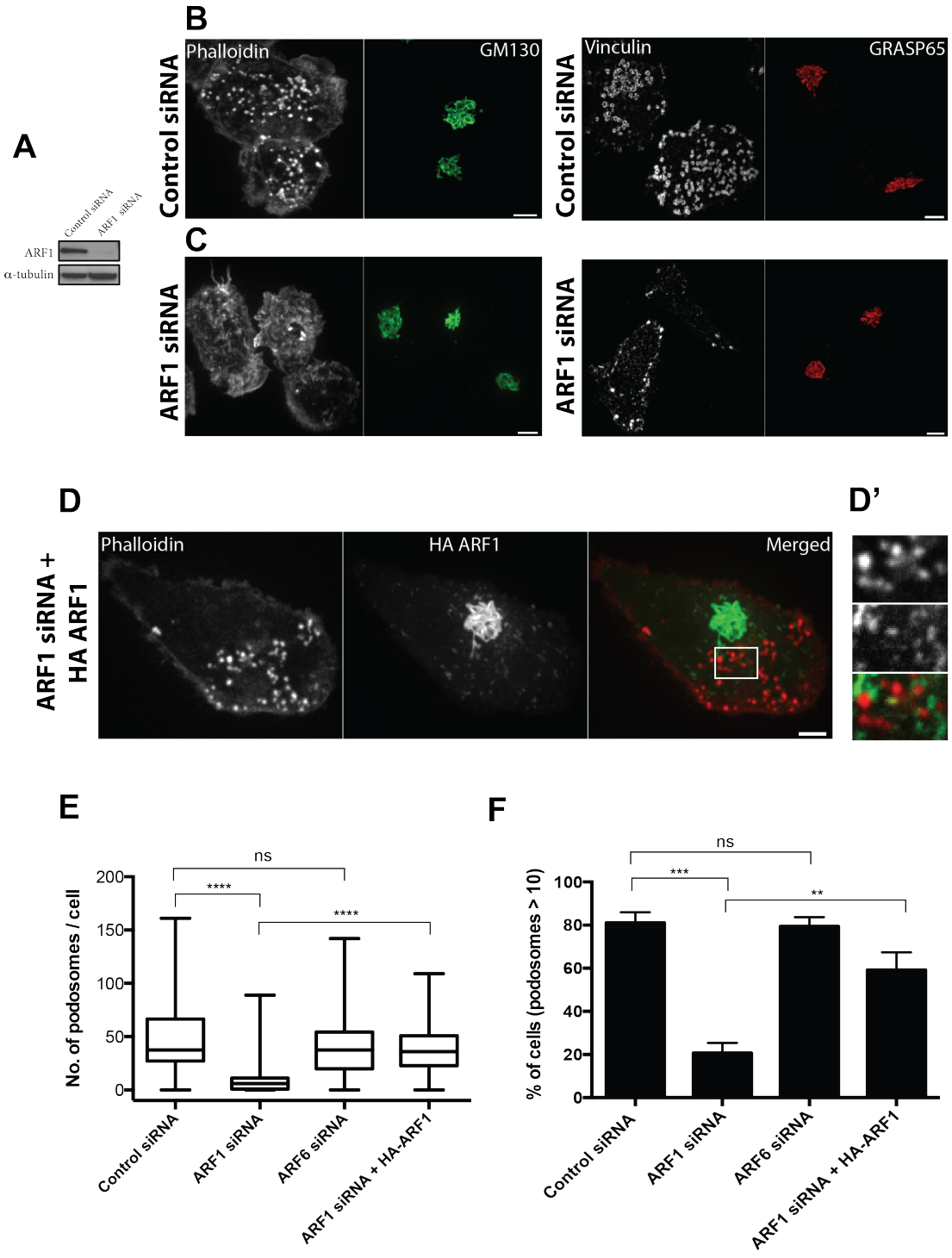

Chapter 2 – Figure 1: Depletion of endogenous ARF1 disrupts podosomes.

(A) Western blot showing ARF1 levels in cells treated with scramble (control) or ARF1 siRNA; α-tubulin was used as a loading control. (B, C) ARF1 knockdown leads to disruption of podosomes but not the Golgi apparatus. Actin labeled with phalloidin (left panel) and vinculin visualized by antibody staining (right panel) in control (B) and ARF1 siRNA-transfected (C) THP1 cells 48 h after TGFβ1 stimulation. The Golgi apparatus in the same cells was visualized by staining with antibody against *cis*-Golgi proteins, GM130 (left panel, green) and GRASP65 (right panel, red). Scale bars, 5 μm. (D) Expression of HA-tagged bovine ARF1 in ARF1-depleted human THP1 cells rescues podosome formation. Podosomes are visualized by phalloidin staining (left and right panels) and HA-ARF1 by immunostaining with anti-HA antibody (central and right panels). HA-ARF1 was localized to Golgi and to punctate structures shown with high magnification in (D') representing the enlarged area boxed in (D). Scale bar, 5 μm. Labeling in (D') shows actin (upper image), HA-ARF1(middle image), and merged image of both (lower panel). Width of the images 7 μm. (E,F) Quantification of the effect of ARF1 and ARF6 knockdown on podosomes integrity. Both number of podosomes per cell (E) and percentage of cells having more than 10 podosomes (F) decreased upon ARF1 but not ARF6 knockdown. This effect was rescued by expression of exogenous HA-ARF1. The graphs represent results of 3 independent experiments with 100-200 cells used for each group. The numbers of podosomes per cell are presented as box-and-whiskers plot while the percentage of cells with more than 10 podosomes as mean ± SD. The significance of the difference between groups was estimated by two-tailed Student's *t*-test, the range of P-values >0.05(non-significant), ≤ 0.05, ≤0.01, ≤0.001, ≤ 0.0001 are denoted by "ns", one, two, three and four asterisks (*), respectively.

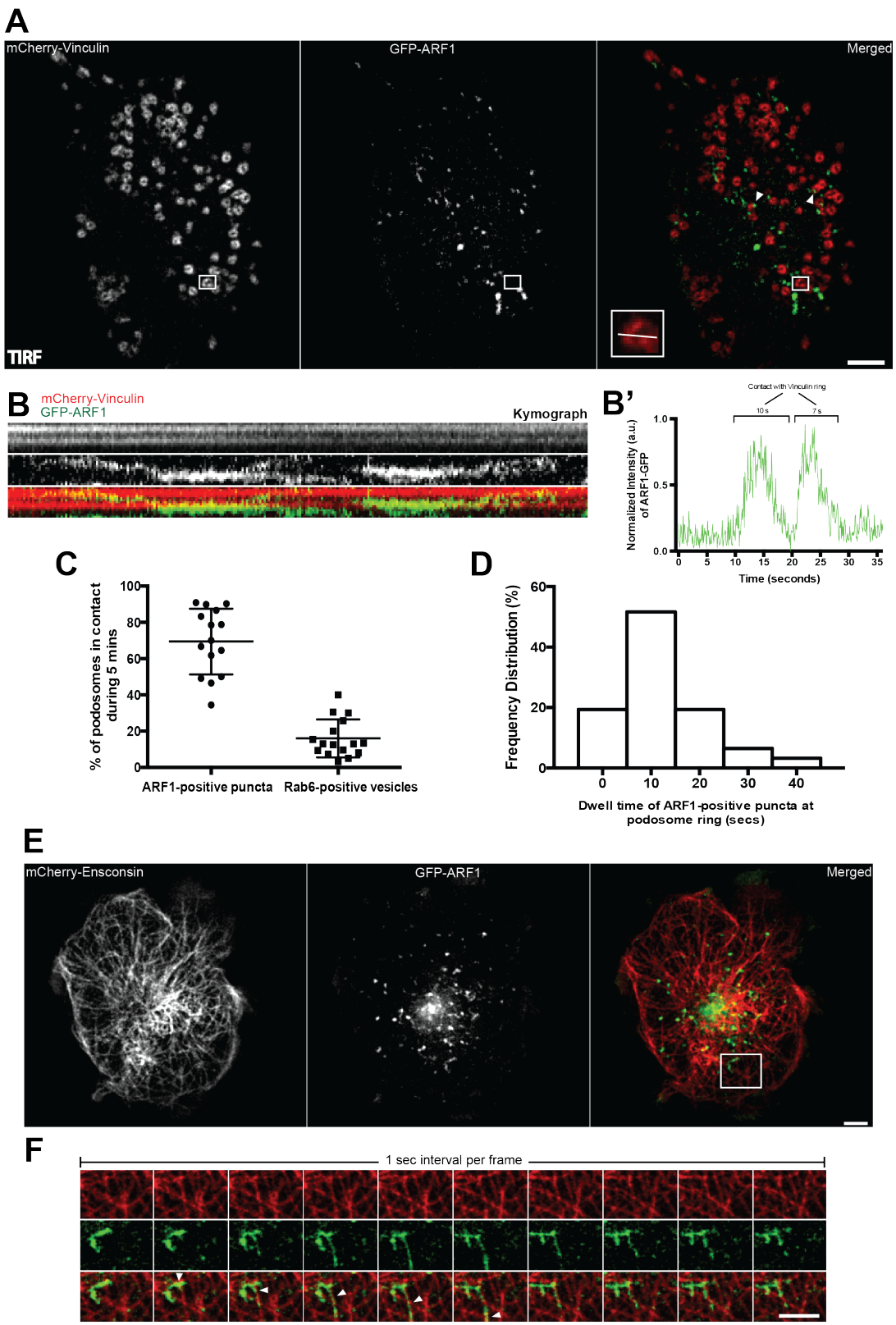

Chapter 2 – Figure 2: Localization and dynamics of ARF1 puncta in TGFβ1-stimulated THP1 cells.

(A) TIRF image of the ventral surface of cell with podosomes labeled by mCherry-vinculin (left panel) and ARF1 puncta labeled by GFP-ARF1 (central panel). Merged image (right panel) shows non-random distribution of ARF1 puncta with a tendency to co-localize to podosome periphery. Scale bar, 5 μm. Boxed area (2.5x2.5 μm^2) contains a podosome, where co-localization dynamics with ARF1 puncta is presented in (B). (B) Kymograph representing fluorescent intensities in a line scan through the podosome boxed in (A). While mCherry-vinculin is stably labeled in the podosome ring (upper panel), GFP-ARF1 was transiently concentrated at one side of the ring (central panel and merged image at the bottom). See also Supplementary movie 1. The time course of fluorescence intensity of GFP-ARF1 at the podosome ring is shown in (B'). (C) Each dot corresponds to a single cell and represents percentage of podosome rings (labeled by vinculin) contacted by either ARF1-containing puncta or Rab6-containing vesicles within 5 minutes of image acquisition. (D) Frequency distribution of the durations of podosome contacts (in seconds) with ARF1-containing puncta (35 podosomes from 10 cells were filmed as shown in kymograph B). (E,F) GFP-ARF1 puncta are moving along microtubules. (E) Left panel: microtubule labeling with 125 kDa microtubule-associated protein, ensconsin (mCherry-ensconsin); central panel: GFP-ARF1 puncta in the same cell; right panel: merged imaged. The dynamics of microtubules and ARF1 puncta in the boxed area (8 x 7.5 μm^2) of C is shown in (F). Scale bar, 5 μm. Movement of puncta along the microtubule is indicated by arrowhead. See also Supplementary movie 2.

Figure 3

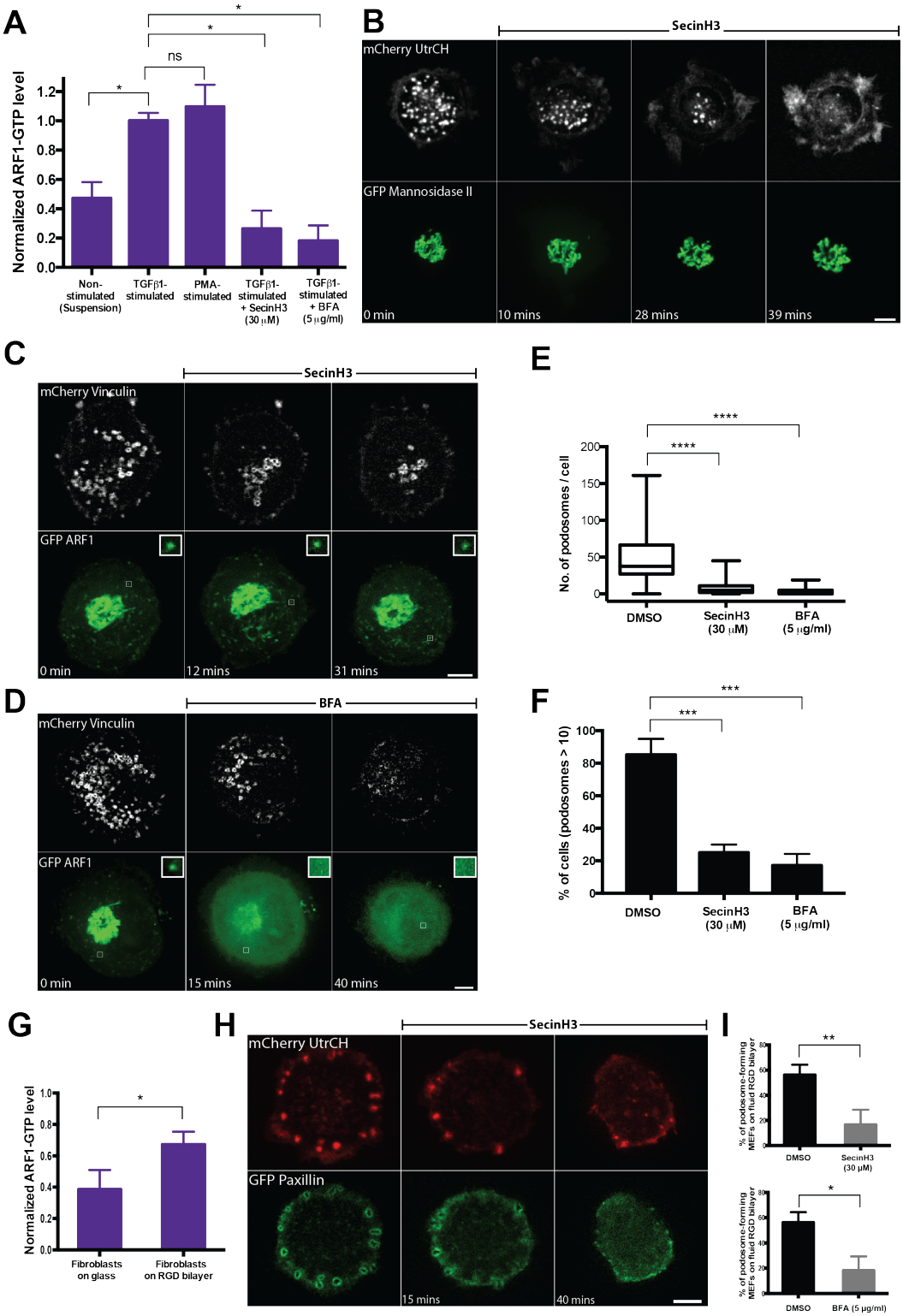

Chapter 2 – Figure 3: ARF1-GTP levels and podosome formation.

(A) Quantification of ARF1-GTP levels by G-LISA assay in control, stimulated and inhibitor-treated THP1 cells. Both TGFβ1 and PMA increased the fraction of GTP-bound ARF1 compared to control, while treatment with SecinH3 or BFA dramatically reduced it. Pooled results of 3 independent experiments are shown. (B) Disruption of podosomes labeled with mCherry-Utrophin (UtrCH) upon treatment with SecinH3 (upper panel). Note that integrity of the Golgi apparatus labeled with GFP-mannosidase II was preserved in the same SecinH3-treated cell (lower panel). See also Supplementary movie 3. (C,D) Disruption of podosomes labeled with mCherry-vinculin by SecinH3 (upper panel of C) and BFA (upper panel of D). Whilst the effect of SecinH3 in these cells is not accompanied by changes in localization of ARF1 to the Golgi and cytoplasmic puncta (lower panel of C), BFA disrupted both Golgi and ARF1 puncta (lower panel in D); Scale bars, 5 μm. Insets (1 x 1 μm^2) show evolution of individual ARF1 puncta in each case. (E,F) Quantification of the effect of SecinH3 and BFA on average number of podosomes per cell (E) and percentage of cells with more than 10 podosomes (F). (G) ARF1-GTP levels increase in fibroblasts plated on a RGD-functionalized fluid lipid bilayer as compared to fibroblasts plated on glass coverslip. (H) Effect of SecinH3 on the integrity of podosome-like structures formed by fibroblasts plated on fluid lipid bilayer. (I) Quantification of the disruptive effect of SecinH3 and BFA on podosome-like structures formed by fibroblasts on lipid bilayer. The percentage of podosome-forming cells significantly decreased upon treatment by each of the inhibitors. The data were presented and the significances of the difference were assessed as indicated in the legend to Figure1. Pooled data of three independent experiments are presented for each group.

Figure 4

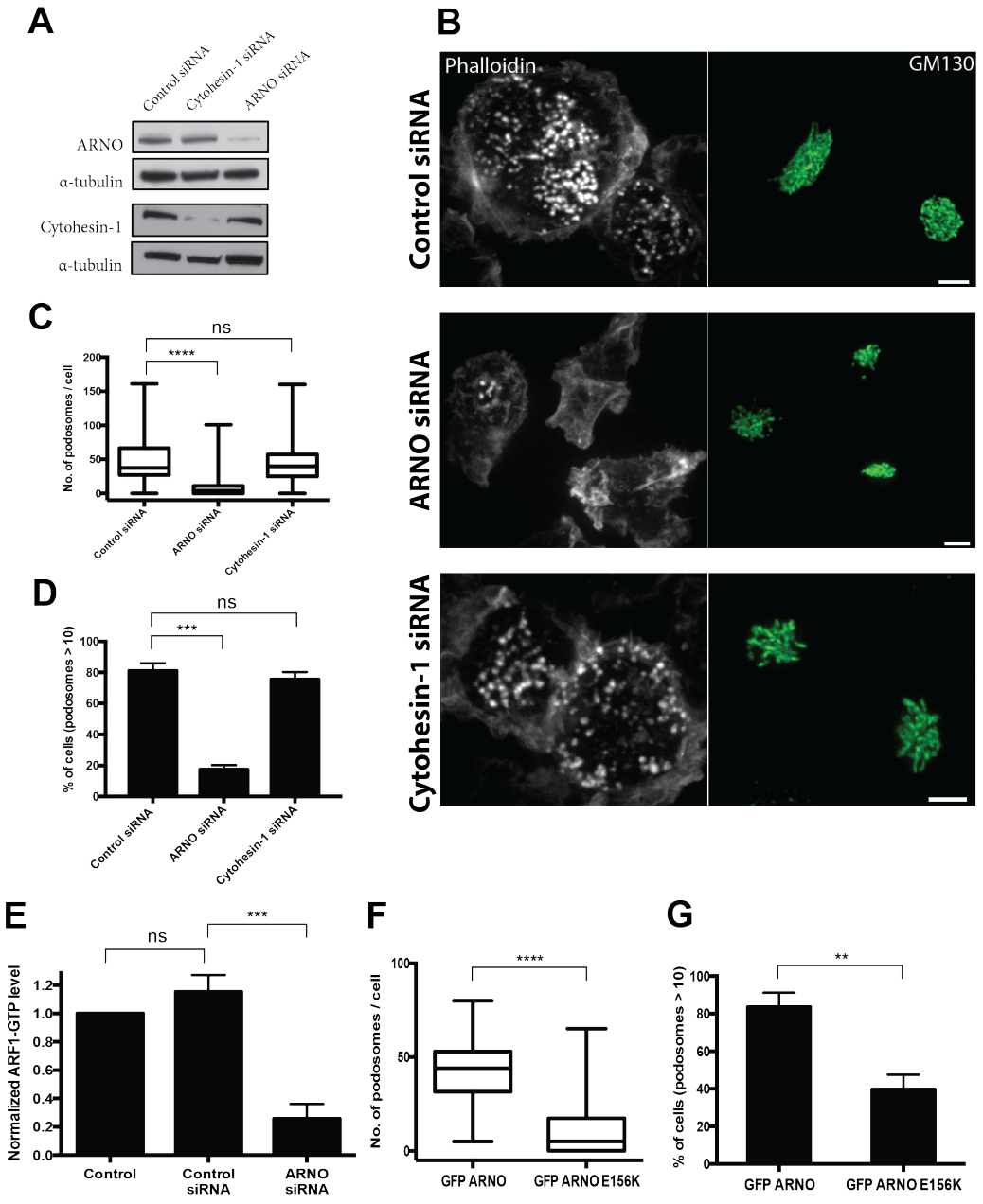

Chapter 2 – Figure 4: Knockdown of ARF1 exchange factor ARNO (cytohesin-2), but not cytohesin-1 leads to podosome disruption.

(A) Western blot showing ARNO and cytohesin-1 levels in cells treated with control (scrambled) siRNA, ARNO or cytohesin-1 siRNAs; α-tubulin was used as a loading control. (B) Upper panel: TGFβ1-stimulated THP1 cells; podosomes labeled with phalloidin and Golgi apparatus labeled by antibody against GM130. Middle panel: siRNA-mediated knockdown of ARNO disrupted podosomes leaving the Golgi undisturbed. Lower panel: Cytohesin-1 knockdown disrupt neither podosomes nor Golgi. Scale bars, 5 μm. (C,D) Quantification of the effect of ARNO and cytohesin-1 knockdowns on average number of podosomes per cell (C) and percentage of cells with more than 10 podosomes (D). (E) G-LISA quantification of ARF1-GTP level in non-transfected control cells, scrambled siRNA-transfected cells, and cells transfected with ARNO siRNA. (F,G) Quantification of the effect of expression of wild-type GFP-ARNO and of dominant negative ARNO mutant (GFP-ARNO E156K) on average number of podosomes per cell (F) and percentage of cells with more than 10 podosomes (G). The data were presented and the significances of the difference were assessed as indicated in the legend to Figure 1. Pooled data of three independent experiments are presented for each group.

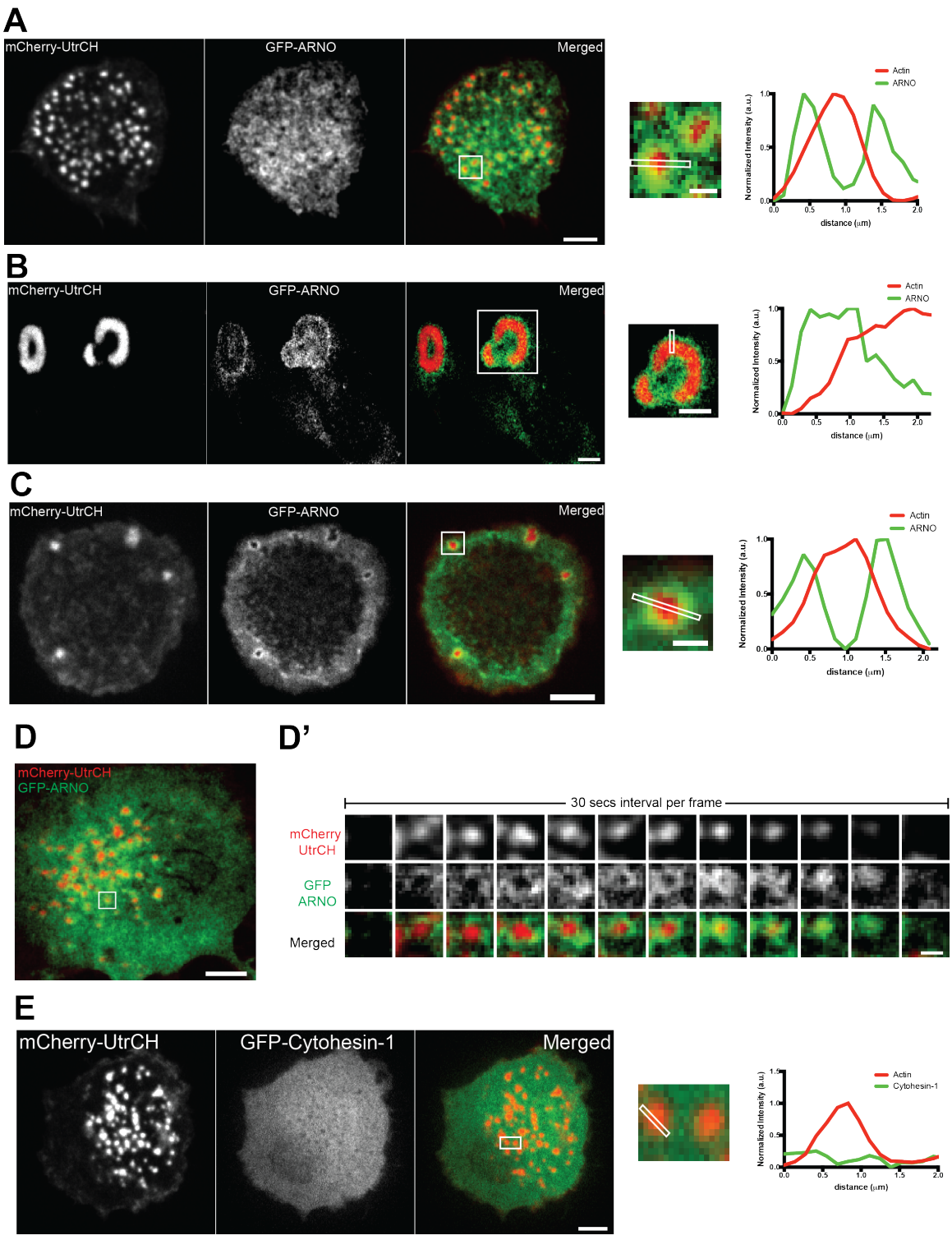

Chapter 2 – Figure 5: ARNO but not cytohesin-1 is localized to podosomes and podosome-like structures in different cell types.

(A,B,C) Localization of F-actin marker, mCherry-UtrCH and GFP-ARNO in TGFβ1-stimulated THP1 cell (A), active Src-transformed fibroblast (B) and fibroblast on a RGD-functionalized fluid lipid bilayer (C). Left panels: F-actin cores of podosomes (A), podosome rosettes (B), and podosome-like structures formed on fluid bilayer (C). Central panels: GFP-ARNO localized to periphery of F-actin cores (A,B,C). Right panels: merged images. The boxed areas (A and B: 2.5 x 2.5 μm^2, Scale bar: 1 μm, C: 14 x 14 μm^2, Scale bar, 5 μm) of merged images are enlarged and line scanned as shown in inset. The graphs on the right demonstrate intensity profiles of F-actin and ARNO in individual podosome (A), podosome "rosette" (B), and podosome-like structure on bilayer (C). (D, D') Time course of ARNO localization to the podosome periphery. Dynamics of F-actin (labeled by mCherry-UtrCH) and GFP-ARNO fluorescence intensities in the podosome shown in the boxed area (3 x 3 μm^2) in D are presented in the sequences in D'. Time interval between frames is 30 seconds. See also Supplementary movie 6. (E) Cytohesin-1 is not localized to podosomes. Left panel: F-actin cores of podosomes in TGFβ1-stimulated THP1 cell. Central panel: GFP-cytohesin-1 localization in the same cell. Right panel: merged image. Line scanning through the individual podosome in the boxed area (4 x 1.5 μm^2) of the merged image shown in inset is quantified in the graph on the right. No enrichment of GFP-cytohesin-1 at podosome core or periphery was detected. Scale bars, 5 μm.

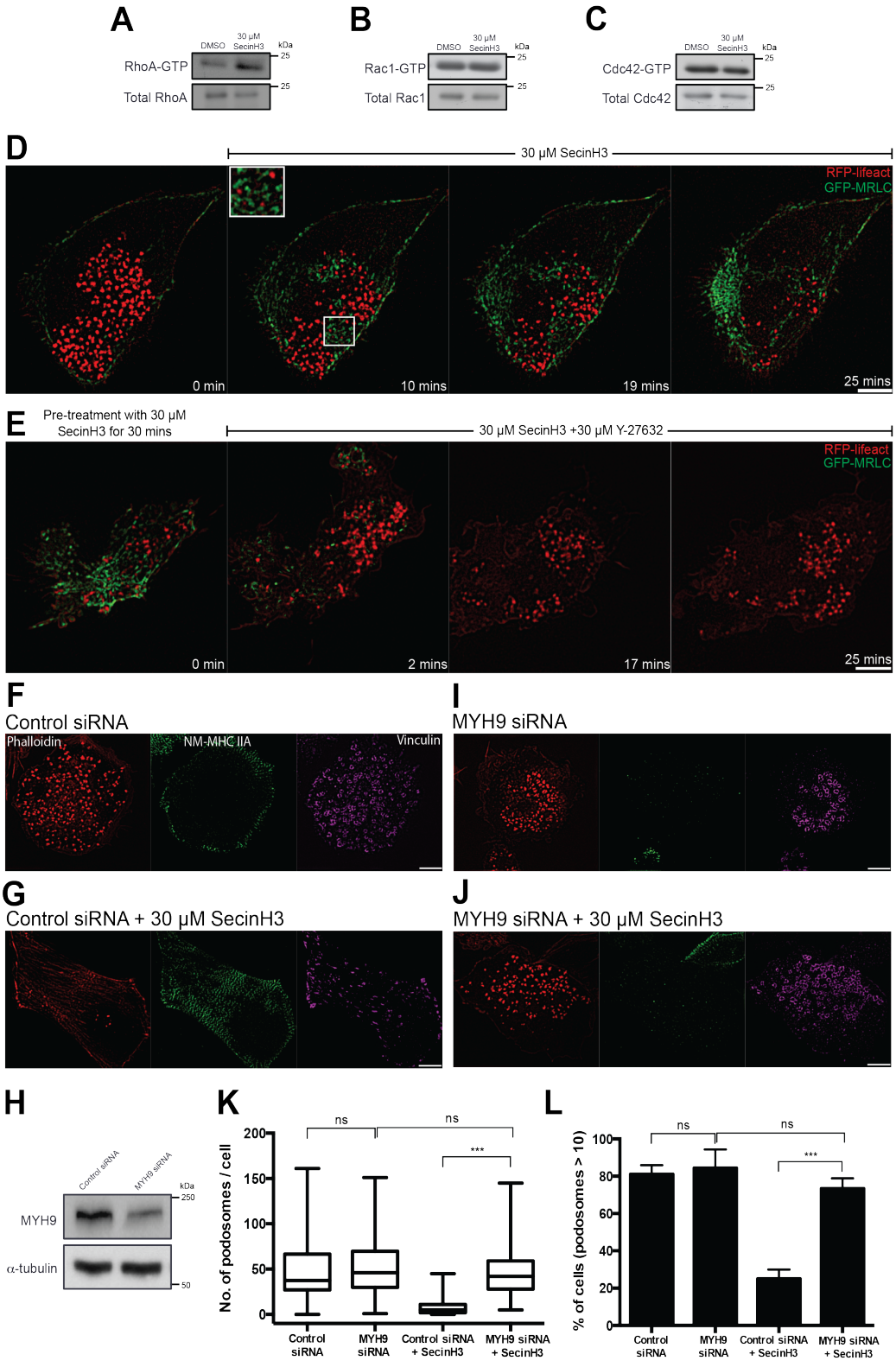

Chapter 2 – Figure 6: Inhibition of ARF1 activity induces RhoA activation.

(A-C) 1 hour incubation of TGFβ1-stimulated THP1 cells with 30 μM SecinH3 led to increase in RhoA-GTP (A) but not Rac1-GTP (B) or Cdc42-GTP (C) fractions as indicated by western blots after pull-down assay. (D-J) Structured-illumination microscopy (SIM) visualization of podosome dynamics in TGFβ1-stimulated THP1. (D and E) Live imaging of cell stably transfected with GFP-MRLC to visualize myosin-II filaments and RFP-lifeact to visualize podosome cores. (D) Cell treated with 30 μM SecinH3 show an increase in myosin-IIA filament assembly (green) and disruption of podosomes (red). Enlarged image of white-boxed area (5 x 4.5 μm^2) of D shows co-localization between appearance of myosin-IIA filaments and podosome disruption (See supplementary movie 7). (E) Time course of podosome re-appearance after addition of 30 μM ROCK inhibitor Y-27632 to cell incubated in secinH3 containing medium. Note that podosomes (red) appeared after disassembly of myosin-II filaments (green). (F-J) TGFβ1-stimulated THP1 cells were transfected with either control scrambled siRNA (F and G) or with siRNA to NM-myosin-IIA heavy chain, MYH9 (I and J) and, after 48 hours, treated with either 0.1% DMSO (F and I) or 30 μM SecinH3 (G and J) for 1 hour. (F, G, I, J) After fixation, the cells were stained with phalloidin (left panels) and antibodies to NM-myosin-IIA heavy chain (middle panels) and vinculin (right panels). (H) Western blot showing protein levels of NM-myosin-IIA heavy chain in control cells (transfected with scrambled siRNA) or in NM-myosin-IIA knockdown cells (transfected with MYH9 siRNA); α-tubulin was used as a loading control. (K and L) Effect of secinH3 treatment of control and NM-myosin-IIA knockdown cells on the average number of podosomes per cell (K) and percentage of cells with more than 10 podosomes (L). The data are presented as indicated in the legend to Figure 1. Pooled data of at least two independent experiments are presented for each group.

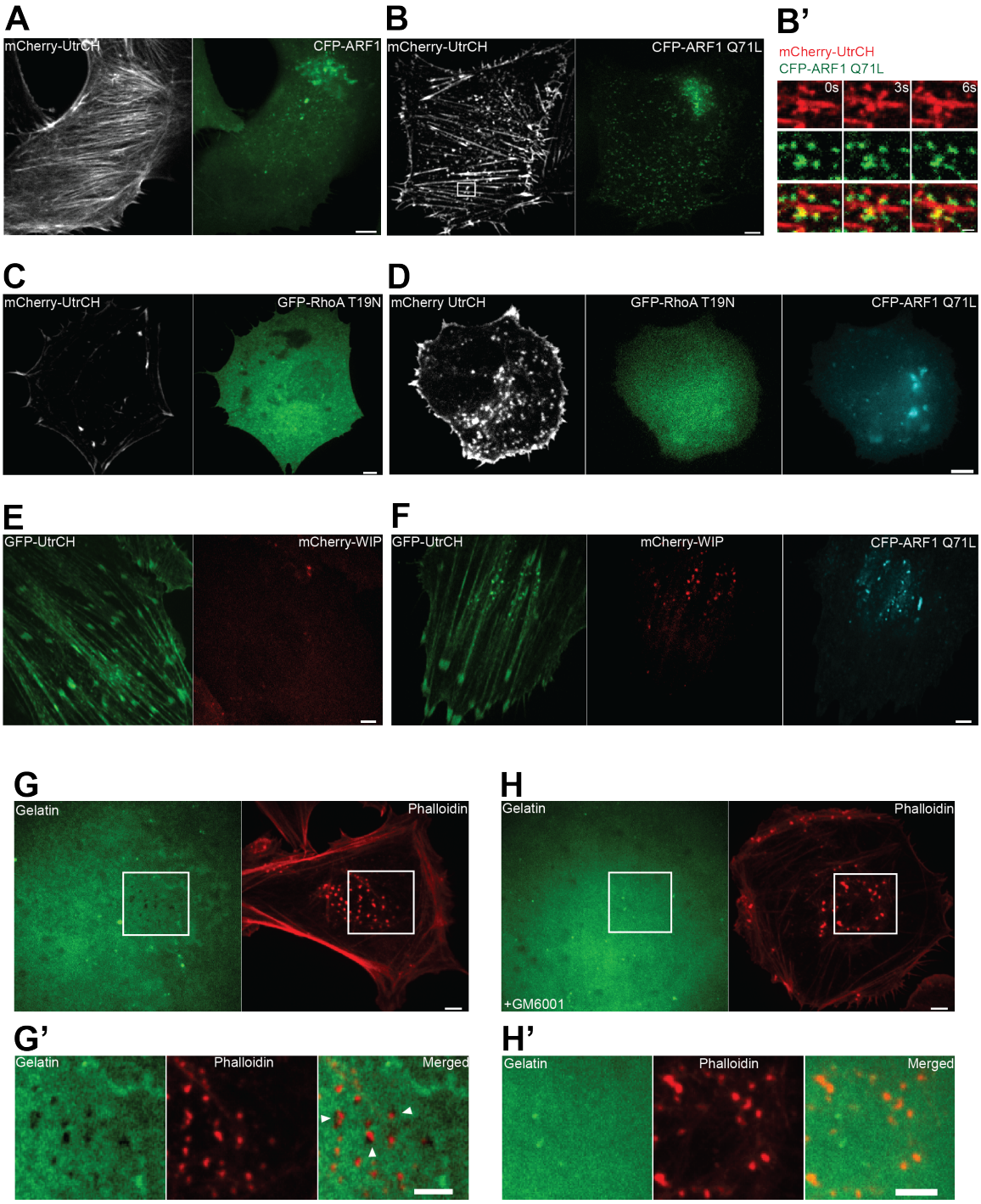

Chapter 2 – Figure 7: Constitutively active ARF1 induces F-actin-rich puncta in mouse fibroblasts.

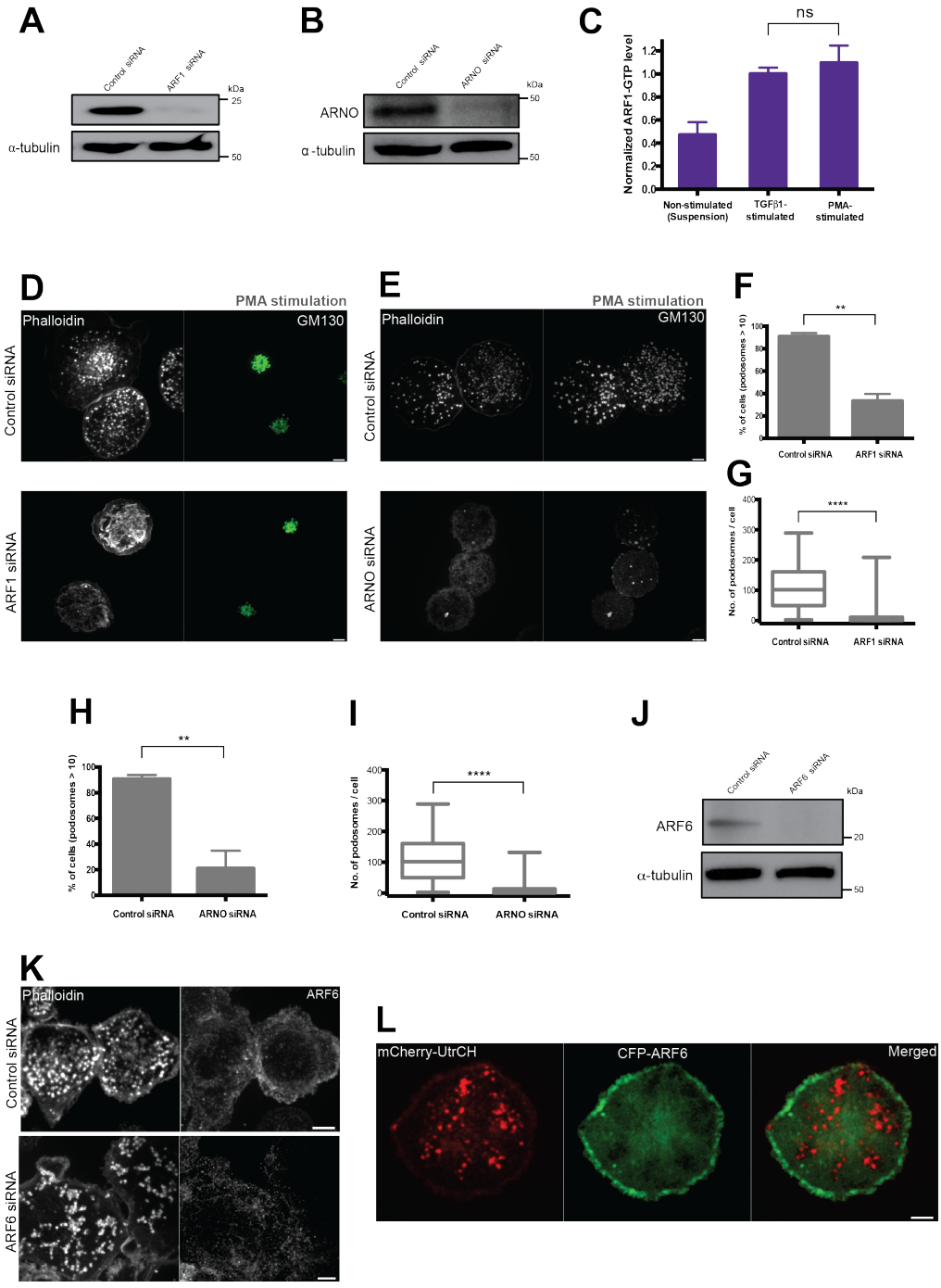

Chapter 2 – Supplementary figure 1: Knockdowns of either ARF1 or ARNO prevent formation of podosomes in THP1 cells stimulated by PMA, while ARF6 is not involved in podosome formation.

(A,B) Western blots showing ARF1 (A) and ARNO (B) levels in cells treated with scramble (control), ARF1- or ARNO-specific siRNAs; α-tubulin was used as a loading control. (C) G-LISA measurement of the fraction of GTP-bound ARF1 in control cells and in cells stimulated by TGFβ1 and PMA. (D,E) Podosomes labeled with phalloidin (D,E, left columns) and vinculin (E, right columns) are abundant in control THP1 cells treated with 50 nM PMA but practically absent from similarly stimulated THP1 cells transfected with ARF1 siRNA (D) or ARNO siRNA (E). The integrity of the Golgi apparatus (labeled with GM130) was not disturbed upon ARF1 knockdown (D, right column). Scale bars, 5 μm. (F,G,H,I) Quantification of the effect of ARF1 (F,G) and ARNO (H,I) knockdowns on percentage of cells with more than 10 podosomes (F, H) and average number of podosomes per cell (G, I). The data were presented and the significances of the difference were assessed as indicated in the legend to Figure 1. Pooled data of two independent experiments are presented for each group. (J) Western blot showing ARF6 levels in cells treated with scramble (control) or ARF6 siRNA; α-tubulin was used as a loading control. (K) Knockdown of ARF6 did not result in any reduction of podosomes in THP1 cells stimulated by TGFβ1. Podosomes are labeled with phalloidin (left column) and endogenous ARF1 is visualized by antibody staining (right column). See quantification of these results in Figure 1E and 1F. (L) ARF6 is not co-localized with podosomes. Podosomes are marked by F-actin labeling with mCherry-UtrCH (left), and ARF6 by expression of CFP-ARF6 (middle). The merged image on the right did not show any co-localization. Scale bars, 5 μm.

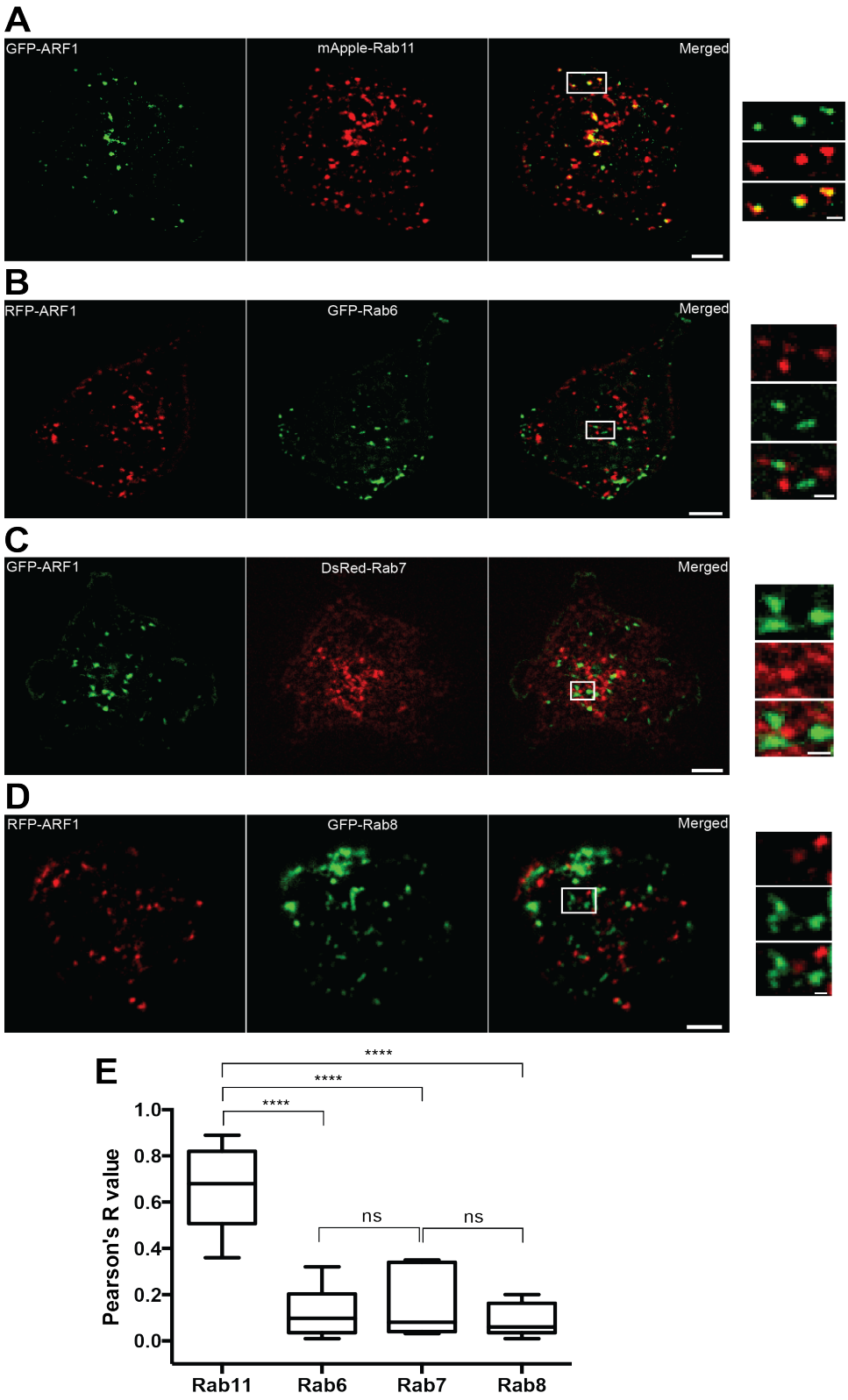

Chapter 2 – Supplementary figure 2: ARF1-containing puncta are positive for Rab11 but not for Rab6, Rab7 or Rab8.

(A,B,C,D) Left column shows images of ARF1 labeled either with GFP (A,C) or RFP(B,D). Central column shows distribution of mApple-Rab11 (A), GFP-Rab6 (B), dsRed Rab7 (C) and GFP-Rab8 (D) in the same cells. Merged images are shown in right column. Scale bars, 5 μm. Boxed areas with heights 4 μm are represented with higher magnification in the insets on the right. Note that ARF1 co-localize only with Rab11 as seen by yellow zones in merged image at the right panel. Scale bars, 1 μm. (E) Graph represents the Pearson's R value of co-localization events between ARF1 and Rab11, Rab6, Rab7 or Rab8. Not less than 8 cells per group were assessed by analyzing the images in four boxed areas (10 x 10 μm2) with Coloc2 plugin software (ImageJ). The significances of the difference were assessed as indicated in the legend to Figure 1.

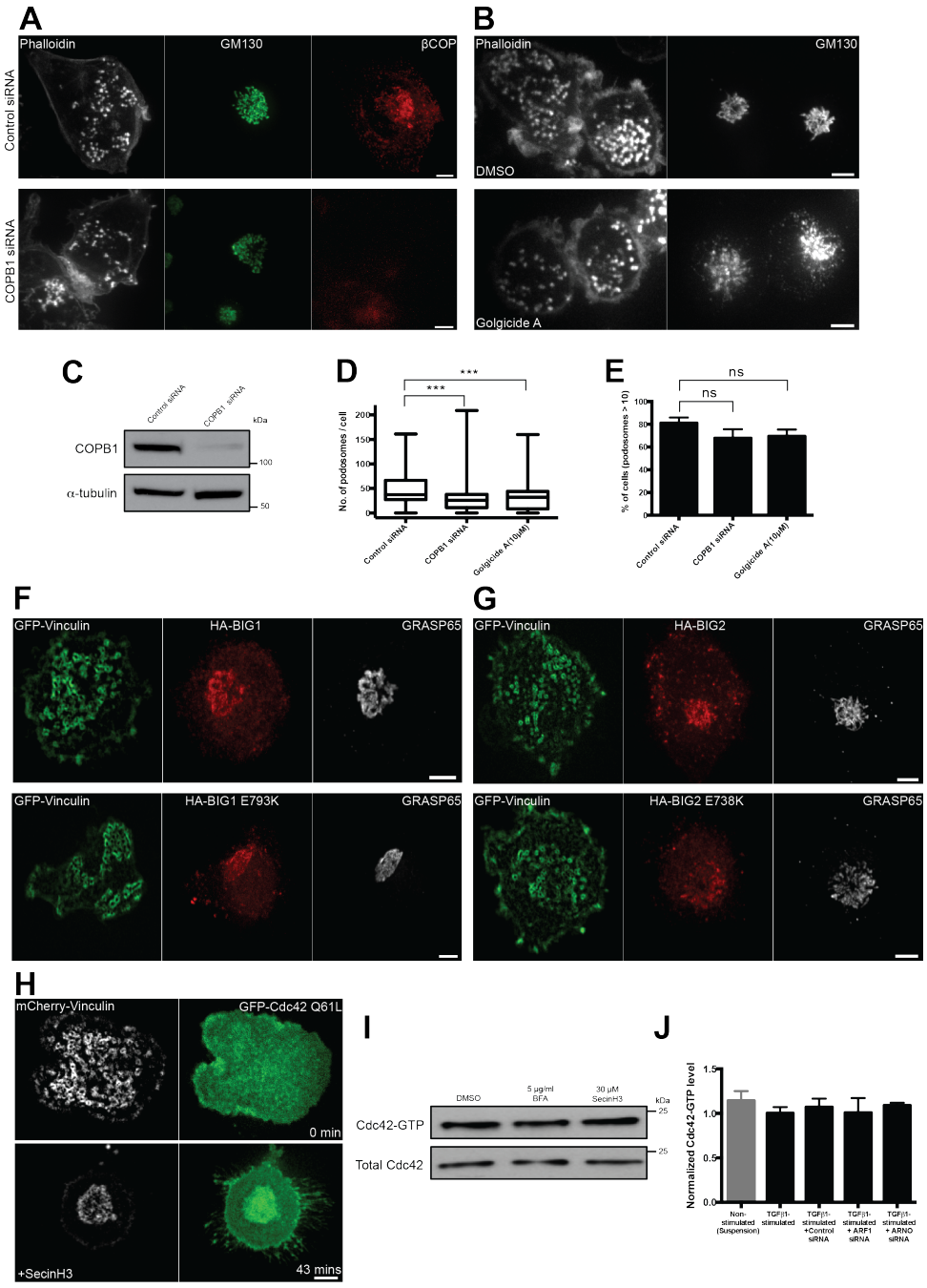

Chapter 2 – Supplementary figure 3: Inhibition of β-COP as well as ARF exchange factors GBF1, BIG1 and BIG2 do not lead to podosome disruption in TGFβ1-stimulated THP1 cells, while ARF1-mediated pathway of podosome formation does not involve Cdc42.

(A) Podosome labeling by phalloidin (left column) in control (upper row) and COPB1 knockdown (lower row) cells. The labeling by GM130 and β-COP antibodies is shown in central and right columns, respectively. (B) Western blot showing β-COP levels in control- and COPB1-siRNA transfected cells; α-tubulin was used as loading control. (C) Podosome marked with phalloidin and Golgi apparatus labeled with GM130 antibody in control cells (upper row) and cells treated with 10 μM Golgicide A for 1 hour. (D) Percentage of cells with more than 10 podosomes and (E) number of podosomes per cell in control cells, COPB1-knockdown cells and Golgicide A-treated cells. The data were presented and the significances of the difference were assessed as indicated in the legend to Figure 1. Pooled data of two to four independent experiments are presented for each group. (F) Podosomes labeled with GFP-vinculin (left column) and Golgi apparatus labeled by GRASP65 (right column) in TGFβ1-stimulated THP1 cells transfected with hemagglutinin (HA)-tagged wild-type exchange factor BIG1 (upper row) and dominant negative mutant of BIG1 (HA-BIG1 E793K). The localization of wild-type (upper panel) and dominant negative (lower panel) BIG1 visualized by anti-HA antibody is presented in the central column. (G) Podosomes labeled with GFP-vinculin (left column) and Golgi apparatus labeled by GRASP65 (right column) in TGFβ1-stimulated THP1 cells transfected with hemagglutinin (HA)-tagged wild-type exchange factor BIG2 (upper row) and dominant negative mutant of BIG2 (HA-BIG2 E738K). The localization of wild-type (upper panel) and dominant negative (lower panel) BIG2 visualized by anti-HA antibody is presented in the central column. Scale bars, 5 μm. (H) Constitutively active Cdc42 (GFP-Cdc42 Q61L) does not prevent disruption of podosomes by SecinH3. Podosomes are labeled with mCherry-vinculin (left column) while the fluorescence of GFP-Cdc42 Q61L is shown in the right column. Control and SecinH3-treated cell is shown in the upper and lower row, respectively. Scale bars, 5 μm. (B,C) ARF1 activity does not alter the GTP-bound fraction of Cdc42. (I) Treatment with BFA (5 μg/ml) or SecinH3 (30 μM) for 1 hour did not reduce the fraction of GTP-bound Cdc42 estimated by pull-down assays using beads coated with the Rac/Cdc42-binding domain of the human PAK1. Typical result of one of four

independent experiments is shown. (J) G-LISA assay showing the normalized level of Cdc42-GTP in cell lysate taken from non-stimulated THP1 cells and TGFβ1-stimulated non-transfected THP1 cells, cells transfected with siRNAs to ARF1, siRNA to ARNO, and a mixture of scrambled siRNAs (control). All data are normalized to the level of Cdc42-GTP in TGFβ1-stimulated non-transfected THP1 cells. Graph represents mean ± SD of two independent experiments. Note that neither stimulation with TGFβ1 nor knockdowns of ARF1 and ARNO affects the level of Cdc42-GTP.

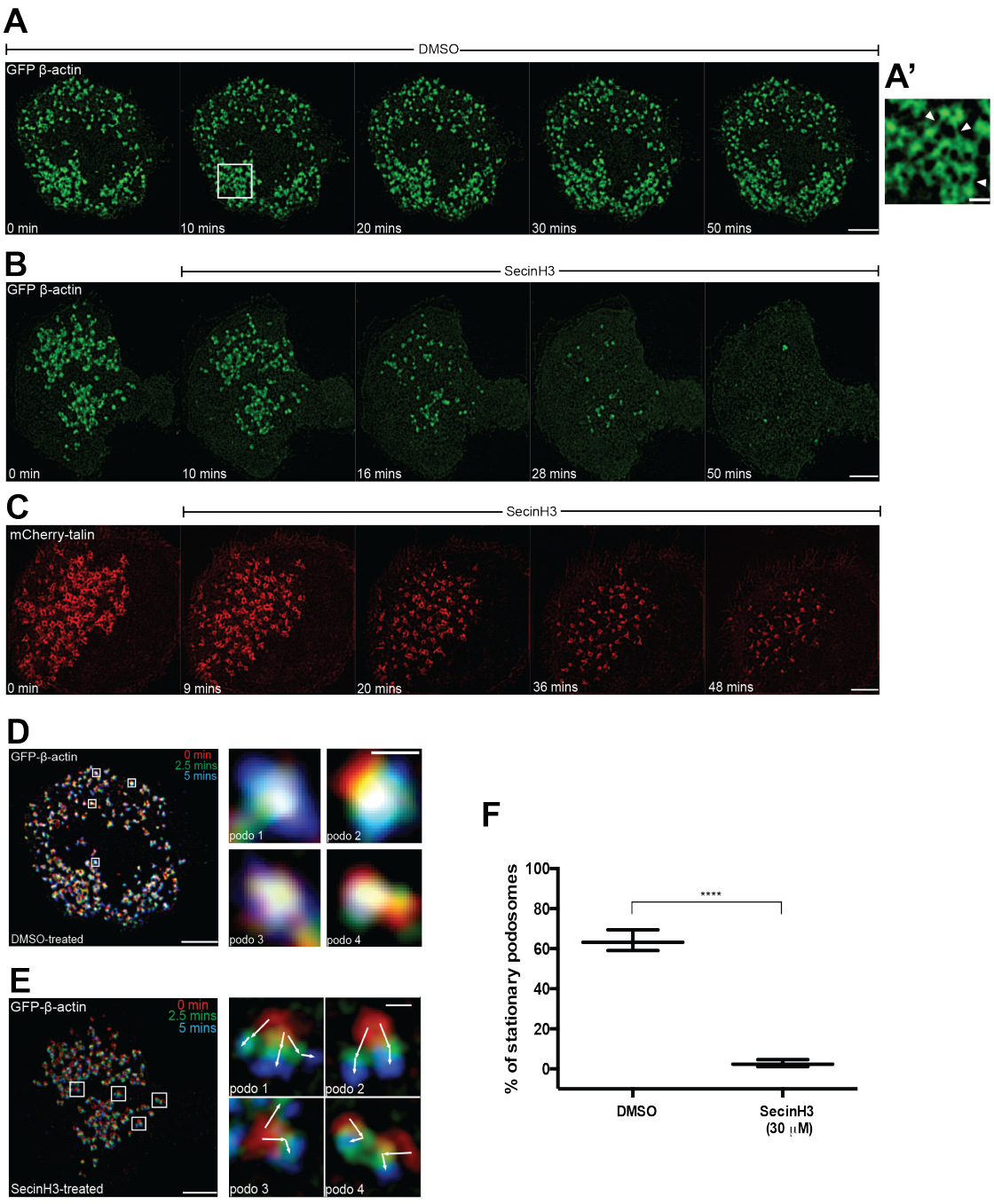

Chapter 2 – Supplementary figure 4: Structured-illumination microscopy (SIM) visualization of podosome dynamics in TGFβ1-stimulated THP1 cells stably transfected with GFP-β-actin and mCherry-talin.

(A) A sequence showing podosomes labeled with GFP-β-actin in TGFβ1-stimulated THP1 cell in the medium with 0.1% of DMSO. (B) A sequence showing disruption of podosomes labeled with GFP-β-actin upon treatment with 30 μM SecinH3. (C) Disruption of podosomes by SecinH3 as visualized by labeling podosomes with mCherry-talin. (D and E) Ratio imaging analysis of podosome displacement in TGFβ1-stimulated THP1 cell. The images of four boxed podosomes were taken from the first 5 minutes of the Supplementary movie 4 and 5 (See also A and B respectively). Three successive frames were computer software-colored and superimposed (insets). (E) Superimposed images of three successive frames in four selected podosomes demonstrated podosomes movements upon addition of secinH3 (white arrows in insets on the right). Scale bars 5 μm in main image and 0.5 μm in insets. (F) Percentage of stationary podosomes in the first 5 minutes after addition of control solvent (0.1% DMSO) or 30 μM SecinH3. Four cells in each group were assessed. The significances of the difference were assessed as indicated in the legend to Figure 1.

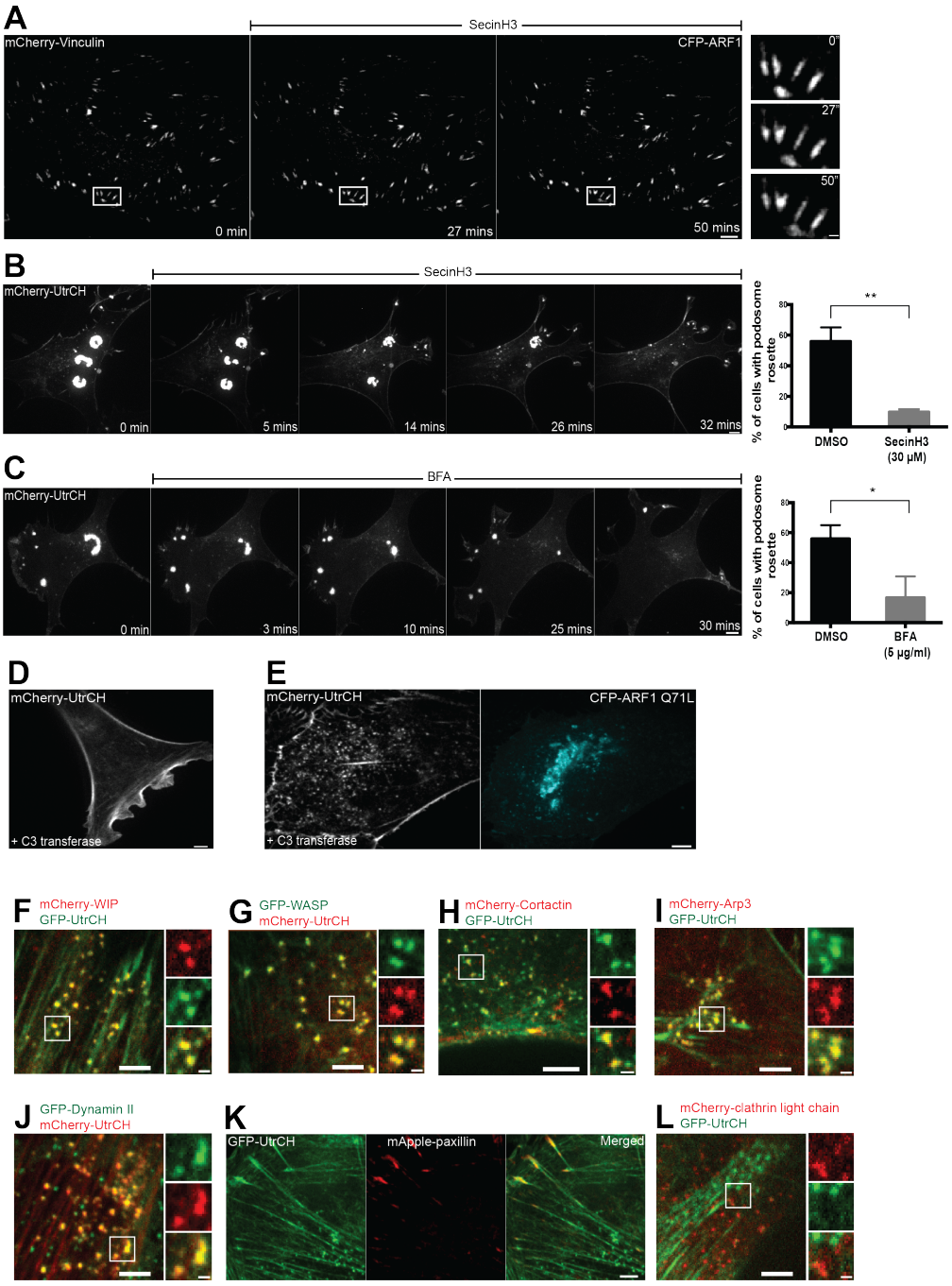

Chapter 2 – Supplementary figure 5: Drugs reducing the level of GTP-ARF1 led to disruption of podosome rosettes induced by constitutively active Src in fibroblast, but did not disrupt focal adhesions. In addition, this figure shows formation of actin-rich puncta upon fibroblast transfection with constitutively active ARF1 and co-localization of podosome core proteins to these puncta.

(A) The treatment of mouse fibroblasts labeled with mCherry-vinculin by SecinH3 did not produce any apparent changes in focal adhesions. Scale bar, 5 μm. Enlarged images of boxed area (8 x 6 μm2) are shown on the right. Scale bar, 1 μm. (B,C) time course of podosome rosettes disruption in mouse fibroblast expressing Src Y527F together with mCherry-UtrCH upon addition of 30 μM of SecinH3 (B) or 5 μg/ml of BFA (C). Graphs showing the decrease in percentage of cells with at least one rosette after 1 hour of incubation with inhibitor are shown on the right. The data were presented and the significances of the difference were assessed as indicated in the legend to Figure 1. Pooled data of three independent experiments are presented for each group. (D) Treatment of mouse embryonic fibroblast (transfected with mCherry-UtrCH) with the Rho inhibitor C3 transferase led to stress fibre disruption. (E) Fibroblast co-transfected with mCherry-UtrCH (left panel) and constitutively active ARF1 (CFP-ARF1 Q71L, right panel) form numerous F-actin-rich puncta. Scale bars, 5 μm. (F-J) Several podosome core markers but not (K) paxilllin and (L) clathrin co-localize with actin in the CFP-ARF1 Q71L-induced F-actin-rich puncta. Cells were triple transfected with CFP-ARF1 Q71L and utrophin (GFP-UtrCH or mCherry-UtrCH) together with protein of interest (GFP-WASP, mCherry-cortactin, mCherry-Arp3, GFP-Dynamin II, mCherry-clathrin light chain). For each montage in figures F-J and L, the larger left photograph represent merged images, while the three small photographs on the right correspond to views of individual transfected proteins (top), utrophin (middle) and merged images (bottom) of the enlarged boxed areas (4 x 4 μm2) of the respective large images. Yellow color of merged image indicates to co-localization between utrophin and protein of interest. Scale bars, 5μm (large images) and 1 μm (boxed images). For cells co-transfected with mApple-paxillin and GFP-UtrCH in montage K, left panel shows utrophin localization, middle panel- paxillin localization to focal adhesions in the same cell, and right panel- the merged image. Scale bar, 5 μm. Note that paxillin does not co-localize with the actin-rich puncta in the central part of the cell.

2.5 - Discussion

In this paper we demonstrate that an ARNO-ARF1 signalling axis is required for the maintenance of podosome integrity (See Figure 8 for flow diagram). First, knockdown of ARF1 but not ARF6 prevents podosome formation by TGFβ1- or PMA-treated THP1 cells. In addition to these "classic" podosomes, we explored podosome-like structures induced in fibroblasts by either expression of constitutively active Src (Tarone et al. 1985) or by plating cells on a fluid substratum (Yu et al. 2013). We checked that specific drugs inhibiting ARF1-activating GEFs, BFA (Yamaji et al. 2000, Niu et al. 2005) and secinH3 (Hafner et al. 2006), led to rapid dissolution of podosomes in THP1 cells and the podosome-like structures in fibroblasts. In addition, we have shown that in both THP1 cells and fibroblasts, treatments inducing podosome formation augmented the fraction of active, GTP-bound ARF1.

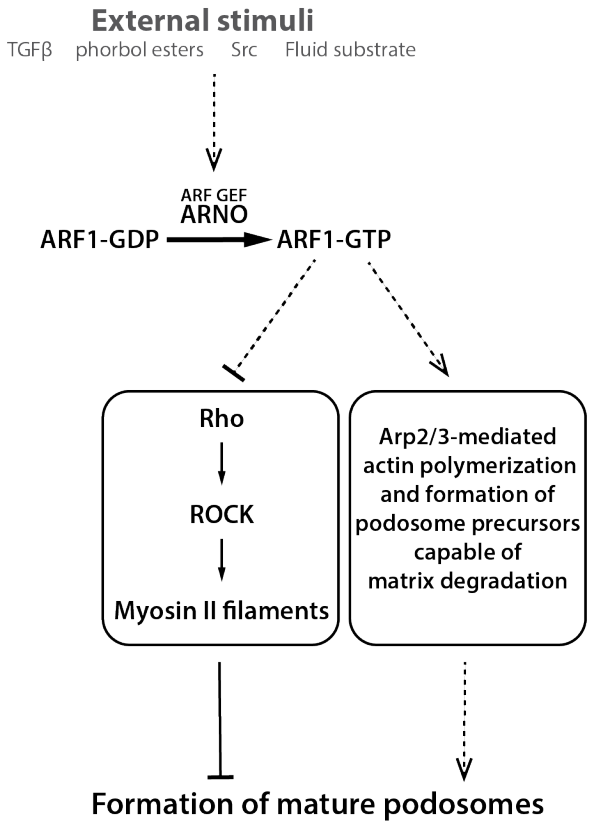

Chapter 2 – Figure 8: A flow diagram illustrating the role of ARNO-ARF1 signaling axis in the podosome formation.

A variety of external factors known to switch cells towards podosome formation activate the ARF GEF ARNO. The ARNO activates ARF1, which in turn induce two major pathways regulating the podosomes. First, ARF1 inhibits Rho, which negatively regulate podosomes via ROCK-dependent formation of myosin-II filaments. Second, ARF1 promotes formation of Arp2/3- and actin-enriched podosome core-like structures associated with matrix degradation sites. The solid arrows represent the direct pathways while the dashed arrows indicate to the existence of unknown intermediate steps in the depicted pathways.

BFA and secinH3 inhibit different classes of ARF1-activating GEFs (Donaldson and Jackson 2011). In our experiments, the BFA-sensitive GEFs (GBF1, BIG1, BIG2) appeared to be functionally unrelated to podosome regulation. The inhibitory effect of BFA could thus be explained by sequestration of ARF1 within the BFA-induced ternary complexes consisting of inhibited GEFs, ARF1-GDP and BFA (Peyroche et al. 1999, Mossessova, Corpina and Goldberg 2003, Zeghouf et al. 2005). At the same time, we found that one of the secinH3-sensitive GEFs, ARNO (cytohesin-2) but not cytohesin-1, is indispensable for podosome integrity in THP1 cells. Possible functions of several other ubiquitous ARF family proteins (ARF3, ARF4, ARF5) as well as other secinH3-sensitive GEFs, cytohesin-3 and -4, remained to be studied in the context of podosome formation.

Localization studies revealed that ARNO (but not cytohesin-1) is stably co-localized with adhesion proteins in the ring domain of podosomes in THP1 cells as well as with podosome-like structures in fibroblasts. This is consistent with biochemical data showing direct association of ARNO with paxillin (Torii et al. 2010). Furthermore, live cell imaging showed transient contacts of vesicles containing ARF1 with the periphery and ring domain of podosomes and podosome-like structures in THP1 cells. We demonstrated that ARF1-containing vesicles are moving along microtubules; so one of the functions of microtubules important for

the podosome maintenance (Linder et al. 2000b) could be delivery of ARF1. It is worth noting that a negative regulator of ARF1 activity, ARF1 GTPase-activating protein ASAP1, was also shown to localize to podosomes (Shiba and Randazzo 2011, Curtis et al. 2015).

How could active ARF1 affect podosome assembly and stability? The first possibility is based on well-documented functions of ARF1 in the Golgi complex and vesicular traffic (Donaldson et al. 2005). It can be conjectured that some of the ARF1-dependent functions of the Golgi are required for podosome integrity. This possibility cannot be entirely excluded; however, it is worth noting that in our experiments integrity of podosomes can be dissected from the integrity of the Golgi. In particular, inhibition of the ARF1 exchange factor GBF1, responsible for ARF1-dependent COPI recruitment to the Golgi, as well as knockdown of the COPI subunit, βCOP, only marginally affected podosome integrity. ARF1 in principle could be involved in integrin turnover and affect podosome formation via regulation of available integrin adhesion receptors. However, in our experiment, experimental manipulations with ARF1 did not affect the integrity or dynamics of another class of integrin-dependent adhesions, focal adhesions. This suggests that other mechanisms should be considered to explain the specific effect of ARF1 depletion/inhibition on podosome integrity.

Podosomes are part of the actin cytoskeleton and as such likely to be regulated by small G proteins of Rho family. We have shown that inhibition of ARF1 triggered significant activation of RhoA but not Rac or Cdc42. Activation of RhoA in turn triggers the assembly of numerous myosin-IIA filaments, which as we have demonstrated led to considerable disruption of podosomes. We have shown that suppression of myosin-IIA filament formation by either inhibition of ROCK or knockdown of myosin-IIA, prevented the disruptive effect of ARF1 inhibition on podosome formation. Thus, our experiments suggest that ARF1 functions in podosome formation as an inhibitor of RhoA activity and subsequent myosin-IIA

filament formation. This conclusion is consistent with our observation that ARF1-dependent activation of podosome formation by plating of cells on fluid bilayer led to inhibition of RhoA (Yu et al. 2013).

Interestingly, apparently the same mechanism based on suppression of Rho and myosin-II by the cytohesin family exchange factor, Steppke, and a Drosophila ARF was found in a completely different system, during cellularization of Drosophila embryos (Lee and Harris 2013). However, the pathway connecting ARF1 and RhoA remains unknown. It is perhaps worth noting that ARF1 can bind the RhoGAP ARHGAP10/21 and deliver it to the Golgi or plasma membrane (Dubois et al. 2005, Menetrey et al. 2007, Kumari and Mayor 2008). ARHGAP10/21 is known to inhibit Cdc42 but also shows some RhoA inhibitory activity *in vitro* (Dubois et al. 2005).

It is also not clear why an excess of myosin-II filaments antagonizes podosome integrity. Myosin-II has been shown to localize to actin links radiating from the podosomes (Dries et al. 2013) but its functional role in podosomes is yet to be established.

In addition to its function as a myosin-II regulator, ARF1 could affect podosomes via regulation of actin polymerization. There are several lines of evidence suggesting involvement of ARF1 in the regulation of Arp2/3 complex-driven actin polymerization: via recruitment of actin nucleation promoting WAVE complex (Humphreys et al. 2012a, Humphreys et al. 2012b), via sequestration and inactivation of Arp2/3 inhibitor, PICK1 (Rocca et al. 2013) and via activation of Cdc42 (Dubois et al. 2005, Heuvingh et al. 2007). We were not able to find evidence of any of these mechanisms in the context of podosome regulation. Neither data from the literature nor our own observations indicate that WAVE or PICK1 are localized to podosomes. Moreover, ARF1 inhibition did not induce any changes in GTP-bound Cdc42 level, and constitutively active Cdc42 did not prevent or overcome the disruption of podosomes seen upon ARF1 inhibition.

Nevertheless, the effect of ARF1 on the polymerization of actin in the context of podosome formation is seen in our experiments with expression of constitutively active ARF1 in fibroblast-type cells, which normally do not produce podosomes. Active ARF1 not only suppresses stress fibre formation but also induces formation of numerous actin and Arp3-containing patches in such cells. The induction of actin polymerization at the plasma membrane by active ARF1 and ARF6 was previously demonstrated (Caviston et al. 2014). Many actin-associated proteins typical of podosomes (N-WASP, WIP, cortactin, dynamin-II) were also found in these puncta. Moreover, a hallmark of podosome function, the local gelatin matrix degradation by MMPs appeared to be associated with these puncta. At the same time, the puncta were not surrounded by any podosome adhesive ring components. The recruitment of certain adhesion components such as paxillin was shown to require dynamic GTP/GDP turnover of ARF1(Liu et al. 2002, Liu et al. 2005). This may explain the lack of adhesive ring surrounding podosome core-like structures induced by constitutively active ARF1. Of note, our data show that matrix degrading and adhesion functions could be dissected under conditions of induction of podosome precursors by constitutively active ARF1.

The pathways downstream of ARF1 underlying formation of these podosome precursors are not the same as Rho and myosin-II inhibitory activity of ARNO-ARF1 characterized above, since expression of dominant negative RhoA did not by itself induce formation of the actin-rich puncta in fibroblasts. We cannot exclude that local changes in Cdc42 activity may still play a role in this process (Heuvingh et al. 2007) even though ARF1 did not affect the total level of Cdc42 activity in our experiments.

In summary, we demonstrate that the signalling axis ARNO-ARF1 plays a critical role in the control of podosome integrity and find that this pathway in macrophage-like cells operates via inhibition of RhoA and myosin-II activity. Other pathway(s) found in fibroblasts downstream of active ARF1 induce formation of F-actin-rich

puncta resembling podosome actin cores that are not associated with the matrix adhesion components but involved in matrix degradation. These findings open new features of the processes of podosome formation and matrix degradation. Investigation of ARNO-ARF1 upstream and downstream pathways provides a rich source of future studies.

Chapter 3 - Microtubule-associated GEF-H1 and myosin-IIA filament assembly suppress podosome formation (manuscript in preparation)

3.1 - Abstract

Disruption of microtubules has been reported to trigger podosome disassembly in macrophages (Linder et al. 2000a), but the mechanism is still unclear. Using structured illumination microscopy, I observed that the nocodazole-induced loss of podosomes in macrophage-like THP1 cells was accompanied by an outburst of myosin II filament assembly. The myosin II bipolar filaments were found to surround podosomes and also localized to the central actin core. Prolonged treatment with nocodazole induced assembly of sarcomeric-like actomyosin structures and larger focal adhesions typically observed in fibroblast-type cells. Furthermore, nocodazole treatment led to significant increase in RhoA-GTP levels in these cells and stimulation of RhoA activity mimicked both the podosome-disrupting and myosin II-filament promoting effects of nocodazole. The nocodazole-induced disassembly of podosomes can be prevented by concomitant inhibition of Rho-associated kinase (ROCK) activity by Y-27632 and were not observed in microtubule-associated guanine nucleotide exchange factor GEF-H1-depleted cells, and in both cases there was no outburst of myosin-II filament assembly. Moreover, even after total disruption of podosomes by nocodazole treatment, podosome formation could be subsequently induced by inhibition of myosin II through use of the ROCK inhibitor. Altogether, these data suggest that disassembly of podosomes after microtubule disruption is due to stimulation of a RhoA/ROCK/Myosin II pathway through the release of GEF-H1 from microtubules, highlighting a switch mechanism controlled by an actomyosin-dependent force generation in two types of integrin-mediated adhesions, namely focal adhesions and podosomes.

3.2 - Introduction

Crosstalk between actin and microtubules regulate physiological processes such as cell division and directed cell migration. Rho GTPases are critical mediators that govern the crosstalk mechanisms between these cytoskeletal networks (Geiger et al. 2001, Even-Ram et al. 2007, Akhshi, Wernike and Piekny 2014). In particular, RhoA activates specific actin nucleators (e.g. formins) and kinases (e.g. Rho-associated kinase) to promote actin polymerization and myosin-dependent contractility, which in turn favors stress fiber formation and focal adhesion maturation (Riveline et al. 2001, Bershadsky et al. 2006, Geiger et al. 2009). However, actin dynamics and myosin II contractility mediated by RhoA must be spatiotemporally controlled to promote processes such as directional migration (Ridley 2001, Bershadsky et al. 2003, Nalbant et al. 2009). Guanine nucleotide exchange factors (GEFs) can activate RhoA through GTP binding, while the GTPase activating proteins (GAPs) promote hydrolysis of GTP-bound RhoA to inactive GDP-bound RhoA, thereby providing a platform for spatiotemporal modulation of RhoA-mediated downstream regulation (Ridley 2001, Geiger et al. 2009).

An example of a cytoskeletal crosstalk concerning RhoA activity is mediated by GEF-H1, also known as ARHGEF2 (Ren et al. 1998). GEF-H1 is a microtubule-associated Rho GEF that becomes activated upon release from the microtubule. Overexpression of GEF-H1 that is deficient in microtubule binding has the most drastic effect in terms of stress fiber formation and actin re-organization (Krendel et al. 2002, Birkenfeld et al. 2008). Treatment of cells with the microtubule de-polymerizing drug, nocodazole, has been shown to induce large focal adhesions and increased stress fiber formation (Bershadsky et al. 1996, Liu, Chrzanowska-Wodnicka and Burridge 1998, Chang et al. 2008). However, the nocodazole-induced increase in cell contractility and focal adhesion size was inhibited in GEF-H1-depleted and ROCK-inhibited cells (Chang et al. 2008) suggesting that disruption of microtubule leads to

release of GEF-H1 that induces a RhoA/ROCK/myosin II -dependent pathway, which in turn enhances cell contractility and focal adhesion maturation.
On the other hand, microtubule disassembly induced by nocodazole disrupts podosome formation in macrophages (Linder et al. 2000). A number of kinesins such as KIF1C (Kopp et al. 2006, Efimova et al. 2014), KIF5B and KIF3A/KIF3B (Wiesner et al. 2010) have been identified as molecular motors that regulate podosome formation, some of which are implicated in the delivery of MT1-MMP for extracellular matrix degradation (Wiesner et al. 2013).

While it is still unclear how microtubules regulate podosome formation, overexpression of GEF-H1 inhibits podosome rosette formation in Src-transformed fibroblasts (Shiba and Randazzo 2011). In addition, RhoA activity has been reportedly low in fibroblast-type cells that assemble podosomes (Pan et al. 2011, Yu et al. 2013). For example, we previously showed that fibroblasts that typically form focal adhesions on glass substrate, switch to form podosome-type adhesions on fluid substrate lacking traction force, with RhoA activity that is much reduced when compared to cells plated on glass surfaces (Yu et al. 2013). In another study, suppression of RhoA activity by the focal adhesion kinase (FAK) was found to be required for podosome rosette assembly (Pan et al. 2011). However, the potential control of podosome formation by a microtubule-dependent RhoA regulation has not been systematically explored.

Here, I propose that the nocodazole-induced disassembly of podosomes in macrophage-like THP1 cells is due to an increase in RhoA activity. Depletion of GEF-H1 and inhibition of ROCK prevented the disassembly of podosomes by microtubule disruption induced by nocodazole in macrophage-like THP1 cells. Using structured illumination microscopy, I found that an increase in RhoA activity induced a global outburst of non-muscle myosin IIA filament assembly and a concomitant loss of podosomes. Treatment of cells with the ROCK inhibitor Y-27632 promoted the disassembly of myosin IIA filaments and immediately stimulated formation of new

podosomes. Furthermore, increase in myosin II activity promoted the formation of larger focal adhesions and prolonged treatment with nocodazole induced formation of sarcomere-like actomyosin structures typically observed in fibroblast-type cells. Our data provides a mechanism for the nocodazole-induced disassembly of podosomes and propose a switch mechanism between podosome and focal adhesion through a ROCK-mediated control of myosin IIA filament assembly.

3.3 - Results

Stimulation of THP1 cells with TGFβ1 induced assembly of podosomes in 85% of cells plated on fibronectin-coated surfaces (see "Results" section of Chapter 2). As mentioned in the previous chapter, we consider a cell as "podosome-forming" if it had more than 10 morphologically identifiable podosomes. In addition, all fixed and live images were captured using structured illumination microscopy (SIM).

3.3.1 - Microtubule disassembly disrupts podosomes and increases RhoA activity

To investigate the role of microtubule in podosome formation, TGFβ1-stimulated THP1 cells plated on fibronectin-coated substrate were treated with nocodazole, a small-molecule inhibitor that binds to tubulin and promotes the depolymerization of microtubule (Hoebeke, Van Nijen and De Brabander 1976). Nocodazole (1 μM) induced gradual disassembly of both podosomes and the F-actin links connecting adjacent podosomes (Figure 1A and B), accompanied by apparent contraction of cell. The percentage of podosome-forming cells can be completely rescued within 2 hours after washout of the drug with complete medium (Figure 1C). Nocodazole-induced microtubule disassembly has been previously associated with cell contractility and increase in active RhoA levels in fibroblasts (Bershadsky et al. 1996, Liu et al. 1998) and HeLa cells (Chang et al. 2008) that typically form focal adhesions and stress fibers. While it is not known if podosome-forming cells behave similarly, RhoA-GTP levels were measure using the GST-tagged rho-binding domain (RBD) of Rhotekin-coated beads in a pull-down assay. The active RhoA levels were significantly (4-fold) higher in nocodazole-treated cells than DMSO-treated control cells (n=4 experiments), indicating that disruption of microtubules led to global increase in RhoA activity, consistent with previous findings (Figure 1D).

3.3.2 - Microtubule disruption leads to an outburst of myosin II filament assembly

To study the nocodazole-induced activation of RhoA activity in podosome-forming cells, the GFP-tagged myosin regulatory light chain of non-muscle myosin IIA (MRLC-GFP) was used to visualize myosin IIA filament assembly, a major downstream consequences of RhoA activation (Bershadsky et al. 2006). The MRLC-GFP and RFP-lifeact constructs were lentivirally transduced to make stable THP1 cells that labeled the N-terminal region of non-muscle myosin IIA and F-actin, respectively. Since myosin IIA assembles into bipolar filaments, the MRLC would appear as "doublets" with a separating distance of 300 nm between the two dots on SIM (Burnette et al. 2014). In TGFβ1-treated THP1 cell, these MRLC "doublets" (Figure 2A, white-boxed inset) were primarily localized to the cortical F-actin network, with little or no localization of MRLC-GFP at regions of podosome assembly (Figure 2A). Furthermore, the normalized average intensity of MRLC-GFP remained relatively constant throughout the hour of image acquisition after bleach correction (Figure 2A, graph). However when RhoA activity was stimulated by 1 μg/ml of CN03, a small peptide that blocks the GAP-mediated GTPase activity of RhoA thereby rendering RhoA to be constitutively active, podosomes were immediately disrupted and there was a concomitant 26-fold increase in MRLC-GFP fluorescence intensity when compared to before addition of CNO3 in TGFβ1-treated THP1 cells (Figure 2B). Surprisingly, addition of nocodazole mimicked the effect observed with RhoA activation by CN03, with an approximately 27-fold increase in MRLC-GFP intensity (Figure 2C). This suggests that disruption of microtubules stimulates a global activation of RhoA leading to an outburst of myosin II filament assembly.

While myosin IIA is scarcely localized to podosomes in control TGFβ1-treated cells (Figure 2A), addition of nocodazole resulted in the assembly of numerous MRLC "doublets" accompanied by attendant loss of podosomes (Figure 2D). These MRLC

"doublets" co-localize or surround the actin core of podosomes as shown in Figure 2E (indicated by white arrows) until the podosomes underwent dissolution. Furthermore, treatment of TGFβ1-stimulated THP1 cells with nocodazole for 1 hour resulted in the appearance of sarcomere-like organization of the actomyosin network usually observed in fibroblast-type cells in about 14.5 ± 2.1% (mean ± SD) of the total cell population (Figure 2G). The percentage of such cells (47.5% ± 2.2%) was further enhanced upon addition of nocodazole for 2 hours (Figure 2F and 2G).

3.3.3 - ROCK inhibition rescues podosome formation in cells lacking microtubules

To investigate the role of myosin IIA filament assembly in the disassembly of podosomes upon disruption of microtubules by nocodazole, Rho-associated kinase (ROCK) activity was inhibited. ROCK activates myosin IIA filament assembly through direct phosphorylation of its regulatory light chain and indirectly by phosphorylating the myosin light chain phosphatase, thereby increasing the pool of phosphorylated and active myosin IIA molecules (Vicente-Manzanares et al. 2009). TGFβ1-stimulated THP1 cells were treated with Y-27632 at doses ranging from 20 to 150 μM and there was close to no detectable fluorescence intensity of MRLC-GFP (cytoplasmic signal of unbound MRLC-GFP proteins are removed after SIM image reconstruction) even at the lowest dose that was used (i.e. 20 μM) in this study. However, podosome formation appeared unaffected even at very high doses (120μM) of Y-27632 (Figure 3B) when compared with DMSO-treated cells (Figure 3A). Intriguingly, when cells were co-treated with both 1 μM nocodazole and 120 μM Y-27632 (Figure 3C), the fluorescence intensity of MRLC-GFP (i.e. bound myosin IIA filaments) was still high at 30 μM Y-27632 in nocodazole-treated cells, and was only completely abolished (i.e. no myosin IIA filaments) at 120μM in 80% of the cells. At this dose, the nocodazole-treated cells with no bound myosin IIA (lack of MRLC-GFP fluorescence) formed podosomes and were strikingly unaffected by

nocodazole-induced microtubule disassembly (Figure 3C). Furthermore, both the percentage and number of podosome-forming cells were similar to control cells when ROCK was inhibited by 120 μM Y-27632 in nocodazole-treated cells (Figure 3D and 3E). In fact, pre-treatment of cells with 120 μM Y-27632 inhibited the outburst of MRLC-GFP bipolar filament assembly when nocodazole was added to these cells (Figure 3F). Conversely, addition of 120 μM Y-27632 in cells pre-treated with nocodazole induces disassembly of myosin II filaments (dissolution of MRLC-GFP signal) and resurrection of new podosomes in these cells despite the lack of an intact microtubule network (Figure 3G). The data collectively suggest that RhoA activates ROCK to induce the assembly of myosin IIA filaments, which in turn disrupts podosome formation in macrophage-like THP1 cells.

3.3.4 - GEF-H1 depletion prevents nocodazole-induced disassembly of podosomes

GEF-H1 is a RhoA-specific guanine nucleotide exchange factor that is connected to microtubules in its inactive state, but becomes active upon its release from microtubules (Krendel et al 2002). To test whether GEF-H1 is involved in the nocodazole-induced increase in RhoA activity, GEF-H1 was depleted in TGFβ1-treated THP1 cells by siRNA. Immediately prior to plating, cells were electroporated with the control or GEF-H1 siRNA constructs and then seeded onto fibronectin in the presence of TGFβ1. Maximum silencing (>80%) was achieved by 48 hours after transfection (Figure 4A). Depletion of GEF-H1 did not affect podosome formation and microtubule assembly in TGFβ1-treated THP1 cells as indicated by the actin, vinculin and myosin II heavy chain staining (Figure 4B). In addition, microtubules labeled by α-tubulin were concurrently visualized in these cells (Figure 4E) since cells deficient in myosin IIA can stabilize microtubules (Even-Ram et al. 2007) and knocking down GEF-H1 can potentially affect its downstream myosin II activity. Strikingly, when these cells were treated with 1 μM nocodazole, podosome

formation was unaffected even with complete disruption of microtubules, unlike cells transfected with control siRNA in similar conditions (Figure 4B and 4E). The percentage of GEF-H1-depleted cells forming more than 10 podosomes in the presence of nocodazole were similar to control siRNA-transfected cells, however, the number podosomes were significantly lower. This might be due to incomplete knockdown of GEF-H1 in each cell or presence of other microtubule-associated RhoA-specific GEFs (e.g. p190 RhoGEF), which can be released upon microtubule disruption (Birkenfeld et al. 2008). More intriguingly, cells treated with nocodazole exhibit a significantly larger size of focal adhesion marked by vinculin (see insets) which was not the seen in GEF-H1 depleted cells treated with 1 μM nocodazole (Figure 4B and 4D). This indicates that increase in myosin IIA filament assembly (marked by the myosin heavy chain staining) via a GEF-H1-mediated RhoA-ROCK activation disrupted podosomes and conversely promoted the assembly of focal adhesions in these cells.

3.4 – Figures

Figure 1

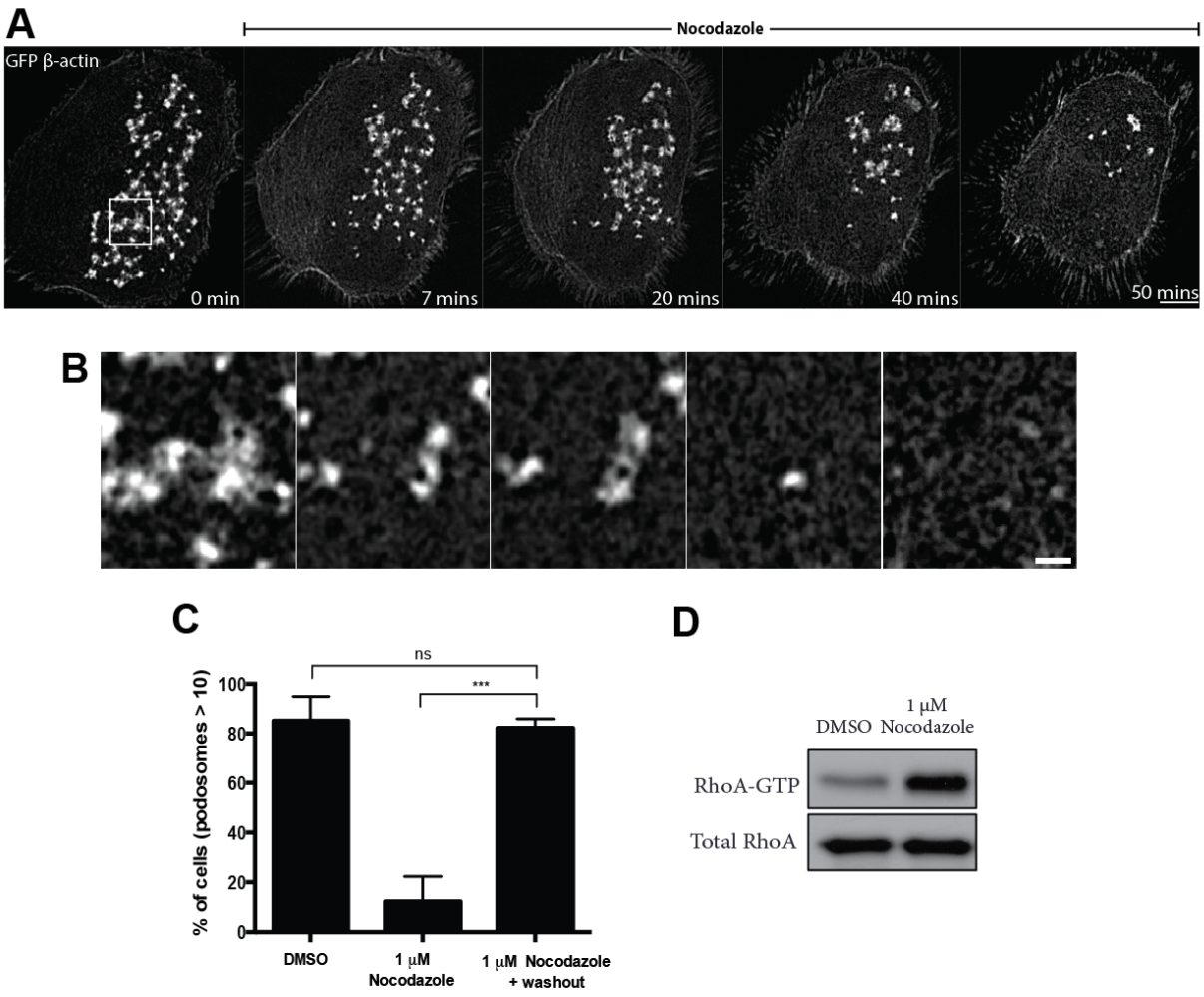

Chapter 3 – Figure 1: Nocodazole induces podosome disassembly.

TGFβ1-stimulated THP1 cell stably transfected with GFP-β-actin was treated with 1 μM nocodazole for 1 hour. (A) Live imaging of the nocodoazole-treated cell showed gradual disassembly of podosomes when visualized on structured illumination microscopy (SIM). Scale bar, 5 μm. (B) Enlarged image of boxed area from (A) revealed disassembly of podosomes and the associated actin links but the cortical

actin meshwork remained intact (most right panel). Scale bar, 1 μm. (C) Graph depicting the percentage of cells having more than 10 podosomes, represented as mean ± SD of 4 independent experiments after addition of DMSO (control), 1 μM nocodazole or washout of the drug with complete medium on podosomes integrity. (D) Pulled-down assay using rhotekin beads showing a 4-fold increase in RhoA-GTP levels in nocodazole-treated cells when compared to DMSO-treated cells. The significance of the difference between groups was estimated by two-tailed Student's *t*-test, the range of P-values >0.05(non-significant), ≤ 0.05, ≤0.01, ≤0.001, ≤ 0.0001 are denoted by "ns", one, two, three and four asterisks (*), respectively.

Figure 2

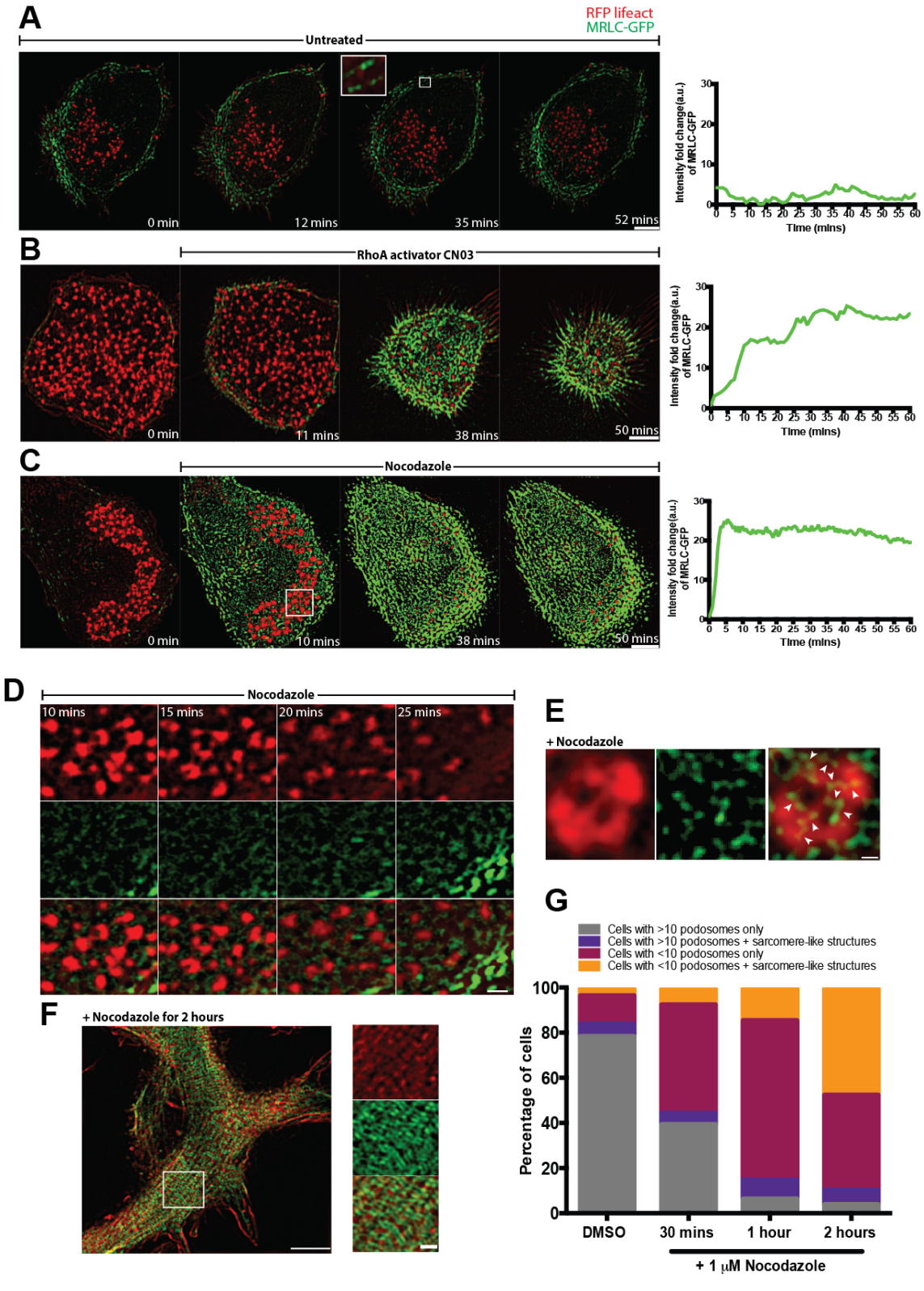
A
RFP lifeact
MRLC-GFP
Untreated
0 min
12 mins
35 mins
52 mins
Intensity fold change(a.u.) of MRLC-GFP
Time (mins)
B
RhoA activator CN03
0 min
11 mins
38 mins
50 mins
C
Nocodazole
0 min
10 mins
38 mins
50 mins
D
Nocodazole
10 mins
15 mins
20 mins
25 mins
E
+ Nocodazole
F
+ Nocodazole for 2 hours
G
Cells with >10 podosomes only
Cells with >10 podosomes + sarcomere-like structures
Cells with <10 podosomes only
Cells with <10 podosomes + sarcomere-like structures
Percentage of cells
DMSO
30 mins
1 hour
2 hours
+ 1 μM Nocodazole

Chapter 3 – Figure 2: Structured-illumination microscopy (SIM) visualization of podosome dynamics in TGFβ1-stimulated THP1 cells stably co-transfected with MRLC-GFP and RFP-lifeact to label myosin II filaments and F-actin, respectively.

(A) A time sequence of merged image of MRLC-GFP (green) and RFP-lifeact (red) showing myosin II filaments were not localized to podosomes but can be found in the cortical actin network. Enlarged imaged of boxed area in third panel of (A) shows four pairs of myosin II bipolar filaments. Right graphs represent time course of MRLC-GFP dynamics for 1 hour with little fluctuations in the total fluorescence intensity. Stimulation of cells with (B) 1 μg/ml RhoA activator, CN03 or (C) 1 μM nocodazole for 1 hour induced burst of myosin IIA filaments and gradual disassembly of podosomes. Scale bars, 5 μm. Right graphs show more than 25-fold increase in total fluorescence intensity of MRLC-GFP in both (B) and (C). (D) Enlarged image of boxed region in (C) with subsequent images captured at 5 minutes interval showing steady myosin II filament assembly (middle row) all over podosomes (top row) and their merged image (bottom row). (E) A closer look at individual podosomes (left panel) indicates numerous myosin II bipolar filaments (middle panel) that were found to surround and co-localize to the actin core of podosomes (white arrowheads of merged image in right panel). Scale bars, 1 μm. (F) Cell treated with 1 μM nocodazole for 2 hours showed assembly of sarcomere-like actomyosin arrangements typically seen in fibroblast-type cells. Enlarged image of boxed area in (F) showing the sarcomere-like arrangement of actin (top panel), myosin II filaments (middle panel) and their merge image (bottom panel). (G) Graph representing percentage of cells forming more than 10 podosomes with or without sarcomere-like actomyosin arrangements in the presence of DMSO (control) or 1 μM nocodazole for 30 minutes, 1 and 2 hours.

Figure 3

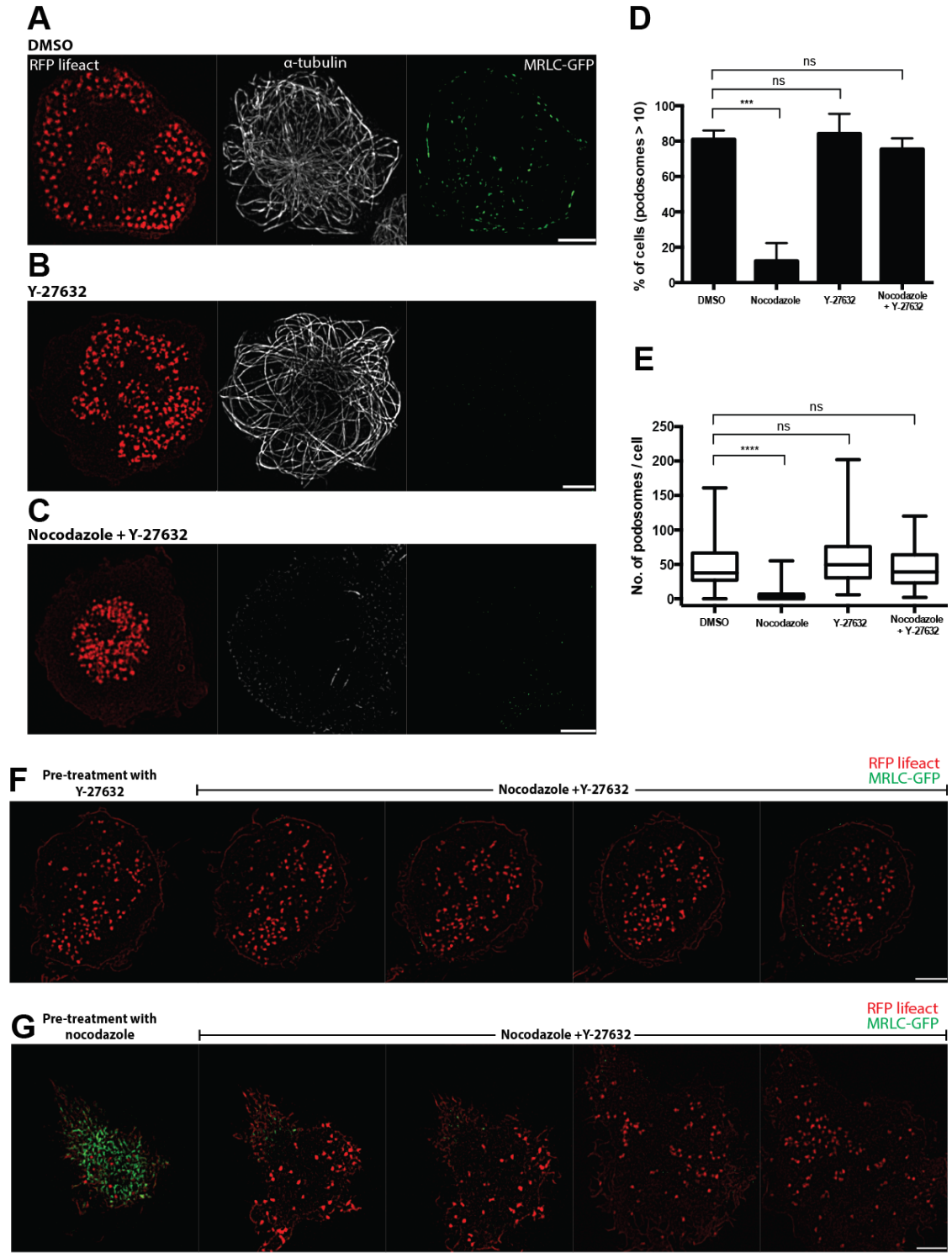

Chapter 3 – Figure 3: Inhibition of Rho-associated kinase (ROCK) rescued podosome formation in nocodazole-treated cells.

(A-C) TGFβ1-stimulated THP1 cells stably co-transfected with MRLC-GFP (right panel) and RFP-lifeact (left panel) were labeled with α-tubulin to visualize microtubule (middle panel) on structured-illumination microscopy (SIM). (A) DMSO-treated cell (control) displaying numerous podosomes with intact microtubule while myosin II filaments were excluded from podosomes. (B) Addition of 120 μM Y-27632 induced disassembly of all myosin II filaments but podosomes and microtubules remained intact. (C) Cell co-treated with 1 μM nocodazole and 120 μM Y-27632 showed disassembly of microtubules and myosin II filaments but podosomes remained intact. (D) Quantification of the effect of Y-27632 and/or nocodazole treatments on podosomes integrity. Both (E) number of podosomes per cell and (F) percentage of cells having more than 10 podosomes were similar to control cells when cells were treated with 120 μM Y-27632 only or co-treated with 120 μM Y-27632 and 1 μM nocodazole for 1 hour but were significantly perturbed in cells treated with 1 μM nocodazole only. (F) Merged image of TGFβ1-stimulated THP1 cell (stably co-transfected with MRLC-GFP and RFP-lifeact) pre-treated with 120 μM Y-27632 for 30 minutes and then co-treated with 1 μM nocodazole for 1 hour prevented both the nocodazole-induced burst of myosin II filaments (MRLC-GFP, green) and disruption of podosomes (RFP-lifeact, red). (G) Pre-treatment of cell with nocodazole for 1 hour and subsequent addition of 120 μM Y-27632 in the presence of 1 μM nocodazole induced disassembly of myosin II filaments (MRLC-GFP, green) and re-assembly of new podosomes (RFP-lifeact, red). Scale bars, 5 μm. The numbers of podosomes per cell are presented as box-and-whiskers plot while the percentage of cells with more than 10 podosomes as mean ± SD. The significance of the difference between groups was estimated by two-tailed Student's *t*-test, the range of P-values >0.05(non-significant), ≤ 0.05, ≤0.01, ≤0.001, ≤ 0.0001 are denoted by "ns", one, two, three and four asterisks (*), respectively.

Figure 4

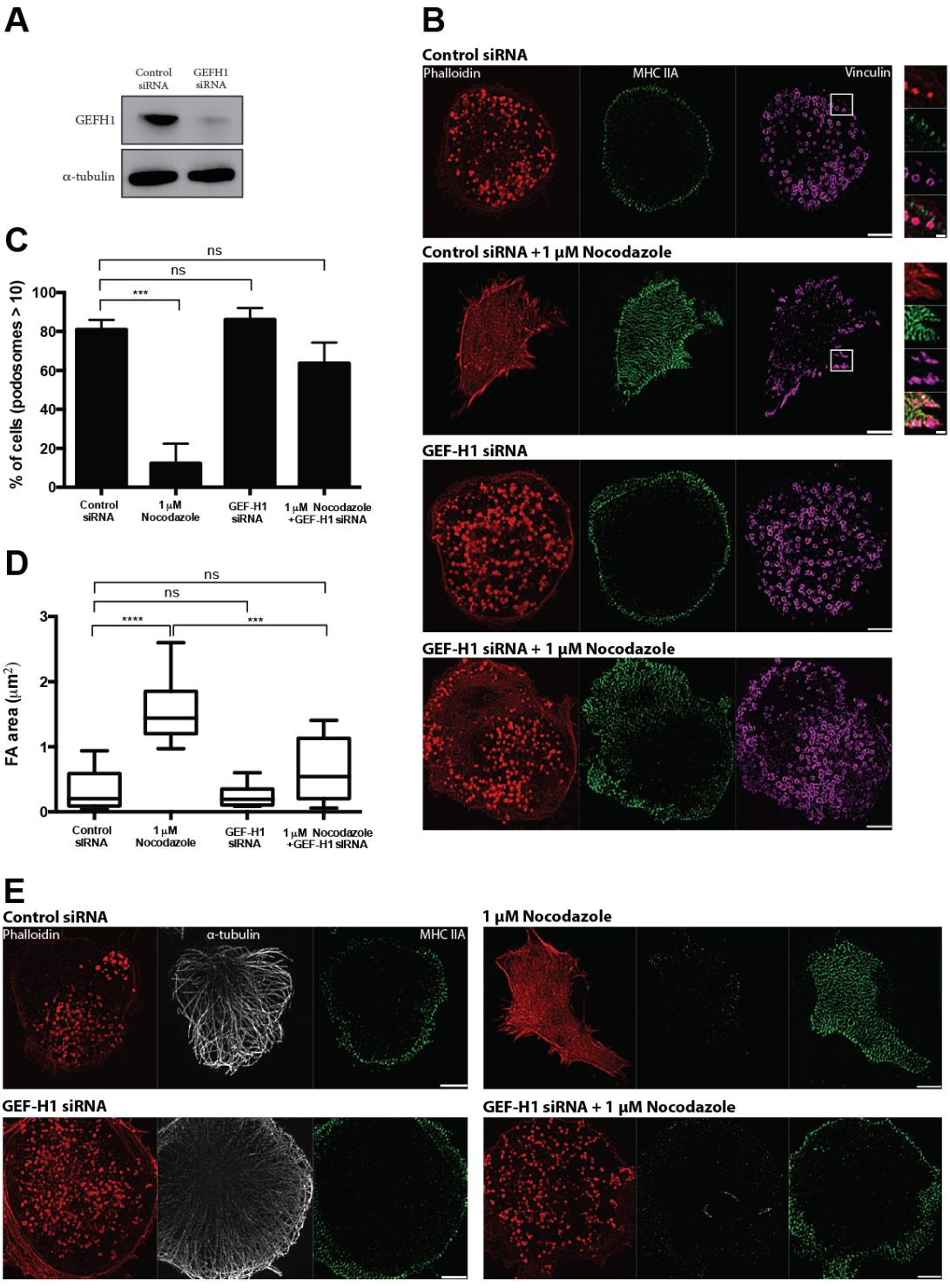

Chapter 3 – Figure 4: Depletion of endogenous GEF-H1 prevented the nocodazole-induced disassembly of podosomes.

(A) Western blot showing GEF-H1 levels in cells treated with scramble (control) or GEF-H1 siRNA; α-tubulin was used as a loading control. (B) Actin labeled with phalloidin (left panel), myosin IIA heavy chain (middle panel) and vinculin (right panel) visualized by antibody staining. TGFβ1-stimulated THP1 cells were transfected with control or GEF-H1 siRNA for 48 hours and then treated with DMSO or 1 μM nocodazole for 1 hour. From top to bottom: Cell transfected and treated with control siRNA and DMSO; control siRNA and 1 μM nocodazole; GEF-H1 siRNA and DMSO, GEF-H1 siRNA and 1 μM nocodazole. Scale bars, 5 μm. Enlarged images represent boxed areas of respective left panels. Scale bars, 1 μm. (C and D) Quantification of the effect of GEF-H1 siRNA and nocodazole on podosome integrity. (C) Graph on the percentage of cells having more than 10 podosomes and (D) size of focal adhesions in accordance to the respective treatments indicated in (B); beginning from top to bottom. Likewise, (E) cell treated with similar conditions as (B) with actin visualized by phalloidin (left panel), microtubule and myosin IIA filaments labeled with α-tubulin (middle panel) and myosin IIA heavy chain (right panel) antibodies.

Figure 5

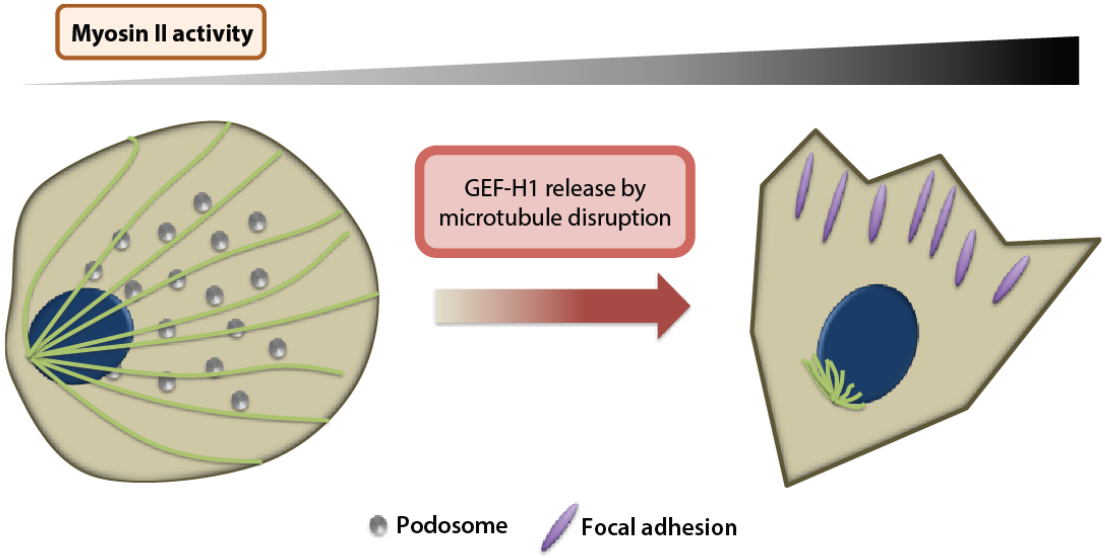

Chapter 3 – Figure 5: Schematic diagram depicting the relationship between microtubule and myosin II activity in switching podosomes to focal adhesions in macrophage-like cells.

Disruption of microtubule by nocodazole induces release of microtubule-bound GEF-H1, which then activates RhoA and downstream ROCK activity to promote myosin IIA filament assembly. Assembly of myosin II filaments induces disassembly of podosomes but enhance formation of focal adhesions.

3.5 - Discussion

The nocodazole-induced disassembly of microtubules has been shown to stimulate cell contractility, stress fiber formation and larger focal adhesions as a consequence of high RhoA activity through the release of microtubule-associated GEF-H1 (Krendel et al. 2002, Birukova et al. 2006, Chang et al. 2008). In contrast, disruption of microtubules by nocodazole led to disassembly of podosomes in macrophages (Linder et al. 2000a). Whilst a number of kinesins have been identified to be involved in regulating podosomes, little is known on how the microtubule-based cytoskeletal network crosstalk with the actin-rich podosome structures.

Here, I demonstrate that microtubules regulate podosome formation in a RhoA and myosin II-dependent fashion, albeit in an opposing direction to focal adhesions (See schematic diagram, Figure 5). Endogenous depletion of the microtubule associated GEF-H1 prevented the nocodazole-induced disassembly of podosomes, suggesting that high RhoA activity induced by GEF-H1 negatively regulates podosomes. In fact, these cells, which typically form small focal complexes in the presence of podosomes, immediately switch to form large focal adhesions in the presence of nocodazole. This observation is consistent with previous studies suggesting that a RhoA-mediated increase in cell contractility induces stress fibers and larger focal adhesions (Bershadsky et al. 1996, Krendel et al. 2002, Chang et al. 2008). In addition, fibroblasts overexpressing constitutively active Src (Pan et al. 2011) or plated on fluid substrate that lacks traction force (Yu et al. 2013), which form podosome rosettes and podosome-like adhesions respectively, have reportedly very low RhoA activity.

Most intriguingly, inhibition of ROCK, downstream of Rho, by Y-27632 prevented and reversed the inhibitory effect of nocodazole on podosome formation (Figure 3D and 3E), suggesting that a GEF-H1-RhoA-ROCK signaling pathway is activated to induce cell contractility that antagonizes podosome formation. On the other hand,

formin inhibition by SMIFH2 (data not shown) did not rescue podosome formation in the presence of nocodazole, indicating that suppression of podosomes by nocodazole is a RhoA-ROCK-myosin IIA-dependent mechanism. The data suggest that formation of podosomes might require active microtubule-dependent RhoA regulation for maintenance of RhoA activity at sites of podosome assembly.

When myosin IIA filaments were visualized by the regulatory light and heavy chain through overexpression of MRLC-GFP or antibody staining respectively, they were predominantly localized to the cortical actin and hardly detectable at sites of podosome assemblies in TGFβ1-stimulated THP1 cells (Figure 2A, 3A, 4B and 4E). However, the increase in RhoA activity as a result of microtubule disruption led to massive assembly of myosin IIA filaments that surround and suppress podosome formation (Figure 2C-E). This suggests that unlike focal adhesions, the activation and local assembly of myosin IIA filaments antagonizes podosome formation.

While disruption of microtubule has been previously shown to increase phosphorylated form of myosin II regulatory light chain (Chang et al. 2008) in fibroblasts, our study provide the first direct visual evidence that levels of active RhoA can be positively correlated with the degree of myosin IIA filament assembly, at least in macrophage-like THP1 cells. In fact, the dose required to inhibit the RhoA-mediated activation of ROCK can be directly visualized by the fluorescence intensity of MRLC-GFP, hence reported doses that inhibit stress fiber formation is insufficient to inhibit the high levels of RhoA activated by the nocodazole-induced release of GEF-H1 into the cytoplasm. More intriguingly, prolonged treatment with nocodazole (>1 hour) promoted the assembly of sarcomeric-like actomyosin structures typically observed in fibroblasts that form defined stress fibers and focal adhesions, indicating that prolonged increased in myosin IIA filament assembly is capable of drastically switching the actin organization of podosome-forming cells to a fibroblast-like organization, potentially changing physiological processes such as matrix degradation and cell migration.

Why does myosin IIA activity promote assembly of focal adhesions but suppress podosome formation? While it is widely known that stimulating RhoA activity promotes increase in focal adhesion size, it is still not clear how myosin IIA contributes to the their maturation. Myosin IIA filaments have both an actin bundling and a contractile role in organizing actin filaments (Vicente-Manzanares et al. 2009). In the first case, bundling of f-actin promotes clustering of adhesion proteins that will consequentially generate a larger focal adhesion size due to the sheer density of these proteins. The actin bundling function has been shown to be sufficient in promoting FA maturation since myosin IIA lacking a functional ATPase motor domain is still capable of promoting adhesion growth and maturation (Choi et al. 2008). In the second case, contraction of myosin IIA bipolar filaments can generate a force that will induce exposure of additional talin and vinculin binding sites for FA growth and maturation (del Rio et al. 2009, Friedland, Lee and Boettiger 2009). Interestingly, the idea of maintaining podosomes via myosin II-dependent contraction mechanism has been previously proposed to control the rate of podosome oscillations during protrusion formation (van den Dries et al. 2013a, Labernadie et al. 2014). If true, then too much myosin II filament assembly at the site of podosomes should exert a net downward pushing force, which will lead to their collapse and disassembly.

Hence, future work includes investigating the effect of overexpressing functionally-deficient (e.g. crosslinking-, motor-deficient) myosin IIA mutants in myosin IIA-depleted cells to investigate how myosin II induces the switch from podosomes to focal adhesions with respect to microtubule integrity.

Chapter 4 - Membrane tension controls the assembly and organization of podosomes

4.1 - Abstract

Cell migration requires continuous remodeling and re-shaping of the lipid bilayer membrane to generate protrusions and extensions at the leading edge of the cell. Such processes require dynamic interaction with the extracellular matrix, but little is known of the relationship between cell-matrix adhesions and lateral tension of the membrane. Here, we focus on podosome-type adhesions in macrophage-like THP1 cells to understand the effect of membrane tension perturbation on podosome dynamics. I demonstrate that existing podosomes undergo dissolution upon increase in membrane tension by exposure to hypo-osmotic shock media and mechanical stretching, while expansion of the membrane (lower tension) by deoxycholate promoted "clustering" of podosomes with shorter connecting actin links than podosomes of control cells. Furthermore, the assembly of podosomes depends on the magnitude of stretch instead of the number of stretch cycles and duration of stretch, and podosome formation can be completely rescued when the strain is released. Collectively, our data provide preliminary but solid evidences that membrane tension plays a central role in the assembly of podosomes, implying that membrane plasticity and/or invagination-related processes such as endocytosis can control the biogenesis and maintenance of podosome-type adhesions.

4.2 - Introduction

Podosomes are multiple micron-sized radially symmetrical units (width; 1μM, height: 2μM) comprising of actin-rich core surrounded by multiple focal adhesion-associated proteins such as talin, paxillin and vinculin (Murphy and Courtneidge 2011, Cox and Jones 2013). While podosomes are constitutively formed in monocyte-derived cells such as macrophages and osteoclasts, their formation can be artificially induced in other cells types such as fibroblasts and endothelial cells by overexpression of constitutively active Src or transforming growth factor beta (TGFβ), respectively (Tarone et al. 1985, Varon et al. 2006, Rottiers et al. 2009).

The plasma membrane is a fluid continuous hydrophobic lipid bilayer that provides the cell its shape and serves as a physical barrier to protect itself from the extracellular environment (Wymann and Schneiter 2008, Kozlov et al. 2014). In addition, physiological processes such as cell motility and division rely on the tension exerted on the membrane in response to cytoskeletal re-organization and signaling events when in contact with the cell extracellular substrate (Kozlov, McMahon and Chernomordik 2010, Gauthier, Masters and Sheetz 2012, Lieber et al. 2013, Kozlov and Chernomordik 2015, McMahon and Boucrot 2015). In particular, tension at the plasma membrane is defined as the force (N) needed to deform a given length (m) of a membrane (N/m). However, tension at the membrane is not only contributed by lipid molecules that constitutes the bilayer, proteins embedded in the membrane and the actin cortex to which the cytoplasmic layer of the membrane is physically attached to are key players that resist the deformation of the membrane and hence contribute to the overall membrane tension of the cell (Vogel and Sheetz 2006, Diz-Munoz, Fletcher and Weiner 2013, Kozlov and Chernomordik 2015). The relationship between the effective membrane tension and tether force (i.e. force exerted to pull an area of membrane by e.g. a micropipette) can be explained by the following equation:

$$T = F^2/(8B\pi^2),$$

where T is the effective membrane tension, F is the tether force and B is the bending

stiffness that accounts for the curvature of the measured membrane (Diz-Munoz et al. 2013).

The plasma membrane responds rapidly to changes in membrane tension through a variety of feedback mechanisms. Processes such as endocytosis and exocytosis can control membrane area through the transport of lipids, which in turn govern the cell membrane tension (Dai and Sheetz 1995, Boulant et al. 2011, Gauthier et al. 2011). For example, artificial increase in membrane tension by osmotic swelling (hypotonic shock) stimulated exocytosis to buffer the increase in tension by supplying more lipids (Gauthier et al. 2011) and likewise, high membrane tension arrested clathrin-coated endocytic pits (Boulant et al. 2011). In addition, generation and disassembly of micron- (e.g. folds and blebs) and submicron- (e.g. caveolae) scaled invaginations can rapidly modulate tension at the membrane (Sinha et al. 2011, Kosmalska et al. 2015). For example, caveolae-mediated invaginations can serve as reservoir to buffer fluctuations in membrane tension through rapid flattening and re-assembly processes in response to mechanical stress and release, respectively (Sinha et al. 2011).

While there is currently no direct method to visualize changes in membrane tension, changing the osmolarity (e.g. hypotonic shock), addition of detergent-like reagents (e.g. deoxycholate, organic solvents) and physical manipulations such as mechanical stretching have been widely accepted as means to perturb tension at the membrane (Dai and Sheetz 1995, Raucher and Sheetz 2000, Vogel and Sheetz 2006, Diz-Munoz et al. 2013). To quantify membrane tension, tethering using tweezers (laser or magnetic) or atomic force microscopy, has been used to estimate the apparent tension exerted on the membrane (Vogel and Sheetz 2006, Diz-Munoz et al. 2013).

Despite the fact that very little is known of the relationship between integrin-mediated adhesions and membrane tension, the actomyosin machinery has been shown to influence processes such as endocytosis and exocytosis, which in turn can

influence the tension exerted on the membrane (Cai et al. 2010, Gauthier et al. 2011, Kozlov and Chernomordik 2015, Tsujita, Takenawa and Itoh 2015). Podosome-type adhesions have been generally described to be protrusive (Gawden-Bone et al. 2010, Labernadie et al. 2014) to allow processes such as transmigration and invasion to take place (Carman et al. 2007a, Seano et al. 2014, Linder and Wiesner 2015). Structurally, this suggests that while podosomes are connected to the substratum via integrins, the actin core of podosomes have to maintain a continuous connectivity to the plasma membrane, so as to favor local protrusive activity.

In this study, I show that assembly dynamics of podosomes in macrophage-like THP1 cells respond to fluctuations in membrane tension. Membrane tension was perturbed using prevailing methods such as osmotic shock, low concentration of the detergent deoxycholate, and mechanical stretching using two different methods, uniaxial and radial stretch directions to increase/decrease membrane tension at the plasma membrane. Our results indicate that podosome formation was hindered during acute mechanical stress and clusters to form numerous domains of closely associated podosomes when tension at the plasma membrane was decreased. Collectively, our data suggest that formation of podosomes is favored when membrane tension is low and perturbed at high tension.

4.3 - Results

To understand how podosomes respond to changes in membrane area and shape, THP1 cells were stimulated with 1ng/ml TGFβ1 as usual and the plasma membrane tension was subsequently perturbed using (i) osmotic shock, (ii) deoxycholate and (iii) mechanical stretching 24 hours after seeding on fibronectin-coated surfaces. Podosomes were visualized using phalloidin/GFP-β-actin and/or vinculin to label the actin core and ring regions of podosomes, respectively.

4.3.1 - Osmotic swelling disperses podosomes and promote their disassembly

TGFβ1-treated THP1 cells were exposed to media containing 50% (0.5x hypotonic) and 90% (0.1x hypotonic) reduction in osmolarity for 15 minutes to acutely increase the cell volume, which exerts pressure on the membrane and consequently result in an increase in membrane tension. Cells incubated with 0.5x hypotonic medium showed reduction in podosome assembly as compared to cells treated with isotonic medium (Figure 1A and 1B) as indicated by actin and vinculin staining, with some podosomes appearing smaller than the usual diameter (Figure 2G). A 90% increase in osmolarity resulted in cell lysis (Figure 1C, Figure 2E-F). The cortical actin of the cells held in 0.1x hypotonic medium was not preserved and cells display numerous actin projections (Figure 1C). Live imaging under structured illumination microscopy (SIM) using GFP-β-actin showed initial dispersion of podosomes followed by dissolution of some podosomes but not all when cell was exposed to 0.5x hypotonic medium (Figure 1D and Figure 2E-F). In fact, the size and fluorescence intensity of GFP-β-actin at these podosomes (yellow arrowheads) were much lower than the podosomes captured before (white arrowheads) addition of 0.5x hypotonic medium even after bleach correction (Figure 1E). The quantification of podosomal actin size, fluorescence intensity and circularity are based on live SIM images of 4-6 cells as shown in Figure 2G-I. Interestingly, podosomes exposed to

0.5x hypotonic medium are much "rounder"(based on circularity index) than podosomes in control cells (Figure 2I).

4.3.2 - Decreasing membrane tension by deoxycholate enhances the clustering of podosomes

Cells were initially perturbed with 200 mM sucrose-containing medium (hypertonic medium) to decrease membrane tension. However, TGFβ1-treated cells immediately underwent shrinkage due to reduction in cell volume, which affected the membrane surface area in contact with the substrate. As a result, podosome number was lower as a consequence of the reduction in spread area, but their assembly was still observed at regions where the cell membrane is in contact with the substrate (data not shown).

In order to decrease membrane tension without significantly perturbing the ventral spread area of the cell, small concentrations of the detergent, deoxycholate, were used to expand the lipid bilayer (Raucher and Sheetz 2000). Surprisingly, addition of 400 μM deoxycholate induced "clustering" of podosomes without increasing the number of podosomes per cell (Figure 2B and 2F). Furthermore, a closer look at the podosome clusters revealed that podosomes in control cells are more distributed and the actin links associated between them are longer than those treated with 400 μM deoxycholate (white arrowheads, boxed images, Figure 2A and B) when visualized on SIM. In fact, these clusters assemble into numerous "domains" of closely associated podosomes connected by the actin links. Live imaging of TGFβ1-treated THP1 cell overexpressing GFP-β-actin using SIM revealed that these clusters are dynamic, and contain numerous actin links connecting adjacent podosomes (Figure 2C and 2D). While treatment with deoxycholate affects the density of podosomes at a given area, there is no significant difference in the actin size, fluorescence intensity of GFP-β-actin and circularity of these podosomes compared

to control ones (Figure 2G-I). The quantification of the podosomal actin size, fluorescence intensity and circularity are based on live SIM images of 4-6 cells (Figure 2G-I). Quantification of the actin links will require better segmentation through super-resolution microscopy such as STORM/PALM since it is difficult to distinguish each individual link based on the SIM images. It is also important to note that the clustering effect induced by deoxycholate lasted for a maximum of 30 minutes, beyond that time, podosomes were found to re-distribute back to their original density observed in podosomes of control cells, suggesting that cells probably have other means to buffer the reduction in membrane tension.

4.3.3- Mechanical stretching induces bleb formation and loss of podosomes

Membrane tension can also be perturbed by acutely changing the cell spread area by mechanically stretching the substrate to induce strain on cells (Kozlov et al. 2014, Kosmalska et al. 2015). Cells were plated on PDMS surfaces and stretched either radially or uniaxially, to which only data obtained from radial stretching are shown in Figure 3, since both stretching methods yielded the same outcome. The radial stretching employed the use of gas generator to induce a positive pressure that pushes the loading post upwards and deforms the bottom part of the PDMS radially where the cells are seeded on (Cui et al. 2015), while the uniaxial stretching method uses a manual sliding unit where the percentage of stretch is proportional to the change in lateral distance from the original non-stretched condition (See supplementary Figure 1 for details on the set-up of both devices).

When cells were submitted to 30 seconds of 5% radial stretch, there was a slight decline in the number of podosomes but the percentage of podosome-forming cells were not significantly different from non-stretched cells (Figure 3A and 3B). However, when the stretch magnitude was increased to 15% with the same duration, podosomes were completely disrupted and cells were accompanied by

numerous bleb formations (Figure 3C, left image, white arrowheads). The application of 15% stretch is not strong enough to break cell-cell junctions (Figure 3C, right image, yellow arrowheads), suggesting that a 15% stretch did not induce any visible mechanical breakage or detachment of the cell membrane. When cells were stretched at the same magnitude for a shorter duration i.e. 10 seconds, podosomes were completely disrupted upon strain application as compared to non-stretched cells when visualized for actin and vinculin (Figure 3E and 3F). These blebs disappear and podosomes re-assembled when the strain was released for 1 hour after single (Figure 3G) and even multiple (data not shown) times of repeated stretching and release at the same magnitude and duration. More intriguingly, around 40% of cells were found to align their podosomes in a cross-like organization when cells were fixed for 24 hours after strain release (Figure 3H). The alignment of podosomes was due to uneven PDMS deformation as a result of radial stretching and subsequent strain release. This is surprising because focal adhesions and stress fibers do not "sense" this deformation in a similar device set-up (Cui et al 2015). Podosomes on the other hand preferred to assemble at regions when the deformation of PDMS is more pronounced than flat surfaces, a strong indication that the lipid bilayer topology that engulfs individual podosomes is not flat and is possibly "bent" to favor formation of podosome-type adhesions.

To examine the effect of repeated (cyclic) stretching, cells were subjected to 5% and 15% cyclic stretching for 2-8 hours at 0.01-0.1 Hz. Data representing cells cyclically stretched with a magnitude of 5 or 15% at 0.1 Hz for 6 hours are presented in Figure 3I and 3J, respectively. At 5% cyclic stretch, podosome formation was slightly perturbed but the percentage of cells forming podosomes was not significantly different from non-stretched cells (Figure 3D). In contrast, podosomes were completely abrogated when stretched at 15% magnitude with numerous bleb formations, similar to a single stretch for 10 (Figure 3F) and 30 seconds (Figure 3C). Collectively, the data indicate that podosomes respond strongly to the magnitude of stretch but not to the duration and cycles of stretch, and cells are capable of forming

new podosomes once the strain was released (Figure 3G and 3H).

4.3.4 - Inhibition of dynamin II but not clathrin-mediated endocytosis perturbed podosome formation

High membrane tension inhibits endocytosis and assembly of membrane invaginations (Raucher and Sheetz 1999, Boulant et al. 2011, Gauthier et al. 2012, Kozlov and Chernomordik 2015). On the other hand, knockdown of dynamin II or overexpression of dominant negative mutant (Ochoa et al. 2000, Destaing et al. 2013) in Src-transformed fibroblasts significantly abrogated podosomes. To test whether dynamin II might function via clathrin-mediated endocytosis in macrophage-like cells, we independently perturbed dynamin II and clathrin using the small-molecule inhibitors, dynasore and Pitstop®2, respectively, in TGFβ1-treated THP1 cells plated on fibronectin-coated surfaces. Cells were stained with phalloidin to visualize actin and antibody to vinculin.

Expectedly, treating cells with 80 μM of dynasore for 30 minutes significantly disrupted podosome formation when compared to control cells (Figure 4A and 4B). However, treatment of cells with 25 μM clathrin inhibitor,Pitstop®2, showed no difference from control cells (Figure 4C), suggesting that dynamin II does not function via clathrin-mediated endocytosis to maintain podosome assembly. In my hands dynamin II was found to localize primarily to the ring component of podosomes in TGFβ1-stimulated THP1 cell (Figure 4E and 4F) but not clathrin (marked by clathrin light chain, data not shown). However, this does not rule out endocytosis, since there are a number of dynamin II-dependent endocytic processes that are clathrin-independent such as the CLIC-GEEC (clathrin-independent carrier and GPI-anchored protein enriched in early endosomal compartments) pathways (Gauthier et al. 2012, Johannes et al. 2015). Future work concerning the role of dynamin II in CLIC-GEEC-dependent endocytosis deserves further investigations.

4.4 – Figures

Figure 1

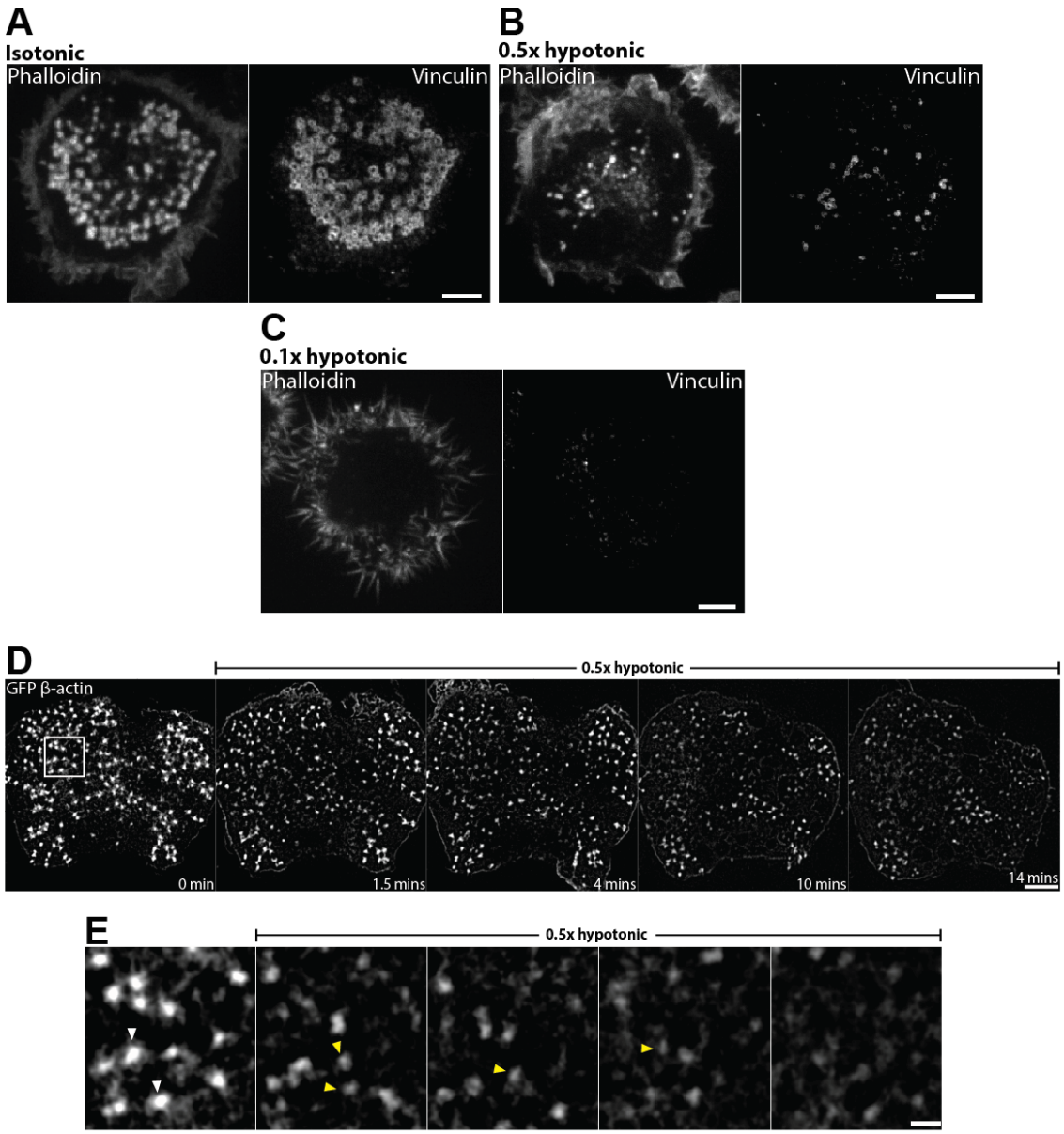

Chapter 4 – Figure 1: Increasing membrane tension by hypo-osmotic shock promotes disassembly of podosomes.

(A) Confocal images of TGFβ1-stimulated cells exposed to isotonic (complete medium), hypotonic medium with (B) 50% and (C) 0% reduction in osmolarity for 15 minutes. Actin labeled with phalloidin (left panel) and vinculin visualized by antibody staining (right panel). Scale bars, 5 μm. (D) Structured-illumination microscopy (SIM) visualization of podosome dynamics in TGFβ1-stimulated THP1 cells stably transfected with GFP-β-actin. Time-lapse images showing dispersion and reduction in the number of podosomes labeled with GFP-β-actin upon addition of 0.5x hypotonic medium (50% reduction in osmolarity). Scale bar, 5 μm. (E) Time sequence of enlarged area boxed in (D) with white and yellow arrowheads showing individual podosomes before and after addition of 0.5x hypotonic shock, respectively. Scale bar, 1 μm.

Figure 2

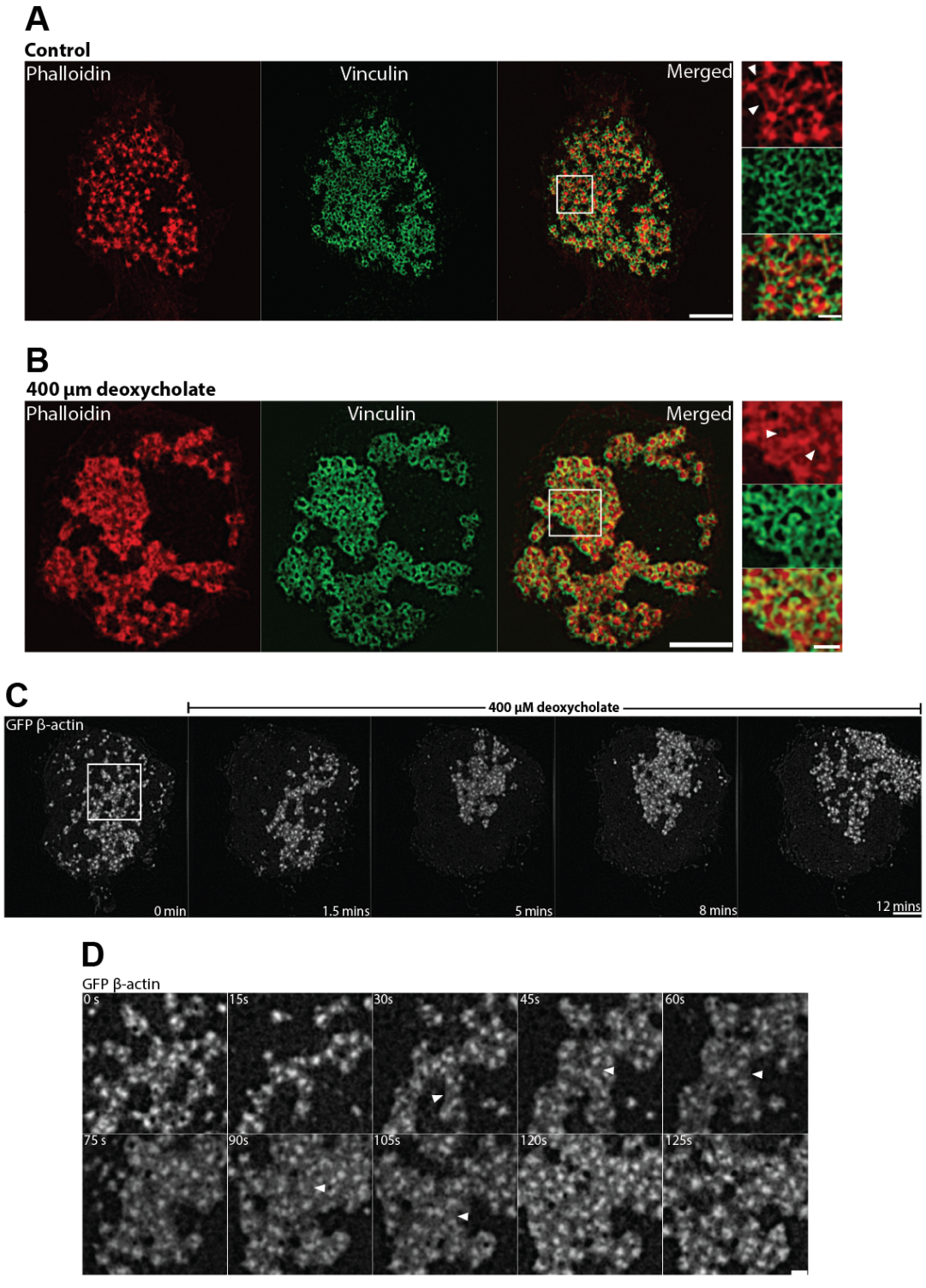
A
Control
Phalloidin
Vinculin
Merged
B
400 µm deoxycholate
Phalloidin
Vinculin
Merged
C
400 µM deoxycholate
GFP β-actin
0 min
1.5 mins
5 mins
8 mins
12 mins
D
GFP β-actin
0 s
15s
30s
45s
60s
75 s
90s
105s
120s
125s

Figure 2

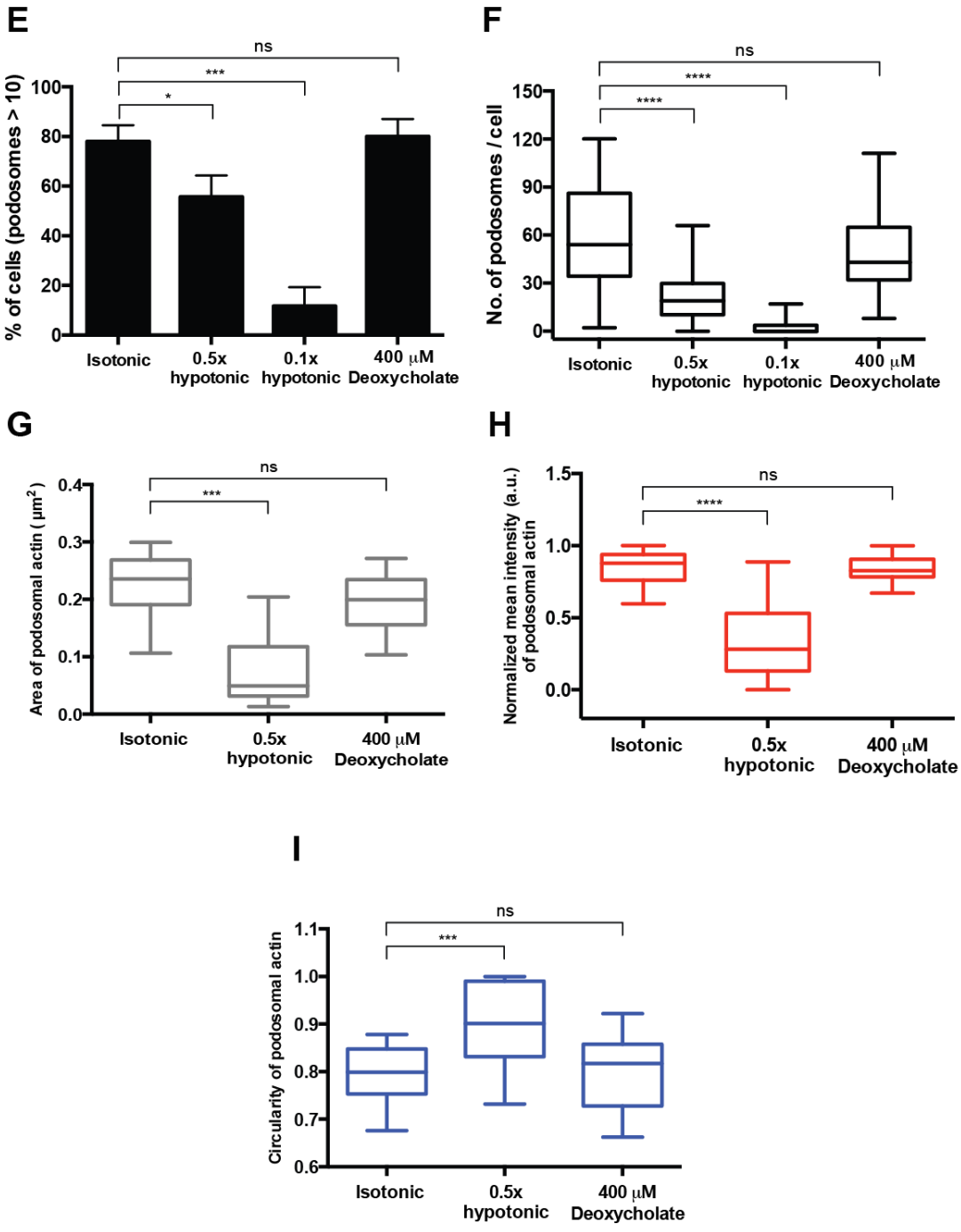

Chapter 4 – Figure 2: Decreasing membrane tension by the detergent deoxycholate promotes podosome "clustering".

Structured-illumination microscopy (SIM) visualization of podosome dynamics in TGFβ1-stimulated THP1 cells exposed to (A) normal complete medium and (B) 400 μM deoxycholate-containing medium for 15 minutes. Actin labeled with phalloidin (left panel), vinculin visualized by antibody staining (middle panel) and their merged image (right panel). Scale bars, 5 μm. Boxed images represent cropped area of (A) and (B) with white arrowheads showing actin links between adjacent podosomes. Scale bars, 1 μm. (C) Time-lapse images depicting the dynamic "clustering" effect of deoxycholate on TGFβ1-stimulated THP1 cell stably transfected with GFP-β-actin. Scale bar, 5 μm. (D) Time sequence of enlarged area boxed in (C) showing numerous actin links connecting adjacent podosomes (see white arrowheads). Scale bar, 1 μm. (E and F) Quantification of the effect of osmotic shock (0.5x and 0.1x) and deoxycholate treatments on podosomes integrity. Both (E) number of podosomes per cell and (F) percentage of cells having more than 10 podosomes are significantly perturbed when exposed to hypotonic media. Quantification of the (G) area, (H) fluorescence intensity and (I) circularity of GFP-β-actin before (isotonic) and after addition of 0.5x hypotonic or deoxycholate-containing media. Figures E and F represent results of 2-3 independent experiments. At least 20 podosomes were analyzed for each group in Figure G-I. The significance of the difference between groups was estimated by two-tailed Student's *t*-test, the range of P-values >0.05(non-significant), ≤ 0.05, ≤0.01, ≤0.001, ≤ 0.0001 are denoted by "ns", one, two, three and four asterisks (*), respectively.

Figure 3

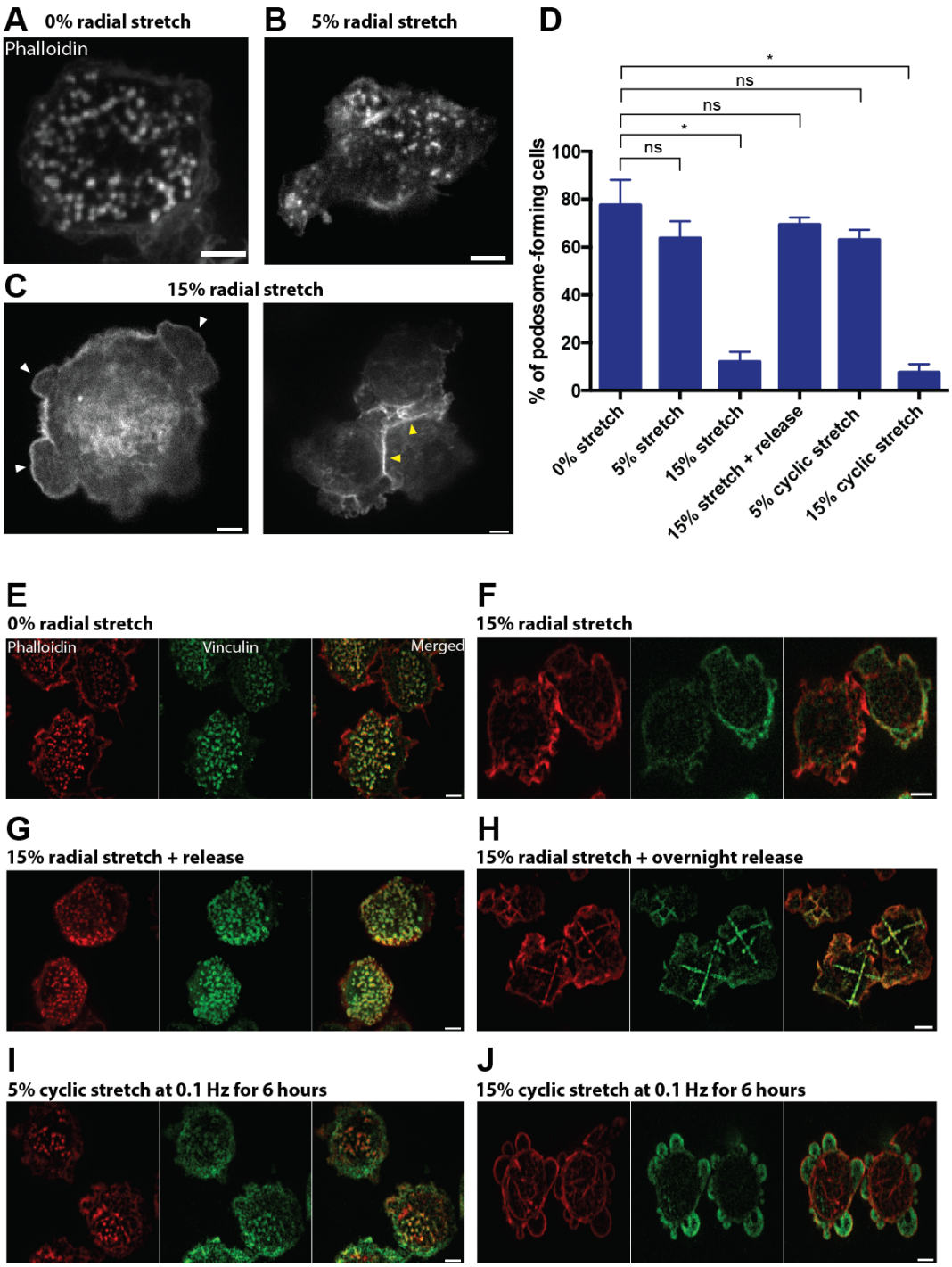

Chapter 4 – Figure 3: Mechanical stretching of cells induced podosome dissolution.

Representative images of TGFβ1-stimulated THP1 cells stained for actin by phalloidin on flat PDMS (polydimethylsiloxane). (A) without stretching and with (B) 5% radial stretching for 30 seconds showed normal podosome formation. (C) 15% radial stretching for 30 seconds completely abrogated existing podosomes with left panel showing bleb formations (white arrowheads) and right panel indicating that cell-cell contacts (yellow arrowheads) were not disrupted at this stretch magnitude. Scale bars, 5 μm. (D) Percentage of podosome-forming cells without stretching (control) and with respective stretching parameters. Graph represents results of 2-3 independent experiments. (E-J) Actin was labeled with phalloidin (left panel), vinculin visualized by antibody staining (middle panel) and their merged image (right panel). (E) Control cells without stretching and with (F) 15% radial stretching for 10 seconds. (G and H) Cells subjected to radial stretching for 10 seconds and then released and fixed 1 hour (G) or 24 hours (H) post-stretching showed re-assembly of podosomes. About 40% of cells (H) aligned with respect to the deformation on the PDMS substrate induced by the pressure-dependent stretching device during the period of stretching. Cells subjected to cyclic stretching of (I) 5% and (J) 15% magnitude at 0.1 Hz for 6 hours did not show significant difference from single stretch experiments shown in (B) and (C). Scale bars, 5 μm.

Figure 4

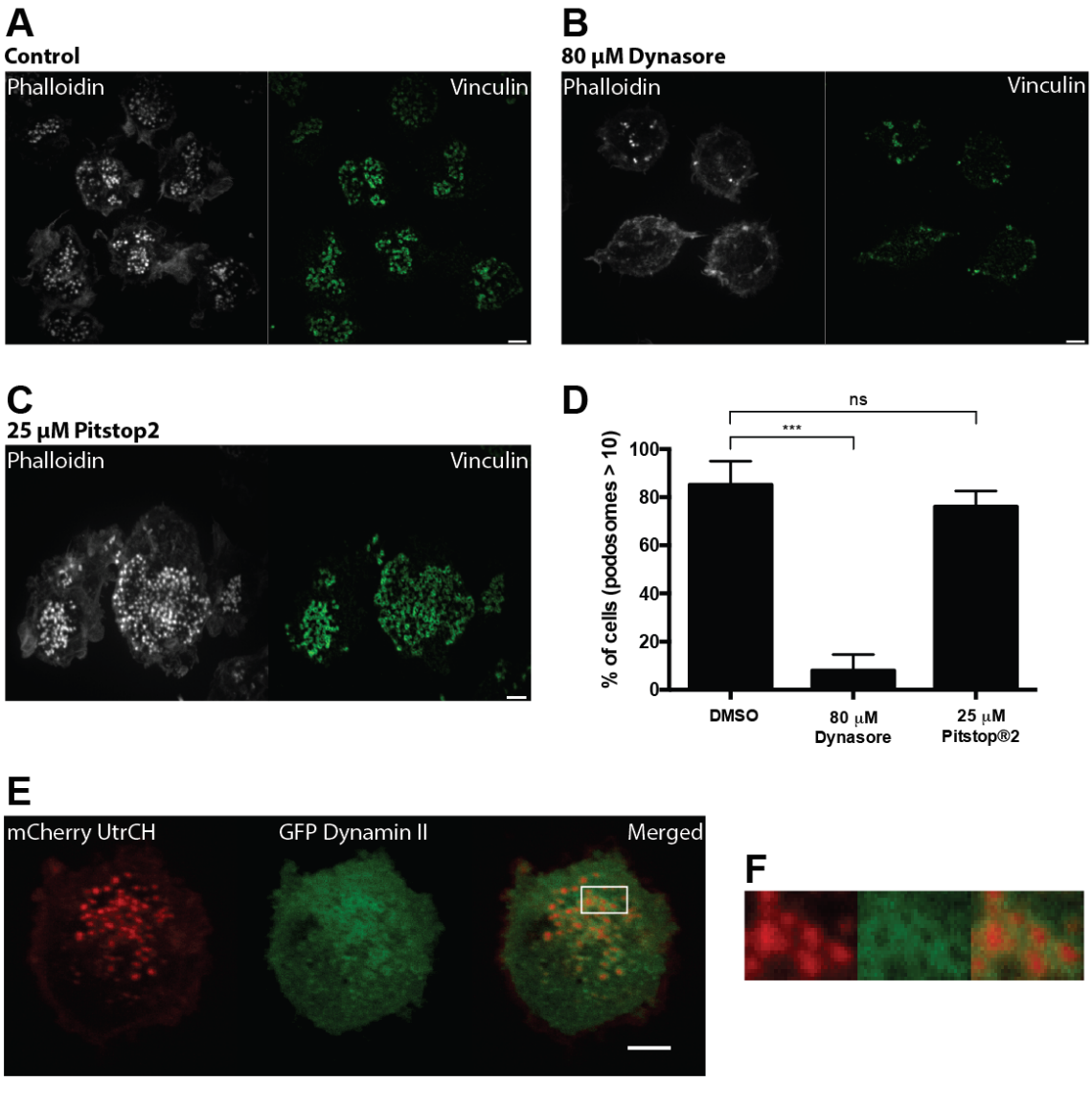

Chapter 4 – Figure 4: Podosome assembly requires dynamin II in a clathrin-independent mechanism.

TGFβ1-stimulated THP1 cells treated with (A) DMSO, (B) 80 µM of the dynamin inhibitor, dynasore and (C) 25 µM of the clathrin inhibitor Pitstop®2. Actin labeled with phalloidin (left panel) and vinculin visualized by antibody staining (right panel). Scale bars, 5 µm. (D) Percentage of cells having more than 10 podosomes

after an hour treatment with DMSO (control), dynamin II and clathrin inhibitors. Graph represents results of 2-3 independent experiments. (E) TGFβ1-stimulated THP1 transfected with mCherry-UtrCH (left panel) and GFP-dynamin II (middle panel) indicate predominant ring localization of dynamin II in podosomes as shown in the overlapped image (right panel) and the (F) enlarged image of the boxed area from (E).

Supplementary Figure 1

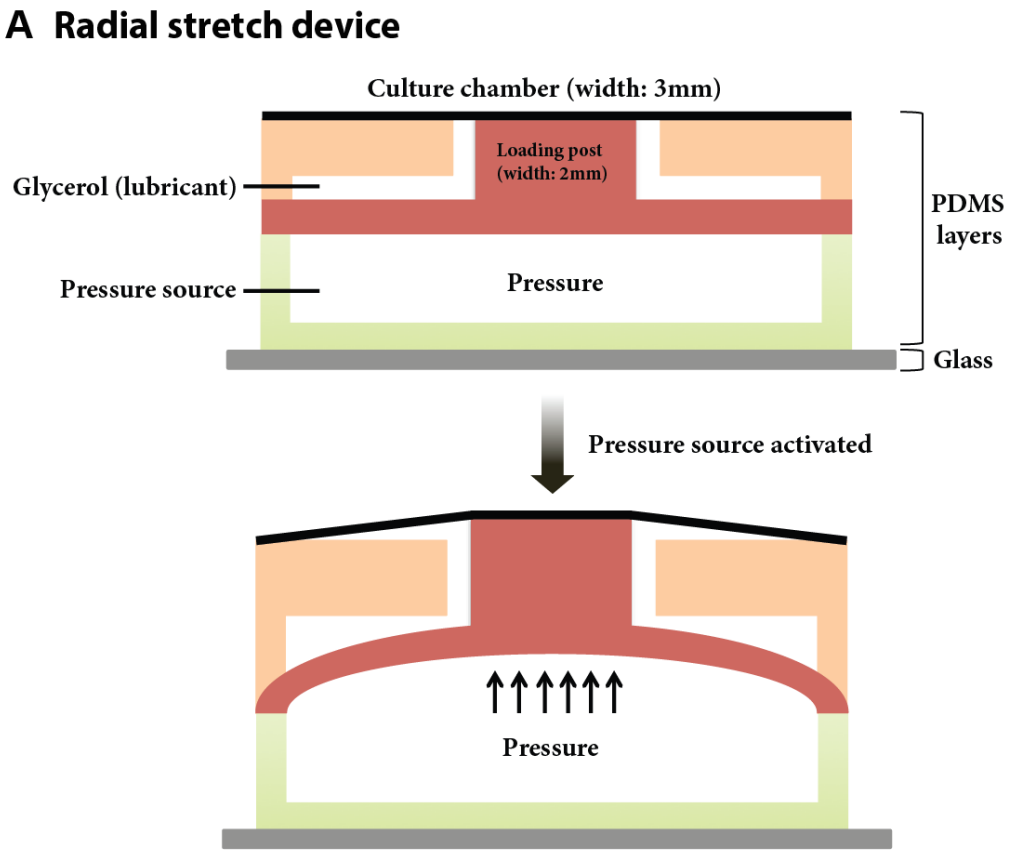

Chapter 4 – Supplementary Figure 1: Design of radial and uniaxial stretch devices.

(A) Vertical cross-section of a radial stretch unit consists of multiple PDMS layers attached to a glass substrate. The culture chamber (3 mm wide) sits on a loading post (2 mm wide and 100 μm in height) with an underlying PDMS layer that is attached to a PDMS cavity bound to the glass substrate. (B) Pressure in the cavity expands the PDMS layer above it, which then pushes the loading post and deforms the uppermost PDMS where the cells are seeded. THP1 cells were stimulated with TGFβ1 and plated for 24 hours on the fibronectin-coated culture chamber prior to any stretch experiments. (C) Uniaxial stretch device employs manual pulling of the sliding unit to stretch the PDMS chamber. The "pulled" distance is proportional to the stretch magnitude. Data obtained from stretching on the uniaxial stretch device are not shown in this chapter but provide similar outcome with the radial stretching approach.

4.5 - Discussion

In this study, I showed that podosomes respond to changes in membrane tension using different methods of perturbation such as osmotic shock, detergent-induced expansion of the membrane and mechanical stretching (uniaxial and radial directions) of the substrate. In particular, increasing membrane tension by addition of 50% hypo-osmotic medium and mechanical stretching (magnitude of 15%) led to reduction and complete abrogation of podosomes, respectively. In fact, disruption of podosomes was independent of the stretch cycles and duration, indicating that sudden increase in membrane tension exerts an acute effect on the stability of podosomes. Both osmotic- and stretch -induced perturbation influence membrane tension differently through increase in cell volume (osmolarity changes) and cell spread area (stretching), suggesting that flattening or tightly-packed lipid bilayer (high stress) do not favor the assembly of podosomes. Surprisingly, decreasing membrane tension did not increase the number of podosomes, instead podosomes were closely connected to one another in clusters upon treatment with deoxycholate.

One possible explanation to relate membrane tension in the context of podosome is to assimilate podosomes with lamellipodia, since their actin polymerization is primarily mediated by the Arp2/3 complex and both exert protrusive forces towards the membrane which is lateral for lamellipodia and downwards for podosomes. Increase in membrane tension by osmolarity changes stopped the lateral lamellipodia protrusions in fibroblasts (Gauthier et al. 2011) and sperm cells (Batchelder et al. 2011). For example, Batchelder et al. (2011) showed that cells under hypotonic shock exhibit smoother lamellipodial membrane as compared to deoxycholate-treated cells, which displayed a much more “wavy” membrane with numerous lateral protrusions. Likewise in the context of podosome formation, cells subjected to hypotonic medium have a smoother membrane, thereby making it harder for actin to protrude towards the substratum due to the higher “pushing”

force. On the other hand, decreasing membrane tension by deoxycholate makes "curvier" membranes that can promote clustering of podosomes as a result of enhanced membrane flexibility.

To favor local protrusive activity, formation of podosomes must be tightly correlated to continuous remodeling of the underlying plasma membrane, and this will require low lateral tension at sites of podosome assemblies to permit vertical growth of the actin core network. Indeed, our earlier work (Yu et al. 2013) showed that fibroblast-type cells that typically do not form podosomes develop podosome-like adhesions on fluid RGD-functionalized lipid bilayer that lacks traction force but not on very soft substrates (2kPa). The absence of traction force on a fluid substrate suggests that mobile surfaces can provide an energetically favorable environment for the existence of a flexible (or more deformable) plasma membrane –i.e. low membrane tension, thereby promoting efficient membrane remodeling.

More intriguingly, despite evidences indicating that podosomes are protrusive structures (Gawden-Bone et al. 2010, Labernadie et al. 2014), podosomes are comprised of membrane-deforming proteins such as N/F-BAR-domain containing proteins (FBP17, endophilin, GRAF1) and dynamin II (Ochoa et al. 2000, Tsuboi et al. 2009, Doherty et al. 2011, Tsujita et al. 2013), all of which are typically involved in the formation of invaginations such as endocytic structures. For example, siRNA knockdown of dynamin II (Ochoa et al. 2000) and inhibition of dynamin II by a small-molecule inhibitor, dynasore (Figure 4) significantly abrogate podosome formation. Membrane tension can affect assembly of curvature-generating proteins and their downstream processes (Simunovic and Voth 2015). Future work will include depletion of one or more of these proteins with concomitant reduction in membrane tension (e.g. addition of deoxycholate) to test if such situations can rescue podosome formation. Finally, quantifying membrane tension at the ventral side of cells has technological limitations, since measuring membrane tension requires physical access and tethering to podosomes at the substrate

APPENDICES

Materials and Method

Cell culture and transfection procedures

THP1 human monocytic leukemia cell line was obtained from Health Protection Agency Culture Collections (Porton Down, Salisbury, UK) and cultured using Roswell Park Memorial Institute (RPMI-1640) supplemented with 10% HI-FBS and 50 μg/ml 2-Mercaptoethanol (Sigma-Aldrich) at 37°C and 5% CO_2.

Cells were transiently transfected with DNA plasmids using electroporation (Neon Transfection System, Life Technologies) in accordance to manufacturer's instructions. Specifically, suspended THP1 cells were transfected with two pulses of 1400V for 20 milliseconds. These suspended THP-1 cells were differentiated into adherent macrophage-like cells either with 1 ng/ml human recombinant cytokine TGFβ1 (R&D Systems) or 50 nM Phorbol 12-myristate 13-acetate (Sigma-Aldrich) for 48 hours on fibronectin-coated glass substrates. 35-mm ibidi (Cat. 81158) glass-bottomed dishes were coated with 1 μg/ml of fibronectin (Calbiochem, Merck Millipore) in phosphate buffered saline (PBS) for 1-2 hours at 37°C, washed with PBS twice, and incubated in complete medium prior to seeding of cells.

For siRNA transfection, THP1 cells were treated with 100nM of ARF1 siRNA (Dharmacon, ON-TARGETplus SMARTpool siRNA, catalogue no. L-011580-00-0005), 150nM of ARF6 siRNA (Dharmacon, ON-TARGETplus SMARTpool siRNA, catalogue no. L-004008-00-0005) or 100nM of COPB1 siRNA (Dharmacon, ON-TARGETplus SMARTpool siRNA, catalogue no. L-017940-01-0005). For control experiments, cells were transfected with (Dharmacon, ON-TARGETplus Non-targeting pool siRNA, catalogue no. D-001810-10) at a concentration similar to individual gene-targeted siRNAs.

For knockdown of ARF GEFs in THP1 cells, siRNA duplex 'GCAAUGGGCAGGAAGAAGU' (Oh et al 2010) against human ARNO sequence and 'AUGGAGGAGGACGACAGCUAC' (Sendide et al 2005) against human cytohesin-1 with dT-dT overhangs were purchased from Sigma-Aldrich. For rescue experiments in Figure 1D, ARF1 siRNA transfected THP1 cells were co-transfected with HA-ARF1 (bovine origin, non-sensitive to aforementioned ARF1 siRNA) and fixed 48 hours after plating on fibronectin.

Immortalized rptp-α(+/+) mouse embryonic fibroblasts (Su et al 1999) that will be termed MEFs from now onwards, were obtained from the Sheetz laboratory (Mechanobiology Institute, Singapore). MEFs were cultured in Dulbecco's modified Eagle's Medium high glucose (DMEM), supplemented with 10% heat-inactivated fetal bovine serum (HI-FBS, Gibco), 1% L-Glutamine, and 100 IU/mg penicillin-streptomycin (Invitrogen) at 37°C and 5% CO_2. MEFs were transiently electroporated with a single pulse of 1400V for 20 milliseconds. MEFs were either seeded on fibronectin-coated 35-mm ibidi or 27-mm IWAKI (Japan) glass-bottomed dishes for 24 hours post-transfection. For plating on supported lipid bilayer membrane, transfected MEFs were seeded on 6-well Nunc (Thermo Fisher Scientific) plastic dishes for 24 hours post-transfection. These MEFs were then treated with trypsin solution, TrypLE™ (ThermoFisher Scientific), for 5 mins and kept in suspension for 15 minutes in complete medium to recover from trypsinization prior to seeding on supported lipid bilayer membrane.

Plasmids

mCherry-WIP and GFP-WASP were described in (Vijayakumar et al 2015); GFP-β-actin and mCherry-Talin – in (Cox et al 2012). The following plasmids described in corresponding references were kindly provided by the following researchers. EGFP-ARNO (Santy et al 1999) and EGFP-ARNO E156K (Hernández-Deviez et al 2003) –

by Dr James Casanova (University of Virginia, VA, USA); EGFP-Cytohesin-1 (Bourgoin et al 2002) – by Dr Sylvain Bourgoin (CHU de Québec Research Center, University of Laval, Quebec, Canada); ARF1-RFP (Hsu et al 2010) – by Dr Nihal Altan-Bonnet (NIH, Bethesda, MD, USA); GFP-Vinculin (Zamir et al 1999) and mCherry-Vinculin – by Dr Michael Davidson (Florida State University, FL, USA); GFP-Paxillin and mApple-Paxillin (Kanchanawong et al 2010) – by Dr Pakorn Kanchanawong (Mechanobiology Institute, Singapore); constitutively active Src Y527F – by Dr Keiko Kawauchi (Mechanobiology Institute, Singapore); EGFP-Rab6A (Miserey-Lenkei S et al 2010) – by Dr Stéphanie Miserey Lenkei (Institute of Curie, Paris, France); GFP-Mannosidase II (Galen J et al 2014) – by Dr Vivek Malhotra (Center of Genomic Regulation, Barcelona, Spain); mApple Rab11A (verified in-house) – by Dr Vicki Allan (University of Manchester, UK); GFP-Dynamin II (Ochoa et al 2000) – by Dr Pietro De Camilli (Yale University, USA); All BIG constructs (HA-BIG1, HA-BIG2, HA-BIG1 E793K, HA-BIG2 E738K (Ishizaki et al 2008) – by Dr Hye-won Shin (Kyoto University, Kyoto, Japan).

The following plasmids described in corresponding references were purchased from Addgene (Cambridge, MA, USA): ARF1-GFP (Chun et al 2008, Addgene #39554), ARF1-ECFP (Beemiller et al 2006, Addgene #11381), ARF1(T31N)-ECFP (Beemiller et al 2006, Addgene #11384), ARF1(Q71L)-ECFP (Beemiller et al 2006, Addgene #11385), HA-ARF1 (Furman et al 2002, Addgene #10830), GFP-Rab11 (Choudhury et al 2002, Addgene #12674), mCherry UtrCH (Burkel et al 2007, Addgene #26740), EMTB-mCherry (Miller et al 2009, Addgene #26742), GFP-RhoA (T19N) (Subauste et al 2000, Addgene #12967), ARF6-CFP (Beemiller et al 2006, Addgene #11382), mCherry-Arp3 (Taylor et al 2011, Addgene #27682), mCherry-Cortactin (Taylor et al 2011, Addgene #27676), mCherry-clathrin light chain (Taylor et al 2011, Addgene #27680), dsRed Rab7 (Choudhury et al 2002, #Addgene 12661), GFP-Rab8A (Guizetti et al 2011, Addgene #31803).

Supported lipid bilayer membrane

Methodologies of supported lipid bilayer preparation and membrane functionalization have been described in Yu *et al* 2011 and Yu *et al* 2013. Briefly, 1,2-dioleoyl-sn-glycero-3-phosphocholine (DOPC) and 1,2-dipalmitoyl-sn- glycero-3-phosphoethanolamine-N-(cap biotinyl) (16:0 biotinyl-Cap-PE) were purchased from Avanti Polar Lipids. The lipids (0.2 mol% of biotinyl- Cap-PE and 99.8 mol% of DOPC) were mixed with an equal volume of PBS and then pipetted onto cleaned glass substratum where a 25-mm coverslip was placed over it for self-assembly of lipid vesicles. The lipid-coated coverslips were immersed into a deionized water bath and then placed and sealed in an Attofluor cell chamber (Life Technologies). The supported lipid bilayer membrane ensemble was kept under aqueous environment at all times. For membrane functionalization, the supported lipid membrane was blocked with 50 μg/ml of Casein. A total of 0.1 μg/ml of Cascade blue neutravidin (Life Technologies) was added onto supported lipid membranes, followed by 1 μg/ml of biotinylated RGD, cyclo (Arg-Gly-Asp-D-Phe-Lys [Biotin-PEG-PEG]; Peptides International). Cells were then added onto the RGD-functionalized lipid bilayer membrane and imaged or fixed within 2-3 hours of preparation.

Drug treatment

For drug inhibition studies, podosome-forming cells were treated with 30μM SecinH3 (Tocris), 10μM Golgicide A (Santa Cruz Biotechnology), 5μg/ml Brefeldin A (Sigma-Aldrich) in complete medium for 1-2 hours at 37°C with 5% CO_2 and subsequently fixed with 4% PFA. For live cell imaging, cells were imaged immediately after addition of appropriate inhibitors, which remained in the medium during the entire period of image acquisition. To study effect of inhibitors on podosomes formed by MEFs plated on RGD lipid bilayer, the cells were treated with appropriate inhibitors 30-45 minutes following cell seeding on the bilayer.

Immunoblotting

For verification of knockdown experiments, cells were lysed in RIPA buffer 48 hours after transfection and extracted proteins were separated by 4-20% SDS-polyacrylamide gel (Thermo Fisher Scientific) and transferred to PVDF membranes (Bio-Rad) before incubation at 75V for 2 hours and blocked for 1 hour with 5% non-fat milk (Bio-Rad) or bovine serum albumin (BSA, Sigma-Aldrich). The PVDF membranes were incubated overnight at 4°C with appropriate antibodies: anti-ARF1 (Abcam, catalogue no. ab108347, dilution 1:1000); anti-ARF6 (Abcam, catalogue no. ab77581, dilution 1:1000); anti-ARNO (Abcam, catalogue no. ab56510, dilution 1:1000); anti-cytohesin-1 (Merck Millipore, catalogue no. MABT14, dilution 1:500); anti-α-tubulin (Sigma-Aldrich, catalogue no. T6199, dilution 1:3000); Anti-βCOP (Abcam, catalogue no. ab2899, dilution 1:1000); anti-HA (Cell Signaling Technology, catalogue no. 2367, 1:1000); anti-Cdc42 (Cell Signaling Technology, catalogue no. 2462, 1:1000).

After three washes (10 minutes each), appropriate secondary antibodies conjugated with horseradish peroxidase (Bio-Rad) were incubated with the membrane for 1 hour, washed three times (15 minutes at room temperature), and detected by Pierce™ ECL western blotting substratum (Thermo Fisher Scientific) using CL-Xposure film (Thermo Fisher Scientific).

ARF1 and Cdc42 activity assay

Total cell lysates were collected and immediately quantified by the G-LISA ARF1 or Cdc42 Activation Assay Biochem Kit (colorimetric-based) and performed as per manufacturer's protocol (Cytoskeleton, Inc.). Samples were run in duplicates, averaged and then normalized to the total ARF1 or Cdc42 levels detected by immunoblotting. For each set of experiment, data were normalized to TGFβ1-treated THP1 cells giving a fold-change value from zero (minimum) to one (maximum). Pull-down assay using GST-tagged Rac/Cdc42-binding domain of PAK1

(PBD) beads, which precipitates GTP-bound Rac or Cdc42 proteins, was used to determine the amounts of active Cdc42 levels in THP1 cells. Pulled-down Cdc42 were immunoblotted using antibodies against Cdc42 as described above.

Immunofluorescence

Cells were fixed with 3.7% paraformaldehyde in PBS, washed twice and permeabilized with 0.5% triton X-100 (Sigma-Aldrich) in PBS for 10 minutes, and then washed twice. Fixed cells were blocked with 5% BSA or 5% FBS for 1 hour at room temperature or overnight at 4°C prior to incubation with appropriate primary antibodies: anti-GM130 (BD Biosciences, catalogue no. 610822, dilution 1:400); anti-GRASP65 (Abcam, catalogue no. ab30315, dilution 1:500); anti-HA (Cell Signaling Technology, catalogue no. 2367, dilution 1:400), anti-vinculin (Sigma-Aldrich, catalogue no. V9131, dilution 1:400); anti-ARF6 (Abcam, catalogue no. ab77581, dilution 1:200); Anti-βCOP (Abcam, catalogue no. ab2899, dilution 1:200). Cells were washed thrice with PBS and incubated with Alexa Fluor-conjugated secondary antibodies (Thermo Fisher Scientific) for 1 hour at room temperature followed by three washes in PBS. Actin staining was carried out using either Alexa Fluor 488 Phalloidin (Thermo Fisher Scientific), Phalloidin-TRITC (Sigma-Aldrich) or CF680R Phalloidin (Thermo Fisher Scientific).

Live cell imaging and confocal microscopy

Cells were imaged in complete medium (unless stated otherwise) at an acquisition rate from 5 seconds to 1 minute intervals using a spinning-disc confocal microscope (PerkinElmer Ultraview VoX) attached to an Olympus IX81 inverted microscope, equipped with a 100x oil immersion objective (1.40 NA, UPlanSApo), an EMCCD camera (C9100-13, Hamamatsu Photonics) for image acquisition, and Volocity software (PerkinElmer) to control the acquisition protocol. Fixed samples and live imaging were also imaged with a Nikon confocal A1R system and Nikon structured

illumination microscopy (N-SIM) attached to a Nikon Ti-E inverted microscope with Perfect Focus System (PFS) using a 100x oil immersion objective (1.40 NA, CFI Plan-ApochromatVC). The cameras, from Andor technology Neo sCMOS and DU-897 were used to acquire images for confocal A1R and N-SIM systems respectively, with the Nikon NIS-Elements AR software to control the acquisition protocol. For z stack images, cells were imaged at a step-size of 0.2-0.5 μm with a total height of 15-20 μm.

Image processing and data analysis

Image processing and analysis were performed with ImageJ or Volocity Software. The number of podosomes (marked by core or ring marker) was quantified automatically using an ImageJ-based tool for counting Nuclei (ImageJ plugin), which was manually verified for the first ten cells in the specimen to account for undetected podosomes (less than 10%). Line intensity measurements (arbitrary unit, a.u.) of GFP-ARNO, GFP-Cytohesin-1 and mCherry-UtrCH were quantified by measuring the mean intensity of GFP or mCherry fluorescence per area (μm^2), background subtracted and normalized with values ranging from 0 (lowest) to 1 (highest).

Statistical analyses

Prism version 6 (GraphPad Software) was used to plot, analyze and represent the data. Significance of the differences was determined using two-tailed unpaired Student's *t*-test or one-way ANOVA for more than two groups. The methods for statistical analysis and sizes of the samples (n) are specified in the results section or figure legends for all of the quantitative data. Differences were accepted as significant for $P < 0.05$.

Integrin-matrix clusters form podosome-like adhesions in the absence of traction forces (Yu, Rafiq *et al* Cell Rep. 2013)

Cell Reports
Article

Integrin-Matrix Clusters Form Podosome-like Adhesions in the Absence of Traction Forces

Cheng-han Yu,[1,*] Nisha Bte Mohd Rafiq,[1,2] Anitha Krishnasamy,[1] Kevin L. Hartman,[1] Gareth E. Jones,[2] Alexander D. Bershadsky,[1,3] and Michael P. Sheetz[1,4,*]
[1]Mechanobiology Institute, National University of Singapore, Singapore 117411, Singapore
[2]Randall Division of Cell & Molecular Biophysics, King's College London, London SE1 1UL, UK
[3]Department of Molecular Cell Biology, Weizmann Institute of Science, Rehovot 76100, Israel
[4]Department of Biological Sciences, Columbia University, New York, NY, 10027, USA
*Correspondence: chyu@nus.edu.sg (C.-h.Y.), ms2001@columbia.edu (M.P.S.)
http://dx.doi.org/10.1016/j.celrep.2013.10.040

SUMMARY

Matrix-activated integrins can form different adhesion structures. We report that nontransformed fibroblasts develop podosome-like adhesions when spread on fluid Arg-Gly-Asp peptide (RGD)-lipid surfaces, whereas they habitually form focal adhesions on rigid RGD glass surfaces. Similar to classic macrophage podosomes, the podosome-like adhesions are protrusive and characterized by doughnut-shaped RGD rings that surround characteristic core components including F-actin, N-WASP, and Arp2/Arp3. Furthermore, there are 18 podosome markers in these adhesions, though they lack matrix metalloproteinases that characterize invadopodia and podosomes of Src-transformed cells. When nontransformed cells develop force on integrin-RGD clusters by pulling RGD lipids to prefabricated rigid barriers (metal lines spaced by 1–2 μm), these podosomes fail to form and instead form focal adhesions. The formation of podosomes on fluid surfaces is mediated by local activation of phosphoinositide 3-kinase (PI3K) and the production of phosphatidylinositol-(3,4,5)-triphosphate (PIP3) in a FAK/PYK2-dependent manner. Enrichment of PIP3 precedes N-WASP activation and the recruitment of RhoA-GAP ARAP3. We propose that adhesion structures can be modulated by traction force development and that production of PIP3 stimulates podosome formation and subsequent RhoA downregulation in the absence of traction force.

INTRODUCTION

Activation of integrin receptors by extracellular ligand binding mediates the formation of cell-matrix adhesions (Miranti and Brugge, 2002). The clustering of activated integrins and integrin-associated proteins locally promotes the activation of downstream signal transduction paths leading to events such as cell migration (Huttenlocher and Horwitz, 2011), differentiation (Engler et al., 2006), and cancer metastasis (Levental et al., 2009). The recruitment of actin-binding proteins, such as talin and vinculin, provides structured linkages between integrins and the actin cytoskeleton (Vogel and Sheetz, 2006; Wehrle-Haller, 2012). While the initial clustering of integrin receptors upon binding mobile Arg-Gly-Asp (RGD) moieties is independent of traction forces (Yu et al., 2011, 2012a), contraction-mediated maturation of integrin clusters results in stable adhesion formation (Moore et al., 2010). More importantly, the physical characteristics of extracellular matrix (ECM) can initiate differential assembly of the actomyosin cytoskeletal network (Geiger et al., 2009). For example, fibroblasts on a rigid ECM substrate (100 kPa) are flat, polarized cells with actin stress fibers across the cell body. On softer but chemically identical ECM substrates (10 kPa), fibroblasts fail to polarize and exhibit fewer and less robust actin stress fibers (Prager-Khoutorsky et al., 2011). Despite numerous studies, the interplay among actin assembly, force generation, and adhesion structure remains unclear.

Podosomes and focal adhesions are both integrin-mediated multimolecular assemblies for cell adhesion (Calle et al., 2006; Geiger et al., 2001; Machesky et al., 2008). Many adherent cells, such as epithelial cells or stromal fibroblasts cultured in vitro, maintain stable adhesions to the substratum via focal adhesions, adhesion structures interconnected by an actomyosin contractile network (Cai and Sheetz, 2009; Vogel and Sheetz, 2009). On the other hand, monocytic-lineage-derived cells such as macrophages utilize an alternative structure known as a podosome as their primary adhesion machinery (Cox et al., 2012; Murphy and Courtneidge, 2011). Podosomes characteristically contain WASP, cortactin Arp2/Arp3, and actin filaments in the center (podosome core, usually 1 μm in diameter and 2 μm in height), which is surrounded by a ring of integrin and integrin-associated proteins, such as talin, vinculin, and paxillin. Alternatively, transformation of fibroblasts by constitutively active Src kinase will also drive podosome or invadopodia formation with N-WASP substituting for leukocyte-restricted WASP. N-WASP/WASP and Arp2/Arp3 are regarded as markers of podosomes as they are not seen at focal adhesions, but otherwise the two adhesive structures share many molecular components, though

the spatial organization of these components is very different (Gimona et al., 2008). Although a wealth of experimental detail is now available, the underlying mechanism of podosome assembly and whether it is force dependent comparable to the situation with focal adhesions are largely unknown.

Mobile RGD ligands on nanopatterned supported lipid membranes provide a simple means to study force-mediated signal transduction events at the cell membrane and have been widely used in various cell biological investigations, such as studies of the immunological synapse (Mossman et al., 2005), ephrin-mediated cancer metastasis (Salaita et al., 2010), and force-modulated integrin adhesion (Yu et al., 2011, 2012a). Previously, we have utilized RGD-tagged lipids in supported membranes (RGD biotin bound to Cascade blue neutravidin bound to biotin lipid) with or without nanopartitioned lines to trigger integrin activation and to investigate force-dependent and independent functions during early cell spreading (Yu et al., 2011). Continuous films of RGD membranes generally exhibited long-range lateral mobility (diffusion coefficient 2 $\mu m^2/s$) and were substrates with infinitesimal elasticity (Evans and Yeung, 1994; Evans and Hochmuth, 1978) (zero rigidity/shear modules, equivalent film viscosity 0.1 N-s/m^2). When the long-range mobility of the RGD membrane was locally restricted by fabricating metal lines as nanopartitions within the bilayers (typically 100 nm line width and 5 nm thick with 1–4 μm line pitch, passivated by BSA or casein) (Yu and Groves, 2010; Yu et al., 2010), mobile RGD-integrin clusters assembled stable adhesions across the adjacent partitions with 1 and 2 μm, but not with 4 μm, pitch through force generation and adhesion maturation. This system was ideal for testing matrix-dependent mechanical regulation of adhesion formation.

Various signal transduction pathways can regulate cell-matrix adhesions. Anionic phospholipids, such as phosphatidylinositol (4,5)-bisphosphate (PIP2) and phosphatidylinositol (3,4,5)-triphosphate (PIP3) are dynamically regulated in plasma membranes (McLaughlin et al., 2002; Xu et al., 2003). Local enrichment of these negatively charged lipids can initiate N-WASP/WASP-mediated actin polymerization at plasma membranes (Papayannopoulos et al., 2005; Pollitt and Insall, 2009). Class IA phosphoinositide 3-kinase (PI3K) is composed of two subunits, p85 (regulatory) and p110 (catalytic), that phosphorylate PIP2 to generate PIP3 (Vanhaesebroeck et al., 2012), raising local PIP3 concentrations. On the other hand, PTEN dephosphorylates PIP3 to PIP2, decreasing PIP3 concentrations. While the biochemical interaction of p85beta and focal adhesion kinase (FAK) has been reported previously (Chen et al., 1996), N-WASP and Arp2/Arp3 actin polymerization complexes are absent at tension-loaded focal adhesions. Here, we report that spatiotemporal recruitment of PI3K and local enrichment of PIP3 at integrin-mediated adhesion sites on traction-force free RGD membranes play an important role in differential signal transduction leading to podosome formation.

RESULTS

Formation of Podosome-like Adhesion Follows Initial Integrin Clustering of RGD Lipids

Although THP1 monocytic cells treated with transforming growth factor $\beta 1$ have been used as a model system to study podosomes on regular matrix-coated substrates (Monypenny et al., 2011), fibroblasts generally do not form podosomes on matrix-coated substrates unless transformed by Src (Oikawa et al., 2008; Tarone et al., 1985). It was therefore surprising to see that nontransformed fibroblasts (RPTP$\alpha^{+/+}$ mouse embryonic fibroblasts and REF52 rat fibroblasts) formed podosome-like adhesions when plated on freely diffusive RGD lipids (Figure 1A) without artificially elevated Src activity. About 70% of REF52 fibroblasts developed podosome-like adhesions after 45 min of initial adhesion (Figure 1B; total of 321 cells in four experiments), while the same cells seeded on immobilized RGD-coated glass consistently formed classic focal adhesions (Figure 1A). In parallel, we also observed podosome formation in THP1 cells on RGD-supported bilayers (Figure 1D; Movie S1).

To understand the development of podosome-like adhesions in fibroblast cells, we examined the process of adhesion formation on RGD membranes. We found that cells assembled RGD-integrin clusters during the early adhesion process, as we described previously (Yu et al., 2011, 2012a). Similar to the case of focal complex and focal adhesion formation, the activated RGD-integrin receptors promptly recruited various integrin-binding proteins such as talin and paxillin and nucleated micrometer-sized clusters as nascent adhesion structures. However, RGD-integrin clusters on continuous RGD lipid bilayers were not interconnected by actin stress fibers and developed into podosomes after 45 min of initial adhesion (Figure 1C; Movie S2). The formation of podosome-like adhesions on RGD membranes was characterized by actin filament assembly in the podosome core at the center of individual RGD-integrin clusters (Figure 1D). Integrin-associated proteins, such as talin, paxillin, and vinculin, were consequently repartitioned into the ring structure (podosome ring) surrounding the actin core (Figures 1D and 1F).

Podosome-like Adhesions Have the Same Components as Classic Podosomes

To better identify the molecular organizations of podosome-like adhesion on RGD membranes, we rigorously examined more than 20 different molecular components (Table S1) that have been identified previously (Linder and Kopp, 2005). We found that podosome-like adhesions shared identical components in classic podosomes in macrophages. Therefore, we refer to podosome-like adhesions on RGD membranes as "podosomes" in the rest of this article. Podosome cores were enriched in F-actin and other characteristic molecular markers, such as Arp2/Arp3, WIP, and N-WASP, that were absent in classic focal adhesions (Figures 1F and S2A). The metalloproteinase, MMP-14 (MT1-MMP), was not enriched at podosomes of nontransformed fibroblasts or THP1 macrophages (Figure S1B). However, Src-transformed fibroblasts exhibited a high level of MMP-14 at invadopodia or long-lasting podosomes (Figure S1B), as previously reported (Wu et al., 2005). In addition, Tks5, a key adaptor protein in invadopodia formation, was not enriched at podosomes in nontransformed fibroblast on RGD membranes (Figure S1C).

Podosomes Are Dynamic Structures Formed by Arp2/Arp3-Mediated Actin Polymerization

Intense F-actin polymerization within RGD-integrin clusters as visualized by LifeAct was a signature of podosome formation

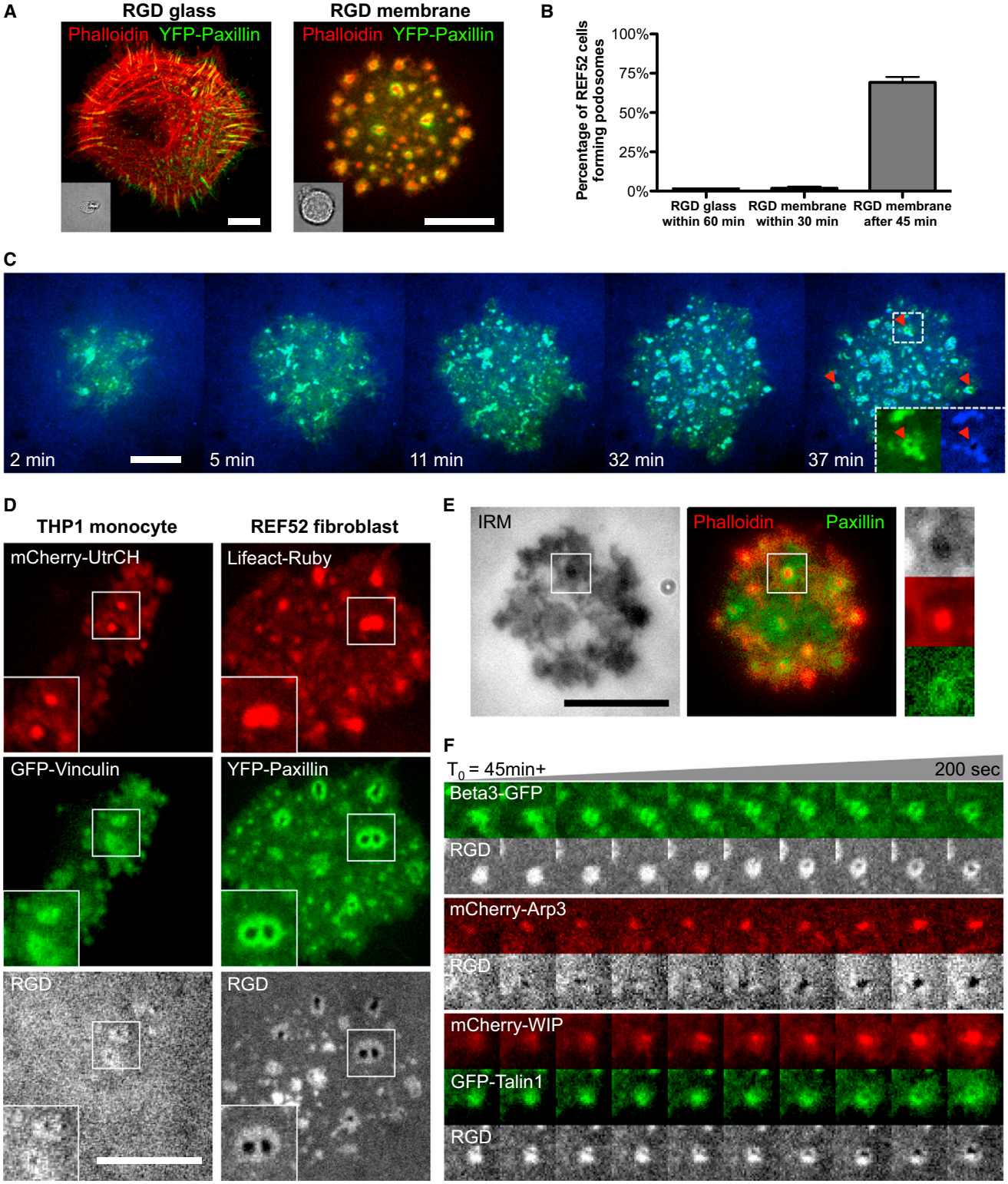

Figure 1. Podosome Formation on RGD Membrane

(A) REF52 fibroblast forms regular focal adhesion on RGD glass but developed podosomes on RGD membrane after 45 min of initial adhesion.

(B) Percentage of REF52 fibroblast cells forming regular adhesion and podosomes on RGD-coated glass or RGD membrane. A total 321 cells in four experiments were used.

(legend continued on next page)

at prepodosomal RGD clusters, and Arp2/3 was enriched at podosome cores (Figure 1F). The Arp2/Arp3 inhibitor CK-666 (Nolen et al., 2009) effectively abolished podosome formation (100 μM, 28 cells in two experiments; Figure S1). Formins, such as mDia1, DAAM1, and FHOD1, were not enriched at the podosomes (Figure S2A). SMIFH2 has been shown to inhibit mDia1- and mDia2-mediated actin polymerization in vitro and in vivo (Rizvi et al., 2009). However, SMIFH2 formin inhibitor did not suppress podosome formation in RPTP$\alpha^{+/+}$ mouse embryonic fibroblasts (Figure S2B). Thus, the actin cores of these podosomes were assembled by Arp2/Arp3-dependent actin polymerization and were not dependent on formin activity. Myosin-II, visualized by myosin regulatory light chain (MLC) was not enriched at podosomes. The disassembly of podosomes correlated with sparse recruitment of MLC around the dissociating actin core (Movie S3; Figure S4C) and a return to prepodosomal RGD-integrin clusters. The transition between podosome and adhesion clusters often repeated multiple times. Unlike long-lasting invadopodia (stable for hours), each podosome on RGD membranes exhibited a lifespan of 2–20 min.

Previously, interference reflection microscopy (IRM) was used to highlight close-contact zones at the cell-matrix interface (Holt et al., 2008), and the podosome core indeed showed close contact to the supporting substrate (Figure 1E). The tight contact revealed by destructive interference between two closely apposed interfaces indicated that the podosomes were protrusive (Evans et al., 2003; Monypenny et al., 2011). Intriguingly, the intensity of RGD fluorescence at the podosome core was diminished and immediately recovered after podosome disassembly (Figure S3B), which indicated that either the cell protrusive force was pushing out the RGD ligands and/or was creating a void in the bilayer. When bilayer continuity was tested with fluorescent lipid probes, such as Texas red-labeled 1,2-dihexadecanoyl-sn-glycero-3-phosphoethanolamine (Texas red DHPE), doped into the supported bilayer, the fluorophores remained evenly distributed at the podosome core (Figure S3A), suggesting that the podosomes were indeed protrusive.

Along with Arp2/Arp3, cortactin, and WIP accumulation (Figure S2A), RGD depletion from the core was another unique phenomenon observed during the transformation from prepodosomal RGD clusters to podosomes. In more than 20 independent experiments with both macrophages and nontransformed fibroblasts, we rigorously examined and confirmed that F-actin polymerization and RGD depletion were always concurrent. While prepodosomal RGD clusters can be in an arbitrary ring shape, we always verified podosome formation by classic podosome markers and RGD depletion inside the RGD ring during live cell imaging (Table S1; Figure 3B). Thus, the podosomes in fibroblasts on RGD membranes exhibit the normal protrusive behavior, morphology, and dynamics of podosomes in macrophages.

Force Generation in Nanopartitioned RGD Membranes Suppresses Podosome Formation

To test whether or not force on adhesions would affect podosome formation, we spread cells on nanopartitioned RGD bilayers where it was previously shown that cells would generate force on adhesions and stabilize them (Yu et al., 2011). The RGD bilayers were partitioned by nanofabricated metal lines (typically 100nm line width and 5nm in height) that provided passive resistance to adhesion movement. Previously, we demonstrated that the line pitch of partitioning barriers on an RGD membrane was inversely related to cell adhesion area. A smaller line pitch between barriers provided a higher density of barriers to RGD-integrin cluster movement and cells spread over larger areas. Cells formed focal adhesions with stress fibers, but they did not form podosomes when plated on nanopartitioned RGD membranes with a 1 μm line pitch (10% surface density). The immobilized RGD-integrin clusters were linear and were linked by actin fibers (hollow arrows in Figure 2A) after 60 min of initial adhesion. Furthermore, when cells were plated on nanopartitioned RGD membranes with a 4 μm line pitch that did not support force generation, podosome formation was restored. At the beginning, cells nucleated RGD clusters adjacent to nanopatterned lines with a 4 μm pitch, but there were no actin stress fibers between RGD clusters and cells had a smaller spread area. After 60 min of adhesion, these RGD clusters were also converted to podosomes (white arrowheads in Figure 2A). Interestingly, when RGD membranes were partitioned by dot arrays (300 × 300 nm^2 metal areas with 1 μm pitch, also 9% of surface density) that provided no spatial confinement of RGD ligands, cells failed to develop force-stabilized RGD-integrin clusters and formed podosomes (Figure 2A). With increasing distance between the membrane partitions, fewer force-stabilized adhesion sites were nucleated, and podosome formation consequently increased (Figure 2C; total of 47 cells in three experiments). More surprisingly, when a single cell adhered to both a continuous and a partitioned RGD membrane, podosomes formed only on the continuous region and did not form at the partitioning lines (Figure 2B; Movie S4). Thus, we suggest that force generation by contraction to the lines produced a local signal that suppressed podosome formation within spatially restricted regions.

Recruitment of p85beta Precedes Podosome Formation and Local Enrichment of PIP3

To determine what factors might be involved in stimulating podosome formation in the absence of force, we looked at Src kinase

(C) Transition from initial RGD-integrin clusters to podosomes in REF52 fibroblast adhered on RGD membrane (Movie S2). Inset: podosomes (red arrowheads) were identified by ring formations of both RGD and YFP paxillin. (D) THP1 monocytes and REF52 fibroblasts both formed podosomes on RGD membrane. The dense actin core is surrounded by adhesion proteins, such as paxillin, vinculin, and RGD-integrin clusters. The center of the podosome ring is depleted from RGD. (E) Interference reflection microscopy reveals tight contacts at the protrusive podosome core in REF52 fibroblast cells. Inset (top to bottom): RICM, CF594 phalloidin (F-actin staining), and YFP paxillin.

(F) Development of podosomes (4 × 4 μm^2 each frame) in REF52 fibroblast cells. Integrin β3, talin, and RGD clusters are reorganized to form the podosome ring. Arp3 and WIP are enriched at the podosome core.

Error estimates are SEM. The scale bar represents 10 μm.

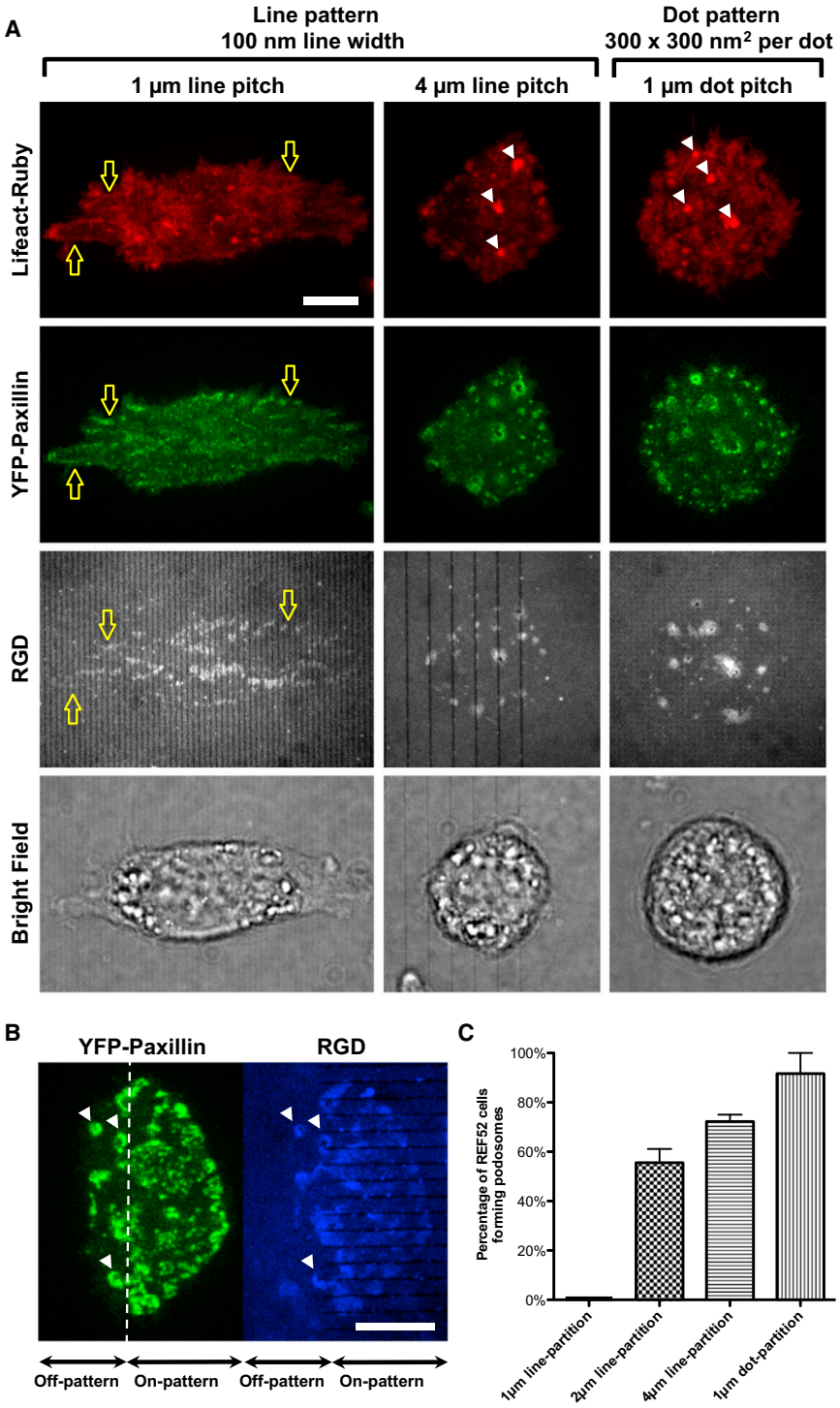

Figure 2. RGD Membrane with Dense Partitioning Barriers Prevents Podosome Formation

(A) Nanopatterned lines (100 nm line width, with 1 to 4 μm line pitch) were prefabricated on glass substrate before RGD membrane deposition. The cell formed regular adhesion and actin stress fibers (white hollow arrows) on line-partitioned RGD membrane with 1 μm pitch. However, podosome formation (white arrowheads) remained when the cell adheres on RGD membrane with a 4-μm-pitch line partition, as well as 1-μm-pitch dot arrays (each dot area: 300 × 300 nm^2).

(B) When a single cell adhered to both a continuous and a partitioned RGD membrane, podosomes (white arrowheads) formed only on the continuous region and did not form between the partitioning lines (Movie S4).

(C) Percentage of REF52 fibroblast cells forming podosomes when adhering on various patterned RGD membranes. Denser line partitions in RGD membranes result in less podosome formation. A total of 47 cells in three experiments were used. Error estimates are SEM. The scale bar represents 10 μm.

activity and PIP3 formation. After inhibition of Src by PP2 (10–20 μm, 2 hr), podosomes still formed, but at only 40% of the frequency of control cells (Figure S6A; total of 104 cells in three experiments). In the case of PIP3 formation, we found the localized recruitment of class 1A PI3K regulatory subunit p85beta at pre-podosomal RGD clusters preceded actin assembly and appeared to trigger podosome formation (Figures 3A and 3B, arrow). During the initial phase of podosome formation, EYFP-p85beta was initially recruited to a subset of preexisting integrin-RGD clusters (Figure S4A) and then it expanded to the podosome rings (Figure 3B; Movie S5). In parallel, we monitored the time-dependence of PIP3 production by measuring the level of Akt-PH binding and we measured a marked increase in Akt-PH binding during the transition from RGD clusters to podosomes (Figure 3C). In addition, N-WASP was recruited at podosome cores (Figure 3D).

To determine if local enrichment of PIP3 triggered podosome formation, we inhibited PI3K activity by Wortmannin (100 nM). Fibroblasts can still develop initial RGD clusters after PI3K inhibition, but podosome formation on RGD membranes was blocked (Figures 4C and S6C; total of 108 cells in four experiments). While p85beta was also found at regular focal adhesions (Figure S5A), there were no significant changes in local PIP3 levels at the adhesions (Figure S5B), and N-WASP was not recruited at focal adhesions (Figure S5C). Thus, we suggest the recruitment of class IA PI3K caused the rise in PIP3 levels that led to F-actin assembly in the transformation of prepodosomal RGD-integrin clusters to podosomes on traction-force-free RGD membranes.

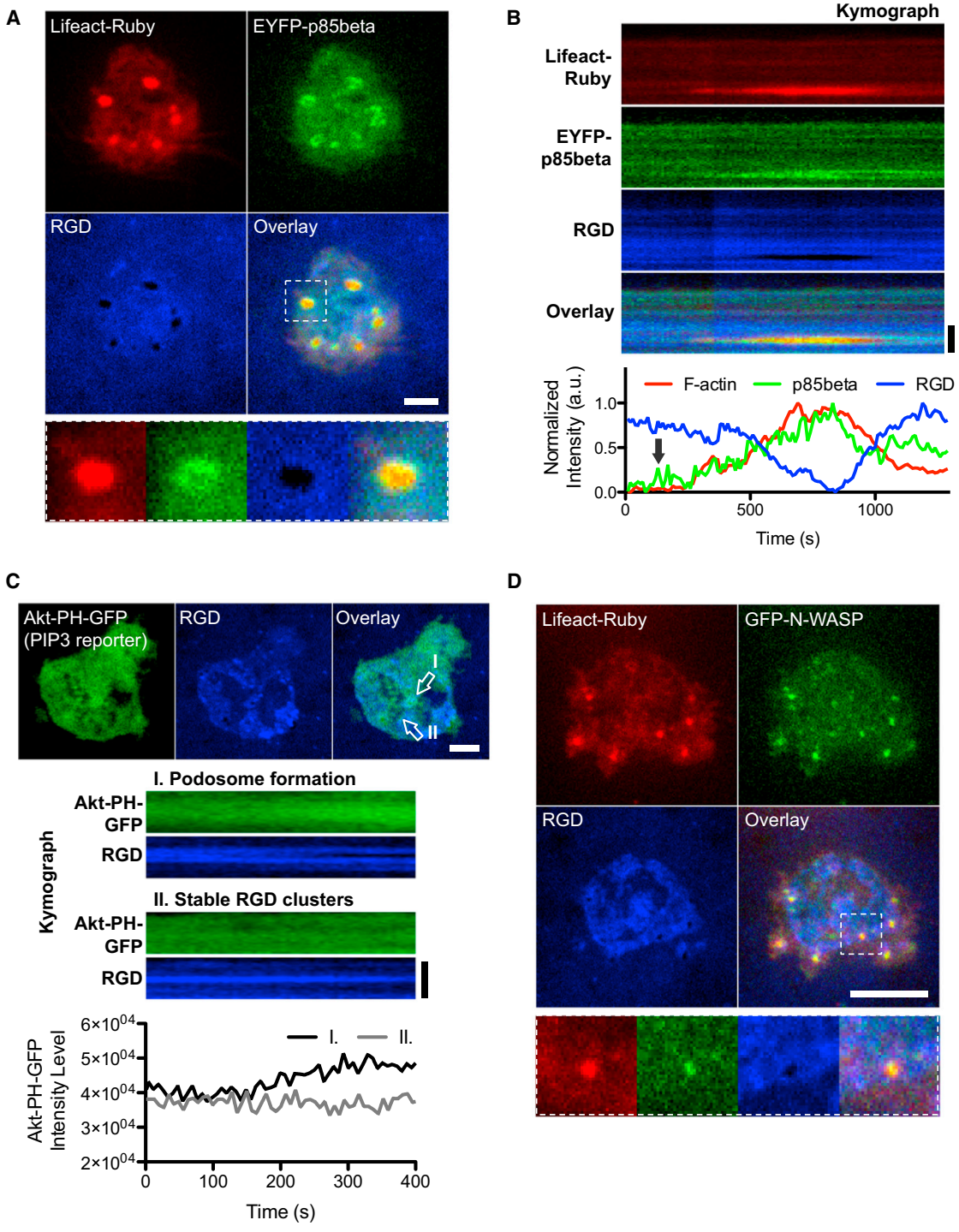

Figure 3. Dynamical p85beta Recruitment and Increased PIP3 Level Turn RGD Clusters into Podosomes

(A) Class IA PI3K regulatory subunit p85beta was recruited at podosomes.

(B) Increased recruitment of p85beta at RGD clusters preceded F-actin polymerization. Spatial-temporal recruitment of F-actin and p85beta were analyzed by kymographs and intensity-time plot. p85beta was recruited at a subset of RGD clusters that subsequently turned into podosomes. As dot-like F-actin started to polymerize podosome core, p85beta reorganized from podosome core to podosome ring (Movie S5).

(C) Local enrichment of PIP3 during podosome formation. PIP3 levels were monitored by Akt-PH. The PIP3 level increased during the void formation within the RGD cluster (zone I) as a result of podosome formation on RGD membranes. The PIP3 level remains unaltered in stable RGD clusters (zone II).

(D) N-WASP was recruited at podosome cores. The scale bar represents 5 μm.

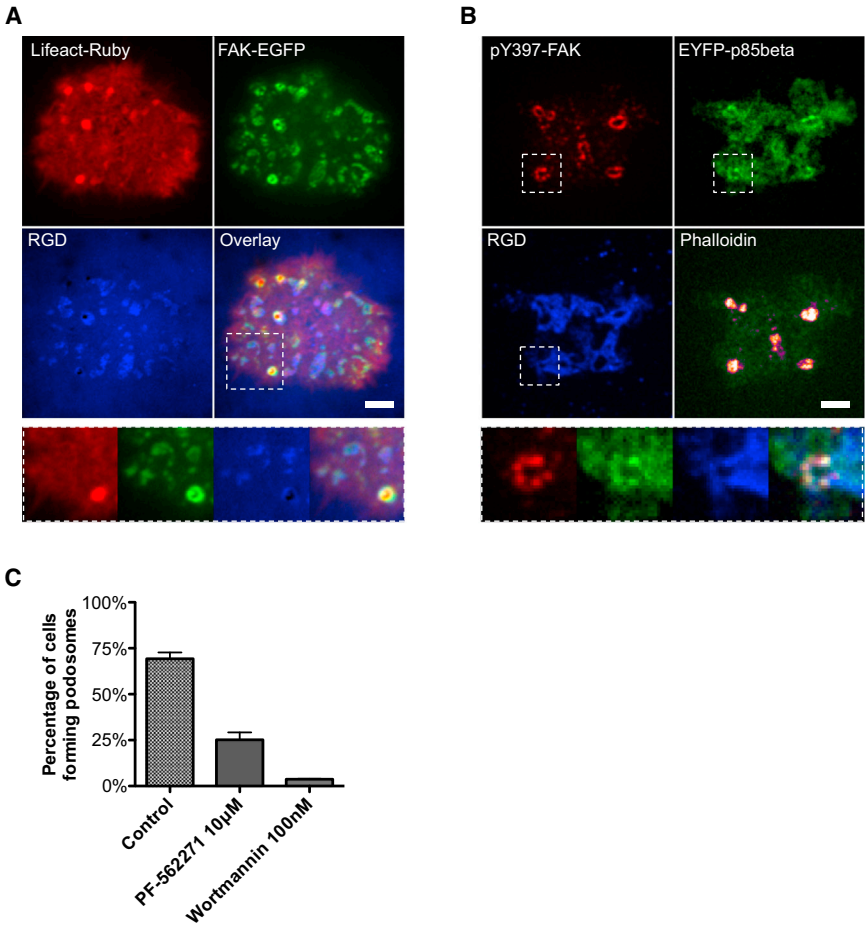

Figure 4. Autophosphorylation of FAK Recruits p85beta at RGD Clusters

(A) FAK was recruited at RGD clusters and was more enriched at podosome rings.

(B) p85beta and pY397 FAK were both enriched at podosome rings.

(C) Podosome formation was suppressed by the FAK/Pyk2 inhibitor PF-562271, which blocked the autophosphorylation of FAK and Pyk2. The PI3K inhibitor Wortmannin also effectively abolished podosome formation. Error estimates are SEM. The scale bar represents 5 μm.

In terms of the degradation of PIP3 and podosome disassembly, PTEN was found at podosomes, but it only appeared after p85beta. It was often found above the focal plane of RGD-integrin clusters and decreased as F-actin disassembled (Figure S4B). In addition, the level of PIP3 decreased with the disassembly of the F-actin core. This suggests that a sustained level of PIP3 is necessary for maintenance of the F-actin core.

Tyrosine Autophosphorylation of Both FAK and PYK2 Regulates p85beta Recruitment

As p85beta is known to bind to substrates with phosphotyrosines via SH2 domains (Songyang et al., 1993), we looked for possible tyrosine kinases that may have been involved. Classical PI3K activation often involved autophosphorylation of receptor tyrosine kinase (RTK), as well as focal adhesion kinase (FAK) (Chen et al., 1996). After testing a number of RTK inhibitors that did not block podosome formation, we tested the dual FAK and Pyk2 kinase inhibitor PF-562271 (Roberts et al., 2008) and found that it efficiently suppressed podosome formation on RGD membranes. We found that FAK was recruited to RGD-integrin clusters (Figure 4A) and Y397 of FAK was autophosphorylated and colocalized with EYFP-p85beta at podosomes (Figure 4B). When FAK/Pyk2 autophosphorylation was inhibited by PF-562271 (10 μM, 4 hr pretreated), fibroblasts can still form initial RGD clusters, but p85beta recruitment was suppressed. Only 25% of fibroblasts were able to form podosomes on RGD membranes (Figures 4C and S6D; total of 139 cells in three experiments). Thus, we suggest autophosphorylation of FAK (Y397) and Pyk2 (Y407) recruited p85beta that triggered local enrichment of PIP3 at prepodosomal RGD clusters.

RhoA-GTP Levels Are Decreased upon Cell Adhesion to Mobile RGD Membranes

Since artificially upregulated RhoA-GTP levels and cellular contractility abolished podosome formation (Schramp et al., 2008; van Helden et al., 2008), we decided to determine if reduced RhoA-GTP was also correlated with podosome formation. Inhibiting Rho-associated protein kinase (ROCK) activity (Y-27632, 10 μM) or downregulating myosin-II-mediated contractility (blebbistatin, 50 μM) did not affect podosome formation on RGD membranes (Figure S6B; total of 60 and 59 cells examined in four experiments, respectively). In contrast, artificially upregulating cellular contractility by the RhoA agonist lysophosphatidic acid (LPA, 40 μM) or expressing a constitutively active RhoA-Q63L mutant effectively inhibited podosome formation (Figure S6B; total of 62 and 87 cells examined in four experiments, respectively). Furthermore, we utilized a fluorescence resonance energy transfer (FRET)-based RhoA biosensor (Pertz et al., 2006) to measure RhoA activity when cells adhered to different substrates (Figure 5B). REF52 cells plated on the mobile RGD membrane had a significantly lower FRET efficiency (0.45 ± 0.01 SEM, n = 30; Figure 5C) than on RGD-coated glass (0.73 ± 0.02 SEM, n = 25; Figure 5C; p value < 0.0001, two-sample t test, two-tailed). Thus, low levels of RhoA-GTP seem to be important for podosome formation.

To further investigate RhoA regulation, we tested two RhoA GTPase-activating proteins (GAPs), DLC1 and ARAP3, which localized to podosomes. While DLC1 was recruited at both focal adhesion and podosome rings through tensin (Schramp et al., 2008), ARAP3 has been shown to bind to PIP3 at plasma membranes (Krugmann et al., 2002, 2004). Indeed, we found that

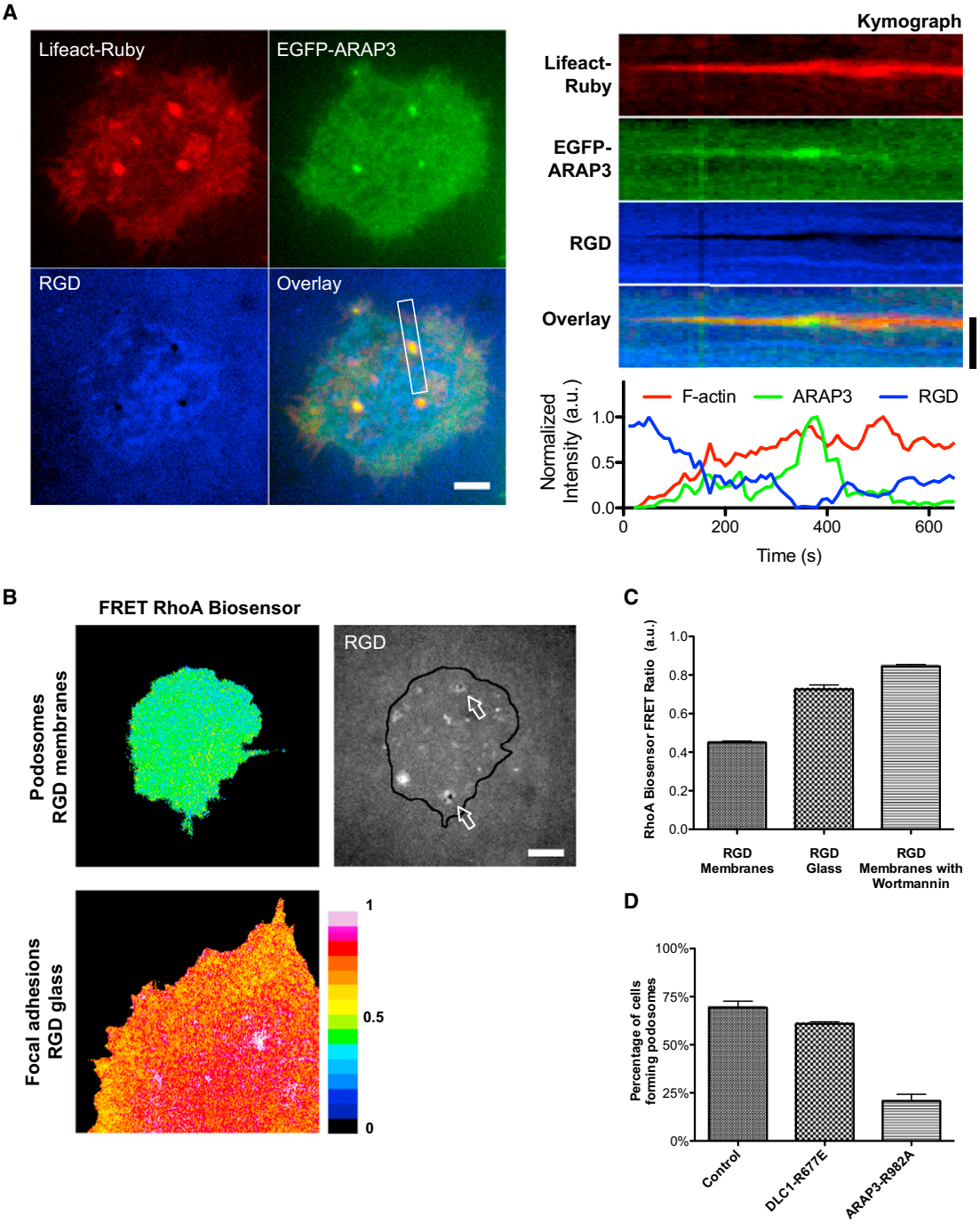

Figure 5. Low RhoA-GTP Levels Accompany Podosome Formation

(A) ARAP3, a PIP3-bound RhoA GAP, was recruited at the podosome core. Recruitment of ARAP3 increased as the F-actin podosome core developed and then decreased before F-actin dissembled. Spatial-temporal recruitment of F-actin and ARAP3 were analyzed by kymographs and intensity time plot.

(B) Color-coded heatmap images of RhoA activity in vivo. RhoA activity measured by a FRET-based RhoA biosensor indicated lower RhoA-GTP levels when REF52 fibroblast cells adhered and formed podosomes on RGD membranes. Higher RhoA-GTP levels were measured as cells adhered and form focal adhesion on RGD-coated glass.

(C) Comparison of RhoA activity via FRET efficiency between cells adhered on RGD membranes (0.45 ± 0.01 SEM, n = 30) and RGD glass (0.73 ± 0.02 SEM, n = 25); p value < 0.0001 (two-sample t test, two tailed). When PI3K was inhibited by Wortmannin, the FRET efficiency of the RhoA biosensor became high (0.85 ± 0.01 SEM, n = 29), even when cells adhered to the mobile RGD membrane.

(D) Differential effects of overexpressing two catalytic-dead RhoA GAP mutants, DLC1-R677E and ARAP3-R982A. Podosome formation was suppressed to 25% in the case of ARAP3-R982A but unaltered in the case of DLC1-R677E. Error estimates are SEM. The scale bar represents 5 μm.

ARAP3 was recruited at PIP3-enriched podosome cores after F-actin core formation (Figure 5A; Movie S6). However, ARAP3 was not recruited to focal adhesions (Figure S5D). We tested whether DLC1 or ARAP3 played important roles in podosome formation by transiently overexpressing catalytic-dead RhoA GAP mutants DLC1-R677E and ARAP3-R982A, respectively. Podosome formation was suppressed to 25% in the case of ARAP3-R982A (Figure 5D), but not significantly disrupted in the case of DLC1-R677E (total of 149 and 114 cells in three experiments, respectively). When PI3K was inhibited, the FRET efficiency of the RhoA biosensor increased significantly (0.85 ± 0.01 SEM, n = 29), even when cells adhered to the mobile RGD membrane (Figure 5C), and podosome formation was suppressed. These observations indicate that the RhoA-GTP level is inversely correlated with podosome formation and that recruitment of ARAP3 and possibly other RhoA-GAPs by local enrichment of PIP3 provided a positive feedback to downregulate cellular RhoA level in podosome-forming cells.

DISCUSSION

In these studies, we have demonstrated for that plating cells onto RGD ligands linked to fluid lipid bilayers caused the formation of integrin-based podosome-like adhesions. Surprisingly, such a response was characteristic not only of cells that produce podosomes under normal culture conditions, such as the macrophage line used here, but also of fibroblasts, which do not produce podosomes when plated onto "normal" rigid substrates. Although large traction forces mediated by RhoA are important for focal adhesion maturation in fibroblasts, there is no evidence that they are major determinants in podosome formation. Notably, macrophages do not develop large traction forces on matrix-coated substrates (Féréol et al., 2009) or mature focal adhesions, but they do form podosomes. The implications are that the components needed to form podosomes are present in fibroblasts and immune cells, but the combination of cell contractility and matrix mechanics plays the critical role in determining which type of adhesion is formed.

The podosome-like adhesions that form in the absence of force in nontransformed fibroblasts are indistinguishable from podosomes in macrophages in terms of morphology, components (Table S1), and protrusive dynamics (Figure 1E). However, their physiological functions, such as chemotaxis and endocytosis/exocytosis, need to be further examined. Spatial depletion of mobile RGD ligands and destructive interference at podosomes by IRM indicated that there was active protrusion of the podosome core (Figures 1E and S3B). While ligands on supported membranes were freely diffusive, the observed spatial exclusion of RGD-neutravidin (5.4 ± 5.8 nm footprint in the x-y dimension; Hendrickson et al., 1989) at the podosome core could not be explained by a simple repartitioning effect from ligation with integrin receptor (8 ± 12 nm footprint in the x-y dimension; Nermut et al., 1988). Nevertheless, supported lipid membrane remains evenly distributed at the podosome core (Figure S3A). The vertical force required to physically penetrate a lipid membrane via biomimetic stealth probes (200 nm in diameter) has been reported as 58 nN (Almquist and Melosh, 2010). We conclude that the protrusive force at podosomes was less than needed to penetrate the membrane but sufficient to block diffusion of RGD-neutravidin into the contact region.

Invadopodia or long-lived stable podosomes (more than 30 min) have been widely investigated in Src-transformed cells (induction of constitutively activated Src kinase) and invasive cancer cell lines (Huveneers et al., 2008; Oikawa et al., 2008). However, podosome-like adhesions on RGD membranes and invadopodia in Src-transformed cells are different in both dynamics and molecular components (Table S1). Constitutively activated Src causes hyperactivation of various downstream targets, such as ARHGEF5 RhoA-GEF (Kuroiwa et al., 2011), phosphorylation of Tks5/Grb2 complexes (Oikawa et al., 2008), and MMP-14 secretion (Poincloux et al., 2009; Wu et al., 2005; Yu et al., 2012b). Notably, Tks5 (Figure S1C) is not enriched at podosomes in nontransformed fibroblast on RGD membranes. In addition, we have examined the potential recruitment of MMP-14 and found that it was present at invadopodia in invasive cancer cells and Src-transformed fibroblasts. However, in nontransformed fibroblasts, most of the MMP-14 remained in endocytic vesicles and there was only a weak recruitment of MMP-14 around the podosomes (Figure S1B). This is all consistent with the hypothesis that podosomes formed in the absence of force are aided by but do not require Src activity.

Likewise, diaphanous-related formins are required for invadopodia formation in invasive MDA-MB-231 breast adenocarcinoma cells (Lizárraga et al., 2009). However, when we treated nontransformed fibroblasts and THP1-differentated macrophages with the formin inhibitor SMIFH2, we still observed podosome formation at a similar density to control cells. Podosomes and invadopodia share many molecular components, but most likely not all. We suggest that podosomes on RGD membranes indeed differ from long-lived invadopodia in Src-transformed cells or invasive cancer cells in their lifespan, formin involvement, Tks5 recruitment, and MMP-14 secretion.

Our data suggest that conventional traction force development and myosin-II activities are dispensable in podosome formation. Mobile RGD membranes with nanopartitioning lines provide a unique platform to examine the force-regulated adhesion structure transformation (Figure 2A). As cells adhere to RGD membranes, initial integrin activation results in RGD clustering without traction force. With dense line-partitioned RGD membranes, such as with 1 or 2 μm line pitch, forces can be generated on RGD-liganded integrins to form traction-force loaded adhesions (Figure 2A) after activation of initial spreading. Because the local contraction units are unable to span the 4 μm spacing (Ghassemi et al., 2012; Yu et al., 2011), the podosomes form as well on the larger line spacing as on continuous bilayers. In addition, myosin-II is not recruited during podosome formation on RGD membrane (Figure S4C). Thus, our data indicate that podosome formation requires minimum traction force development and that the local force generation between RGD-integrin adhesion clusters at dense line-partitioned RGD membranes inhibits podosome formation. When the same cell covers both the 2 μm pitch lines and a continuous membrane (Figure 2B), there is a remarkably local formation of focal adhesions at the lines while podosomes form over continuous membrane regions, indicating that the effect of contractility is local and may involve spatial contact signals.

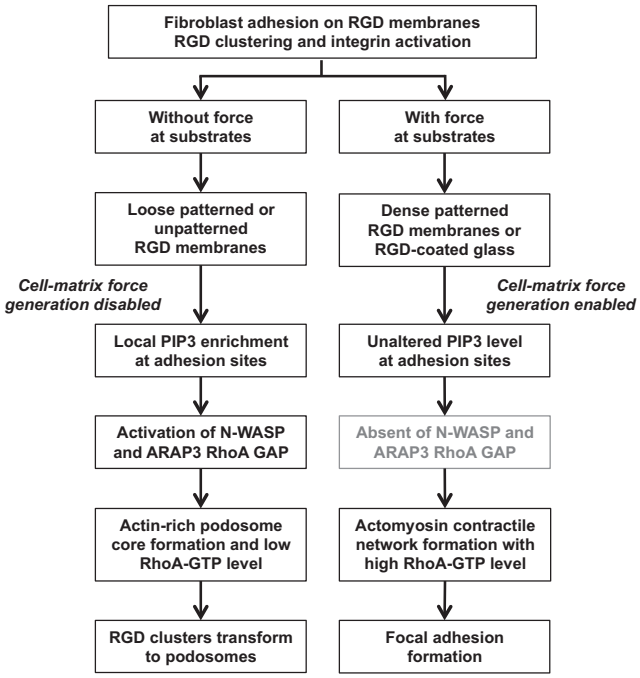

Figure 6. Summary of Force-Mediated Adhesion Transformation Pathway

Early RGD-integrin activation triggered actomyosin contraction. When substratum provides traction force (1 μm line-pitch RGD membranes), cells form classic focal adhesions. When substratum provides no traction force, RGD-integrin clusters can turn into podosomes after 45 min of initial adhesion. Local enrichment of PIP3 by PI3K activation at the prepodosomal RGD cluster triggers N-WASP and Arp2/Arp3-mediated actin polymerization that initiated podosome formation. Recruitment of ARAP3 via local enrichment of PIP3 serves as a positive-feedback mechanism to downregulate RhoA-GTP in podosome-forming cells.

Although we do not fully know how local contractions are translated into inhibition of podosome formation, we find that peak production of PIP3 is the key upstream event to trigger the transformation from prepodosomal integrin-RGD clusters to podosomes (Figure 6). Class IA PI3K regulatory subunit p85beta is first recruited at activated integrins through binding to autophosphorylated FAK and possibly Pyk2, and local production of PIP3 is observed by an increased level of Akt-PH-GFP. Inhibition of FAK and Pyk2 by PF-562271 (Roberts et al., 2008) effectively block podosome formation. Indeed, autophosphorylation site Y397 of FAK can bind p85beta (Chen et al., 1996), and Pyk2 has the same sequence (Y-A-E-I) at its tyrosine autophosphorylation site, Y402. In the case of fibroblasts, the activation of Pyk2 appears to be best correlated with podosome formation on RGD lipids, since FAK$^{-/-}$ cells and cells treated with a FAK-specific inhibitor form podosomes normally (C.-H.Y. and M.P.S., unpublished data). Pyk2 also plays an important role in podosome formation in osteoclasts (Gil-Henn et al., 2007), but we cannot rule out another kinase because there could be off-target inhibition of other kinases by PF-562271. In addition, FAK can phosphorylate N-WASP and promote actin polymerization, and inhibition of FAK kinase activity suppresses N-WASP activity (Tang et al., 2013). However, N-WASP can still be phosphorylated by other kinases, such as Src family kinases (Dovas and Cox, 2010) or Abl kinase (Burton et al., 2005). While N-WASP could be activated by other kinases, N-WASP may fail to be recruited at RGD clusters without local enrichment of PIP3. We suggest that inhibition of FAK and Pyk2 autophosphorylation provides a mechanism to abolish local production of PIP3 by perturbing p85/PI3K association. As expected, inhibition of PI3K also suppresses podosome formation (Figure 4C).

Another protein that binds to PIP3 is PTEN, and it dephosphorylates PIP3, thereby causing the loss of actin polymerizing proteins. It has previously been shown that PTEN is present in and regulates podosome/invadopodia formation (Hoshino et al., 2012; Poon et al., 2010). PTEN associates with podosomes after the actin core is formed and contributes to the disassembly of the podosome F-actin core. Thus, it seems that the cycle of podosome formation and disassembly is primarily dependent upon the local levels of PIP3 on plasma membranes. This can explain the regional differences in podosome formation we see in single cells (Figure 2B; Movie S4) through slower two-dimensional diffusion of PIP3 lipids rather than fast diffusive cytosolic signals.

A factor that could contribute indirectly to the formation of podosomes is RhoA activity. Using the FRET-based RhoA biosensor, lower RhoA-GTP levels are observed when cells develop podosomes, and pharmaceutically activating RhoA-mediated contractility using LPA is seen to abolish podosome formation on RGD membranes, in agreement with previous reports (Schramp et al., 2008; van Helden et al., 2008). More than 70 Rho GAPs have been identified in eukaryotes (Tcherkezian and Lamarche-Vane, 2007), and it remains unclear how RhoA activities are differentially regulated during adhesion formation. While DLC1 is linked to downregulation of RhoA in Src-transformed cells (Schramp et al., 2008), we find that the PIP3-binding protein ARAP3 is another RhoA-regulating factor recruited at podosome cores. ARAP3 contains both RhoA GAP and Arf6 GAP domains, and the RhoA GAP function of ARAP3 is activated by Rap-GTP (Krugmann et al., 2002, 2004). ARAP3's Arf6 GAP function in vivo, however, is still under investigation (Gambardella et al., 2011). Inhibition of PI3K upregulates RhoA-GTP and cellular contractility (Krugmann et al., 2004; Orlova et al., 2007), and our RhoA biosensor measurements also agree with previous findings (Figure 5C). Using overexpressed catalytic-dead RhoA GAP mutants, we find ARAP3-R982A moderately suppresses podosome formation, while DLC1-R677E has no significant effect. However, ARAP3 is recruited largely after podosomes are formed. Recruitment of ARAP3 provides a positive-feedback mechanism to downregulate RhoA-GTP. Thus, our results indicate that manipulations of traction force development at integrin-matrix clusters can serve as a mechanical signal to modulate adhesion phenotype switching and RhoA activities.

In conclusion, we suggest that the development of podosomes as adhesion structures implicates the absence of traction forces between integrin receptors and matrix ligands. Lack of traction forces at activated RGD-integrin clusters results in spatial-temporal recruitment of p85beta and local enrichment of PIP3, which is not observed in force-loaded focal adhesions. This PIP3-dependent pathway of podosome formation does not require

the induction of constitutively activated Src kinase and is further aided by the inactivation of RhoA by PIP3-mediated recruitment of ARAP3. We suggest that local contractions may directly inhibit podosome formation while facilitating focal adhesion formation through a block of the PIP3-dependent pathway. The transformation between prepodosomal RGD-integrin clusters and podosomes is a remarkable example of mechanosensing through cell-adhesion processes. The reorganization of adhesion structures triggered by changing microenvironments has become an emerging theme of adaptive regulation in cellular signaling. Force and matrix ligand and integrin composition are all critical factors regulating adhesion phenotype and turnover.

EXPERIMENTAL PROCEDURES

Cell Culture and Fluorescent Fusion Proteins

Nontransformed RPTP$\alpha^{+/+}$ mouse embryonic fibroblasts (Su et al., 1999), rat embryonic fibroblast (REF52), and THP-1 (human monocytic leukemia cells) were used in this study. Detailed information regarding cell culture, transfection protocol, the plasmids of fluorescent fusion proteins, and microscopy methods can be found in the Supplemental Experimental Procedures.

RGD-Supported Lipid Bilayer Membranes

1,2-dioleoyl-*sn*-glycero-3-phosphocholine (DOPC) and 1,2-dipalmitoyl-*sn*-glycero-3-phosphoethanolamine-N-(cap biotinyl) (16:0 biotinyl-Cap-PE) were purchased from Avanti Polar Lipids. The lipids (0.2 mol% of biotinyl-Cap-PE and 99.8 mol% of DOPC) were mixed with an equal volume of 1× PBS and then pipetted onto cleaned glass substrates for the self-assembly processes. A total of 0.1 μg/ml of Cascade blue neutravidin (Life Technologies) or DyLight 680 neutravidin (Thermo Fisher Scientific) was added onto supported lipid membranes, followed by 1 μg/ml of biotinylated RGD, *cyclo* (Arg-Gly-Asp-D-Phe-Lys[Biotin-PEG-PEG]; Peptides International). Detailed information regarding lipid preparation and membrane functionalization can be found in the Supplemental Experimental Procedures.

Nanopatterned Glass Substrate

Nanoimprint lithography was utilized to fabricate the physical barriers on glass substrates, and detailed preparation methods were previously described (Yu et al., 2011). In brief, a silicon-based imprint mold was fabricated by electron-beam lithography and anisotropic etching processes. First, Coverglasses (Warner Instruments) were cleaned by Piranha solution (sulfuric acid and hydrogen peroxide, mixed in 3:1 ratio) for 15 min, rinsed with deionized water, and then spin-coated with UV-curable imprint polymers. Patterns were then transferred from the mold to the glass by high-pressure stamping the imprint mold onto the polymer-coated coverglass and curing the polymer by UV exposure. After demolding, oxygen plasma etching was used to extend imprinted trenches vertically to the surface of the coverglass. A thin chromium metal layer was deposited onto the exposed glass surface by thermal evaporation. The chromium on imprinted polymers was removed by resist lift-off processing. Typically, metal lines were 100 nm in width and 5 nm in height with a gap distance ranging from 1 to 4 μm. The density of the metal lines remains constant and is about 10% per μm^2.

SUPPLEMENTAL INFORMATION

Supplemental information includes Supplemental Experimental Procedures, six figures, one table, and six movies and can be found with this article online at http://dx.doi.org/10.1016/j.celrep.2013.10.040.

AUTHOR CONTRIBUTIONS

C.-H.Y. and N.B.M.R. conducted and analyzed most of the experiments. A.K. and K.L.H. assisted in sample preparations. C.-H.Y., G.E.J., A.D.B., and M.P.S. supervised this study and prepared the manuscript.

ACKNOWLEDGMENTS

C.-H.Y. acknowledges support from National Science Council of Taiwan (grant NSC98-2917-I-564-165). N.B.M.R. is funded by a joint National University of Singapore and King's College studentship. G.E.J. is supported by the Medical Research Council, UK (G1100041) and a generous provision of a visiting professorship to the Mechanobiology Institute, Singapore.

Received: April 26, 2013
Revised: September 5, 2013
Accepted: October 24, 2013
Published: November 27, 2013

REFERENCES

Almquist, B.D., and Melosh, N.A. (2010). Fusion of biomimetic stealth probes into lipid bilayer cores. Proc. Natl. Acad. Sci. USA *107*, 5815–5820.

Burton, E.A., Oliver, T.N., and Pendergast, A.M. (2005). Abl kinases regulate actin comet tail elongation via an N-WASP-dependent pathway. Mol. Cell. Biol. *25*, 8834–8843.

Cai, Y., and Sheetz, M.P. (2009). Force propagation across cells: mechanical coherence of dynamic cytoskeletons. Curr. Opin. Cell Biol. *21*, 47–50.

Calle, Y., Burns, S., Thrasher, A.J., and Jones, G.E. (2006). The leukocyte podosome. Eur. J. Cell Biol. *85*, 151–157.

Chen, H.C., Appeddu, P.A., Isoda, H., and Guan, J.L. (1996). Phosphorylation of tyrosine 397 in focal adhesion kinase is required for binding phosphatidylinositol 3-kinase. J. Biol. Chem. *271*, 26329–26334.

Cox, S., Rosten, E., Monypenny, J., Jovanovic-Talisman, T., Burnette, D.T., Lippincott-Schwartz, J., Jones, G.E., and Heintzmann, R. (2012). Bayesian localization microscopy reveals nanoscale podosome dynamics. Nat. Methods *9*, 195–200.

Dovas, A., and Cox, D. (2010). Regulation of WASp by phosphorylation: Activation or other functions? Commun. Integr. Biol. *3*, 101–105.

Engler, A.J., Sen, S., Sweeney, H.L., and Discher, D.E. (2006). Matrix elasticity directs stem cell lineage specification. Cell *126*, 677–689.

Evans, E., and Yeung, A. (1994). Hidden dynamics in rapid changes of bilayer shape. Chem. Phys. Lipids *73*, 39–56.

Evans, E.A., and Hochmuth, R.M. (1978). Mechanochemical properties of membranes. In Current Topics in Membranes and Transport, B. Felix and K. Arnost, eds. (New York: Academic Press), pp. 1–64.

Evans, J.G., Correia, I., Krasavina, O., Watson, N., and Matsudaira, P. (2003). Macrophage podosomes assemble at the leading lamella by growth and fragmentation. J. Cell Biol. *161*, 697–705.

Féréol, S., Fodil, R., Laurent, V.M., Balland, M., Louis, B., Pelle, G., Hénon, S., Planus, E., and Isabey, D. (2009). Prestress and adhesion site dynamics control cell sensitivity to extracellular stiffness. Biophys. J. *96*, 2009–2022.

Gambardella, L., Anderson, K.E., Nussbaum, C., Segonds-Pichon, A., Margarido, T., Norton, L., Ludwig, T., Sperandio, M., Hawkins, P.T., Stephens, L., and Vermeren, S. (2011). The GTPase-activating protein ARAP3 regulates chemotaxis and adhesion-dependent processes in neutrophils. Blood *118*, 1087–1098.

Geiger, B., Bershadsky, A., Pankov, R., and Yamada, K.M. (2001). Transmembrane crosstalk between the extracellular matrix—cytoskeleton crosstalk. Nat. Rev. Mol. Cell Biol. *2*, 793–805.

Geiger, B., Spatz, J.P., and Bershadsky, A.D. (2009). Environmental sensing through focal adhesions. Nat. Rev. Mol. Cell Biol. *10*, 21–33.

Ghassemi, S., Meacci, G., Liu, S., Gondarenko, A.A., Mathur, A., Roca-Cusachs, P., Sheetz, M.P., and Hone, J. (2012). Cells test substrate rigidity by local contractions on submicrometer pillars. Proc. Natl. Acad. Sci. USA *109*, 5328–5333.

Gil-Henn, H., Destaing, O., Sims, N.A., Aoki, K., Alles, N., Neff, L., Sanjay, A., Bruzzaniti, A., De Camilli, P., Baron, R., and Schlessinger, J. (2007). Defective

microtubule-dependent podosome organization in osteoclasts leads to increased bone density in Pyk2(-/-) mice. J. Cell Biol. *178*, 1053–1064.

Gimona, M., Buccione, R., Courtneidge, S.A., and Linder, S. (2008). Assembly and biological role of podosomes and invadopodia. Curr. Opin. Cell Biol. *20*, 235–241.

Hendrickson, W.A., Pähler, A., Smith, J.L., Satow, Y., Merritt, E.A., and Phizackerley, R.P. (1989). Crystal structure of core streptavidin determined from multiwavelength anomalous diffraction of synchrotron radiation. Proc. Natl. Acad. Sci. USA *86*, 2190–2194.

Holt, M.R., Calle, Y., Sutton, D.H., Critchley, D.R., Jones, G.E., and Dunn, G.A. (2008). Quantifying cell-matrix adhesion dynamics in living cells using interference reflection microscopy. J. Microsc. *232*, 73–81.

Hoshino, D., Jourquin, J., Emmons, S.W., Miller, T., Goldgof, M., Costello, K., Tyson, D.R., Brown, B., Lu, Y., Prasad, N.K., et al. (2012). Network analysis of the focal adhesion to invadopodia transition identifies a PI3K-PKCα invasive signaling axis. Sci. Signal. *5*, ra66.

Huttenlocher, A., and Horwitz, A.R. (2011). Integrins in cell migration. Cold Spring Harb. Perspect. Biol. *3*, a005074.

Huveneers, S., Arslan, S., van de Water, B., Sonnenberg, A., and Danen, E.H. (2008). Integrins uncouple Src-induced morphological and oncogenic transformation. J. Biol. Chem. *283*, 13243–13251.

Krugmann, S., Anderson, K.E., Ridley, S.H., Risso, N., McGregor, A., Coadwell, J., Davidson, K., Eguinoa, A., Ellson, C.D., Lipp, P., et al. (2002). Identification of ARAP3, a novel PI3K effector regulating both Arf and Rho GTPases, by selective capture on phosphoinositide affinity matrices. Mol. Cell *9*, 95–108.

Krugmann, S., Williams, R., Stephens, L., and Hawkins, P.T. (2004). ARAP3 is a PI3K- and rap-regulated GAP for RhoA. Curr. Biol. *14*, 1380–1384.

Kuroiwa, M., Oneyama, C., Nada, S., and Okada, M. (2011). The guanine nucleotide exchange factor Arhgef5 plays crucial roles in Src-induced podosome formation. J. Cell Sci. *124*, 1726–1738.

Levental, K.R., Yu, H., Kass, L., Lakins, J.N., Egeblad, M., Erler, J.T., Fong, S.F., Csiszar, K., Giaccia, A., Weninger, W., et al. (2009). Matrix crosslinking forces tumor progression by enhancing integrin signaling. Cell *139*, 891–906.

Linder, S., and Kopp, P. (2005). Podosomes at a glance. J. Cell Sci. *118*, 2079–2082.

Lizárraga, F., Poincloux, R., Romao, M., Montagnac, G., Le Dez, G., Bonne, I., Rigaill, G., Raposo, G., and Chavrier, P. (2009). Diaphanous-related formins are required for invadopodia formation and invasion of breast tumor cells. Cancer Res. *69*, 2792–2800.

Machesky, L., Jurdic, P., and Hinz, B. (2008). Grab, stick, pull and digest: the functional diversity of actin-associated matrix-adhesion structures. Workshop on Invadopodia, Podosomes and Focal Adhesions in Tissue Invasion. EMBO Rep. *9*, 139–143.

McLaughlin, S., Wang, J., Gambhir, A., and Murray, D. (2002). PIP(2) and proteins: interactions, organization, and information flow. Annu. Rev. Biophys. Biomol. Struct. *31*, 151–175.

Miranti, C.K., and Brugge, J.S. (2002). Sensing the environment: a historical perspective on integrin signal transduction. Nat. Cell Biol. *4*, E83–E90.

Monypenny, J., Chou, H.C., Bañón-Rodríguez, I., Thrasher, A.J., Antón, I.M., Jones, G.E., and Calle, Y. (2011). Role of WASP in cell polarity and podosome dynamics of myeloid cells. Eur. J. Cell Biol. *90*, 198–204.

Moore, S.W., Roca-Cusachs, P., and Sheetz, M.P. (2010). Stretchy proteins on stretchy substrates: the important elements of integrin-mediated rigidity sensing. Dev. Cell *19*, 194–206.

Mossman, K.D., Campi, G., Groves, J.T., and Dustin, M.L. (2005). Altered TCR signaling from geometrically repatterned immunological synapses. Science *310*, 1191–1193.

Murphy, D.A., and Courtneidge, S.A. (2011). The 'ins' and 'outs' of podosomes and invadopodia: characteristics, formation and function. Nat. Rev. Mol. Cell Biol. *12*, 413–426.

Nermut, M.V., Green, N.M., Eason, P., Yamada, S.S., and Yamada, K.M. (1988). Electron microscopy and structural model of human fibronectin receptor. EMBO J. *7*, 4093–4099.

Nolen, B.J., Tomasevic, N., Russell, A., Pierce, D.W., Jia, Z., McCormick, C.D., Hartman, J., Sakowicz, R., and Pollard, T.D. (2009). Characterization of two classes of small molecule inhibitors of Arp2/3 complex. Nature *460*, 1031–1034.

Oikawa, T., Itoh, T., and Takenawa, T. (2008). Sequential signals toward podosome formation in NIH-src cells. J. Cell Biol. *182*, 157–169.

Orlova, I., Silver, L., and Gallo, G. (2007). Regulation of actomyosin contractility by PI3K in sensory axons. Dev. Neurobiol. *67*, 1843–1851.

Papayannopoulos, V., Co, C., Prehoda, K.E., Snapper, S., Taunton, J., and Lim, W.A. (2005). A polybasic motif allows N-WASP to act as a sensor of PIP(2) density. Mol. Cell *17*, 181–191.

Pertz, O., Hodgson, L., Klemke, R.L., and Hahn, K.M. (2006). Spatiotemporal dynamics of RhoA activity in migrating cells. Nature *440*, 1069–1072.

Poincloux, R., Lizárraga, F., and Chavrier, P. (2009). Matrix invasion by tumour cells: a focus on MT1-MMP trafficking to invadopodia. J. Cell Sci. *122*, 3015–3024.

Pollitt, A.Y., and Insall, R.H. (2009). WASP and SCAR/WAVE proteins: the drivers of actin assembly. J. Cell Sci. *122*, 2575–2578.

Poon, J.S., Eves, R., and Mak, A.S. (2010). Both lipid- and protein-phosphatase activities of PTEN contribute to the p53-PTEN anti-invasion pathway. Cell Cycle *9*, 4450–4454.

Prager-Khoutorsky, M., Lichtenstein, A., Krishnan, R., Rajendran, K., Mayo, A., Kam, Z., Geiger, B., and Bershadsky, A.D. (2011). Fibroblast polarization is a matrix-rigidity-dependent process controlled by focal adhesion mechanosensing. Nat. Cell Biol. *13*, 1457–1465.

Rizvi, S.A., Neidt, E.M., Cui, J., Feiger, Z., Skau, C.T., Gardel, M.L., Kozmin, S.A., and Kovar, D.R. (2009). Identification and characterization of a small molecule inhibitor of formin-mediated actin assembly. Chem. Biol. *16*, 1158–1168.

Roberts, W.G., Ung, E., Whalen, P., Cooper, B., Hulford, C., Autry, C., Richter, D., Emerson, E., Lin, J., Kath, J., et al. (2008). Antitumor activity and pharmacology of a selective focal adhesion kinase inhibitor, PF-562,271. Cancer Res. *68*, 1935–1944.

Salaita, K., Nair, P.M., Petit, R.S., Neve, R.M., Das, D., Gray, J.W., and Groves, J.T. (2010). Restriction of receptor movement alters cellular response: physical force sensing by EphA2. Science *327*, 1380–1385.

Schramp, M., Ying, O., Kim, T.Y., and Martin, G.S. (2008). ERK5 promotes Src-induced podosome formation by limiting Rho activation. J. Cell Biol. *181*, 1195–1210.

Songyang, Z., Shoelson, S.E., Chaudhuri, M., Gish, G., Pawson, T., Haser, W.G., King, F., Roberts, T., Ratnofsky, S., Lechleider, R.J., et al. (1993). SH2 domains recognize specific phosphopeptide sequences. Cell *72*, 767–778.

Su, J., Muranjan, M., and Sap, J. (1999). Receptor protein tyrosine phosphatase alpha activates Src-family kinases and controls integrin-mediated responses in fibroblasts. Curr. Biol. *9*, 505–511.

Tang, H., Li, A., Bi, J., Veltman, D.M., Zech, T., Spence, H.J., Yu, X., Timpson, P., Insall, R.H., Frame, M.C., and Machesky, L.M. (2013). Loss of Scar/WAVE complex promotes N-WASP- and FAK-dependent invasion. Curr. Biol. *23*, 107–117.

Tarone, G., Cirillo, D., Giancotti, F.G., Comoglio, P.M., and Marchisio, P.C. (1985). Rous sarcoma virus-transformed fibroblasts adhere primarily at discrete protrusions of the ventral membrane called podosomes. Exp. Cell Res. *159*, 141–157.

Tcherkezian, J., and Lamarche-Vane, N. (2007). Current knowledge of the large RhoGAP family of proteins. Biol. Cell *99*, 67–86.

van Helden, S.F., Oud, M.M., Joosten, B., Peterse, N., Figdor, C.G., and van Leeuwen, F.N. (2008). PGE2-mediated podosome loss in dendritic cells is dependent on actomyosin contraction downstream of the RhoA-Rho-kinase axis. J. Cell Sci. *121*, 1096–1106.

Vanhaesebroeck, B., Stephens, L., and Hawkins, P. (2012). PI3K signalling: the path to discovery and understanding. Nat. Rev. Mol. Cell Biol. *13*, 195–203.

Vogel, V., and Sheetz, M. (2006). Local force and geometry sensing regulate cell functions. Nat. Rev. Mol. Cell Biol. *7*, 265–275.

Vogel, V., and Sheetz, M.P. (2009). Cell fate regulation by coupling mechanical cycles to biochemical signaling pathways. Curr. Opin. Cell Biol. *21*, 38–46.

Wehrle-Haller, B. (2012). Structure and function of focal adhesions. Curr. Opin. Cell Biol. *24*, 116–124.

Wu, X., Gan, B., Yoo, Y., and Guan, J.L. (2005). FAK-mediated src phosphorylation of endophilin A2 inhibits endocytosis of MT1-MMP and promotes ECM degradation. Dev. Cell *9*, 185–196.

Xu, C., Watras, J., and Loew, L.M. (2003). Kinetic analysis of receptor-activated phosphoinositide turnover. J. Cell Biol. *161*, 779–791.

Yu, C.H., and Groves, J.T. (2010). Engineering supported membranes for cell biology. Med. Biol. Eng. Comput. *48*, 955–963.

Yu, C.H., Wu, H.J., Kaizuka, Y., Vale, R.D., and Groves, J.T. (2010). Altered actin centripetal retrograde flow in physically restricted immunological synapses. PLoS ONE *5*, e11878.

Yu, C.H., Law, J.B., Suryana, M., Low, H.Y., and Sheetz, M.P. (2011). Early integrin binding to Arg-Gly-Asp peptide activates actin polymerization and contractile movement that stimulates outward translocation. Proc. Natl. Acad. Sci. USA *108*, 20585–20590.

Yu, C.H., Luo, W., and Sheetz, M.P. (2012a). Spatial-temporal reorganization of activated integrins. Cell Adhes. Migr. *6*, 280–284.

Yu, X., Zech, T., McDonald, L., Gonzalez, E.G., Li, A., Macpherson, I., Schwarz, J.P., Spence, H., Futó, K., Timpson, P., et al. (2012b). N-WASP coordinates the delivery and F-actin-mediated capture of MT1-MMP at invasive pseudopods. J. Cell Biol. *199*, 527–544.

BIBLIOGRAPHY

Abdul-Manan, N., B. Aghazadeh, G. A. Liu, A. Majumdar, O. Ouerfelli, K. A. Siminovitch & M. K. Rosen (1999a) Structure of Cdc42 in complex with the GTPase-binding domain of the 'Wiskott-Aldrich syndrome' protein. *Nature,* 399**,** 379-383.

--- (1999b) Structure of Cdc42 in complex with the GTPase-binding domain of the 'Wiskott-Aldrich syndrome' protein. *Nature,* 399**,** 379-83.

Adams, J. C. (2001) Cell-matrix contact structures. *Cell Mol Life Sci,* 58**,** 371-92.

Akhshi, T. K., D. Wernike & A. Piekny (2014) Microtubules and actin crosstalk in cell migration and division. *Cytoskeleton (Hoboken),* 71**,** 1-23.

Ang, E. S., N. J. Pavlos, S. M. Chim, H. T. Feng, R. M. Scaife, J. H. Steer, M. H. Zheng & J. Xu (2012) Paclitaxel inhibits osteoclast formation and bone resorption via influencing mitotic cell cycle arrest and RANKL-induced activation of NF-kappaB and ERK. *J Cell Biochem,* 113**,** 946-55.

Batchelder, E. L., G. Hollopeter, C. Campillo, X. Mezanges, E. M. Jorgensen, P. Nassoy, P. Sens & J. Plastino (2011) Membrane tension regulates motility by controlling lamellipodium organization. *Proc Natl Acad Sci U S A,* 108**,** 11429-34.

Beck, R., M. Rawet, F. T. Wieland & D. Cassel (2009) The COPI system: molecular mechanisms and function. *FEBS Lett,* 583**,** 2701-9.

Beemiller, P., A. D. Hoppe & J. A. Swanson (2006) A phosphatidylinositol-3-kinase-dependent signal transition regulates ARF1 and ARF6 during Fcgamma receptor-mediated phagocytosis. *PLoS Biol,* 4**,** e162.

Beese, L., G. Stubbs & C. Cohen (1987) Microtubule structure at 18 A resolution. *J Mol Biol,* 194**,** 257-64.

Bershadsky, A., A. Chausovsky, E. Becker, A. Lyubimova & B. Geiger (1996) Involvement of microtubules in the control of adhesion-dependent signal transduction. *Curr Biol,* 6**,** 1279-89.

Bershadsky, A. D., N. Q. Balaban & B. Geiger (2003) Adhesion-dependent cell mechanosensitivity. *Annu Rev Cell Dev Biol,* 19**,** 677-95.

Bershadsky, A. D., C. Ballestrem, L. Carramusa, Y. Zilberman, B. Gilquin, S. Khochbin, A. Y. Alexandrova, A. B. Verkhovsky, T. Shemesh & M. M. Kozlov (2006) Assembly and mechanosensory function of focal adhesions: experiments and models. *Eur J Cell Biol,* 85**,** 165-73.

Bershadsky, A. D. & A. H. Futerman (1994) Disruption of the Golgi apparatus by brefeldin A blocks cell polarization and inhibits directed cell migration. *Proc Natl Acad Sci U S A,* 91**,** 5686-9.

Birkenfeld, J., P. Nalbant, S. H. Yoon & G. M. Bokoch (2008) Cellular functions of GEF-H1, a microtubule-regulated Rho-GEF: is altered GEF-H1 activity a crucial determinant of disease pathogenesis? *Trends Cell Biol,* 18**,** 210-9.

Birukova, A. A., D. Adyshev, B. Gorshkov, G. M. Bokoch, K. G. Birukov & A. D. Verin (2006) GEF-H1 is involved in agonist-induced human pulmonary endothelial barrier dysfunction. *Am J Physiol Lung Cell Mol Physiol,* 290**,** L540-8.

Block, M. R., C. Badowski, A. Millon-Fremillon, D. Bouvard, A. P. Bouin, E. Faurobert, D. Gerber-Scokaert, E. Planus & C. Albiges-Rizo (2008) Podosome-type adhesions and focal adhesions, so alike yet so different. *Eur J Cell Biol,* 87**,** 491-506.

Bonifacino, J. S. & J. Lippincott-Schwartz (2003) Coat proteins: shaping membrane transport. *Nat Rev Mol Cell Biol,* 4**,** 409-14.

Boulant, S., C. Kural, J. C. Zeeh, F. Ubelmann & T. Kirchhausen (2011) Actin dynamics counteract membrane tension during clathrin-mediated endocytosis. *Nat Cell Biol,* 13**,** 1124-31.

Boulay, P. L., M. Cotton, P. Melancon & A. Claing (2008) ADP-ribosylation factor 1 controls the activation of the phosphatidylinositol 3-kinase pathway to regulate epidermal growth factor-dependent growth and migration of breast cancer cells. *J Biol Chem,* 283**,** 36425-34.

Burger, K. L., A. L. Davis, S. Isom, N. Mishra & D. F. Seals (2011) The podosome marker protein Tks5 regulates macrophage invasive behavior. *Cytoskeleton (Hoboken),* 68**,** 694-711.

Burgstaller, G. & M. Gimona (2005) Podosome-mediated matrix resorption and cell motility in vascular smooth muscle cells. *Am J Physiol Heart Circ Physiol,* 288**,** H3001-5.

Burnette, D. T., L. Shao, C. Ott, A. M. Pasapera, R. S. Fischer, M. A. Baird, C. Der Loughian, H. Delanoe-Ayari, M. J. Paszek, M. W. Davidson, E. Betzig & J. Lippincott-Schwartz (2014) A contractile and counterbalancing adhesion system controls the 3D shape of crawling cells. *J Cell Biol,* 205**,** 83-96.

Burns, S., S. J. Hardy, J. Buddle, K. L. Yong, G. E. Jones & A. J. Thrasher (2004) Maturation of DC is associated with changes in motile characteristics and adherence. *Cell Motil Cytoskeleton,* 57**,** 118-32.

Burns, S., A. J. Thrasher, M. P. Blundell, L. Machesky & G. E. Jones (2001) Configuration of human dendritic cell cytoskeleton by Rho GTPases, the WAS protein, and differentiation. *Blood,* 98**,** 1142-9.

Buschman, M. D., P. A. Bromann, P. Cejudo-Martin, F. Wen, I. Pass & S. A. Courtneidge (2009) The novel adaptor protein Tks4 (SH3PXD2B) is required for functional podosome formation. *Mol Biol Cell,* 20**,** 1302-11.

Cai, Y., O. Rossier, N. C. Gauthier, N. Biais, M. A. Fardin, X. Zhang, L. W. Miller, B. Ladoux, V. W. Cornish & M. P. Sheetz (2010) Cytoskeletal coherence requires myosin-IIA contractility. *J Cell Sci,* 123**,** 413-23.

Cai, Y. & M. P. Sheetz (2009) Force propagation across cells: mechanical coherence of dynamic cytoskeletons. *Curr Opin Cell Biol,* 21**,** 47-50.

Calle, Y., S. Burns, A. J. Thrasher & G. E. Jones (2006) The leukocyte podosome. *Eur J Cell Biol,* 85**,** 151-7.

Calle, Y., H. C. Chou, A. J. Thrasher & G. E. Jones (2004a) Wiskott-Aldrich syndrome protein and the cytoskeletal dynamics of dendritic cells. *J Pathol,* 204**,** 460-9.

Calle, Y., G. E. Jones, C. Jagger, K. Fuller, M. P. Blundell, J. Chow, T. Chambers & A. J. Thrasher (2004b) WASp deficiency in mice results in failure to form osteoclast sealing zones and defects in bone resorption. *Blood,* 103**,** 3552-61.

Cao, H., S. Weller, J. D. Orth, J. Chen, B. Huang, J. L. Chen, M. Stamnes & M. A. McNiven (2005) Actin and Arf1-dependent recruitment of a cortactin-dynamin complex to the Golgi regulates post-Golgi transport. *Nat Cell Biol,* 7**,** 483-92.

Carman, C. V., P. T. Sage, T. E. Sciuto, M. A. de la Fuente, R. S. Geha, H. D. Ochs, H. F. Dvorak, A. M. Dvorak & T. A. Springer (2007a) Transcellular diapedesis is initiated by invasive podosomes. *Immunity,* 26**,** 784-797.

--- (2007b) Transcellular diapedesis is initiated by invasive podosomes. *Immunity,* 26**,** 784-97.

Carvajal-Gonzalez, J. M., S. Balmer, M. Mendoza, A. Dussert, G. Collu, A. C. Roman, U. Weber, B. Ciruna & M. Mlodzik (2015) The clathrin adaptor AP-1 complex and Arf1 regulate planar cell polarity in vivo. *Nat Commun,* 6**,** 6751.

Casanova, J. E. (2007) Regulation of Arf activation: the Sec7 family of guanine nucleotide exchange factors. *Traffic,* 8**,** 1476-85.

Caviston, J. P., L. A. Cohen & J. G. Donaldson (2014) Arf1 and Arf6 promote ventral actin structures formed by acute activation of protein kinase C and Src. *Cytoskeleton (Hoboken),* 71**,** 380-94.

Chabadel, A., I. Banon-Rodriguez, D. Cluet, B. B. Rudkin, B. Wehrle-Haller, E. Genot, P. Jurdic, I. M. Anton & F. Saltel (2007) CD44 and beta3 integrin organize two functionally distinct actin-based domains in osteoclasts. *Mol Biol Cell,* 18**,** 4899-910.

Chang, Y. C., P. Nalbant, J. Birkenfeld, Z. F. Chang & G. M. Bokoch (2008) GEF-H1 couples nocodazole-induced microtubule disassembly to cell contractility via RhoA. *Mol Biol Cell,* 19**,** 2147-53.

Choi, C. K., M. Vicente-Manzanares, J. Zareno, L. A. Whitmore, A. Mogilner & A. R. Horwitz (2008) Actin and alpha-actinin orchestrate the assembly and maturation of nascent adhesions in a myosin II motor-independent manner. *Nat Cell Biol,* 10**,** 1039-50.

Chretien, D. & R. H. Wade (1991) New data on the microtubule surface lattice. *Biol Cell,* 71**,** 161-74.

Cichy, J. & E. Pure (2003) The liberation of CD44. *J Cell Biol,* 161**,** 839-43.

Citterio, C., H. D. Jones, G. Pacheco-Rodriguez, A. Islam, J. Moss & M. Vaughan (2006) Effect of protein kinase A on accumulation of brefeldin A-inhibited guanine

nucleotide-exchange protein 1 (BIG1) in HepG2 cell nuclei. *Proc Natl Acad Sci U S A,* 103**,** 2683-8.

Cornfine, S., M. Himmel, P. Kopp, K. El Azzouzi, C. Wiesner, M. Kruger, T. Rudel & S. Linder (2011) The kinesin KIF9 and reggie/flotillin proteins regulate matrix degradation by macrophage podosomes. *Mol Biol Cell,* 22**,** 202-15.

Cougoule, C., V. Le Cabec, R. Poincloux, T. Al Saati, J. L. Mege, G. Tabouret, C. A. Lowell, N. Laviolette-Malirat & I. Maridonneau-Parini (2010) Three-dimensional migration of macrophages requires Hck for podosome organization and extracellular matrix proteolysis. *Blood,* 115**,** 1444-52.

Cox, S. & G. E. Jones (2013) Imaging cells at the nanoscale. *Int J Biochem Cell Biol,* 45**,** 1669-78.

Cox, S., E. Rosten, J. Monypenny, T. Jovanovic-Talisman, D. T. Burnette, J. Lippincott-Schwartz, G. E. Jones & R. Heintzmann (2012) Bayesian localization microscopy reveals nanoscale podosome dynamics. *Nat Methods,* 9**,** 195-200.

Cui, Y., F. M. Hameed, B. Yang, K. Lee, C. Q. Pan, S. Park & M. Sheetz (2015) Cyclic stretching of soft substrates induces spreading and growth. *Nat Commun,* 6**,** 6333.

Curtis, J., Y. Luo, H. L. Zenner, D. Cuchet-Lourenco, C. Wu, K. Lo, M. Maes, A. Alisaac, E. Stebbings, J. Z. Liu, L. Kopanitsa, O. Ignatyeva, Y. Balabanova, V. Nikolayevskyy, I. Baessmann, T. Thye, C. G. Meyer, P. Nurnberg, R. D. Horstmann, F. Drobniewski, V. Plagnol, J. C. Barrett & S. Nejentsev (2015) Susceptibility to tuberculosis is associated with variants in the ASAP1 gene encoding a regulator of dendritic cell migration. *Nat Genet,* 47**,** 523-7.

D'Souza-Schorey, C. & P. Chavrier (2006) ARF proteins: roles in membrane traffic and beyond. *Nat Rev Mol Cell Biol,* 7**,** 347-58.

Dai, J. & M. P. Sheetz (1995) Regulation of endocytosis, exocytosis, and shape by membrane tension. *Cold Spring Harb Symp Quant Biol,* 60**,** 567-71.

de Pablo, P. J., I. A. Schaap, F. C. MacKintosh & C. F. Schmidt (2003) Deformation and collapse of microtubules on the nanometer scale. *Phys Rev Lett,* 91**,** 098101.

Dehring, D. A., F. Clarke, B. G. Ricart, Y. Huang, T. S. Gomez, E. K. Williamson, D. A. Hammer, D. D. Billadeau, Y. Argon & J. K. Burkhardt (2011) Hematopoietic lineage cell-specific protein 1 functions in concert with the Wiskott-Aldrich syndrome protein to promote podosome array organization and chemotaxis in dendritic cells. *J Immunol,* 186**,** 4805-18.

del Rio, A., R. Perez-Jimenez, R. Liu, P. Roca-Cusachs, J. M. Fernandez & M. P. Sheetz (2009) Stretching single talin rod molecules activates vinculin binding. *Science,* 323**,** 638-41.

Dell'Angelica, E. C., R. Puertollano, C. Mullins, R. C. Aguilar, J. D. Vargas, L. M. Hartnell & J. S. Bonifacino (2000) GGAs: a family of ADP ribosylation factor-binding proteins related to adaptors and associated with the Golgi complex. *J Cell Biol,* 149**,** 81-94.

Destaing, O., S. M. Ferguson, A. Grichine, C. Oddou, P. De Camilli, C. Albiges-Rizo & R. Baron (2013) Essential function of dynamin in the invasive properties and actin architecture of v-Src induced podosomes/invadosomes. *PLoS One,* 8**,** e77956.

Destaing, O., E. Planus, D. Bouvard, C. Oddou, C. Badowski, V. Bossy, A. Raducanu, B. Fourcade, C. Albiges-Rizo & M. R. Block (2010) beta1A integrin is a master regulator of invadosome organization and function. *Mol Biol Cell,* 21**,** 4108-19.

Destaing, O., A. Sanjay, C. Itzstein, W. C. Horne, D. Toomre, P. De Camilli & R. Baron (2008) The tyrosine kinase activity of c-Src regulates actin dynamics and organization of podosomes in osteoclasts. *Mol Biol Cell,* 19**,** 394-404.

DiNitto, J. P., A. Delprato, M. T. Gabe Lee, T. C. Cronin, S. Huang, A. Guilherme, M. P. Czech & D. G. Lambright (2007) Structural basis and mechanism of autoregulation in 3-phosphoinositide-dependent Grp1 family Arf GTPase exchange factors. *Mol Cell,* 28**,** 569-83.

Diz-Munoz, A., D. A. Fletcher & O. D. Weiner (2013) Use the force: membrane tension as an organizer of cell shape and motility. *Trends Cell Biol,* 23**,** 47-53.

Doherty, G. J., M. K. Ahlund, M. T. Howes, B. Moren, R. G. Parton, H. T. McMahon & R. Lundmark (2011) The endocytic protein GRAF1 is directed to cell-matrix adhesion sites and regulates cell spreading. *Mol Biol Cell,* 22**,** 4380-9.

Donaldson, J. G., A. Honda & R. Weigert (2005) Multiple activities for Arf1 at the Golgi complex. *Biochim Biophys Acta,* 1744**,** 364-73.

Donaldson, J. G. & C. L. Jackson (2011) ARF family G proteins and their regulators: roles in membrane transport, development and disease. *Nat Rev Mol Cell Biol,* 12**,** 362-75.

Dovas, A., B. Gligorijevic, X. Chen, D. Entenberg, J. Condeelis & D. Cox (2011) Visualization of actin polymerization in invasive structures of macrophages and carcinoma cells using photoconvertible beta-actin-Dendra2 fusion proteins. *PLoS One,* 6**,** e16485.

Dries, K., M. B. Meddens, S. de Keijzer, S. Shekhar, V. Subramaniam, C. G. Figdor & A. Cambi (2013) Interplay between myosin IIA-mediated contractility and actin network integrity orchestrates podosome composition and oscillations. *Nat Commun,* 4**,** 1412.

Dubois, T., O. Paleotti, A. A. Mironov, V. Fraisier, T. E. Stradal, M. A. De Matteis, M. Franco & P. Chavrier (2005) Golgi-localized GAP for Cdc42 functions downstream of ARF1 to control Arp2/3 complex and F-actin dynamics. *Nat Cell Biol,* 7**,** 353-64.

Efimova, N., A. Grimaldi, A. Bachmann, K. Frye, X. Zhu, A. Feoktistov, A. Straube & I. Kaverina (2014) Podosome-regulating kinesin KIF1C translocates to the cell periphery in a CLASP-dependent manner. *J Cell Sci,* 127**,** 5179-88.

El Azzouzi, K., C. Wiesner & S. Linder (2016) Metalloproteinase MT1-MMP islets act as memory devices for podosome reemergence. *J Cell Biol,* 213**,** 109-25.

Etienne-Manneville, S. & A. Hall (2002) Rho GTPases in cell biology. *Nature,* 420**,** 629-35.

Evans, J. G., I. Correia, O. Krasavina, N. Watson & P. Matsudaira (2003) Macrophage podosomes assemble at the leading lamella by growth and fragmentation. *J Cell Biol,* 161**,** 697-705.

Even-Ram, S., A. D. Doyle, M. A. Conti, K. Matsumoto, R. S. Adelstein & K. M. Yamada (2007) Myosin IIA regulates cell motility and actomyosin-microtubule crosstalk. *Nat Cell Biol,* 9**,** 299-309.

Foxall, E., A. Pipili, G. E. Jones & C. M. Wells (2016) Significance of kinase activity in the dynamic invadosome. *Eur J Cell Biol*.

Friedland, J. C., M. H. Lee & D. Boettiger (2009) Mechanically activated integrin switch controls alpha5beta1 function. *Science,* 323**,** 642-4.

Gauthier, N. C., M. A. Fardin, P. Roca-Cusachs & M. P. Sheetz (2011) Temporary increase in plasma membrane tension coordinates the activation of exocytosis and contraction during cell spreading. *Proc Natl Acad Sci U S A,* 108**,** 14467-72.

Gauthier, N. C., T. A. Masters & M. P. Sheetz (2012) Mechanical feedback between membrane tension and dynamics. *Trends Cell Biol,* 22**,** 527-35.

Gawden-Bone, C., Z. Zhou, E. King, A. Prescott, C. Watts & J. Lucocq (2010) Dendritic cell podosomes are protrusive and invade the extracellular matrix using metalloproteinase MMP-14. *J Cell Sci,* 123**,** 1427-37.

Geiger, B., A. Bershadsky, R. Pankov & K. M. Yamada (2001) Transmembrane crosstalk between the extracellular matrix--cytoskeleton crosstalk. *Nat Rev Mol Cell Biol,* 2**,** 793-805.

Geiger, B., J. P. Spatz & A. D. Bershadsky (2009) Environmental sensing through focal adhesions. *Nat Rev Mol Cell Biol,* 10**,** 21-33.

Gimona, M., R. Buccione, S. A. Courtneidge & S. Linder (2008) Assembly and biological role of podosomes and invadopodia. *Curr Opin Cell Biol,* 20**,** 235-41.

Hafner, M., A. Schmitz, I. Grune, S. G. Srivatsan, B. Paul, W. Kolanus, T. Quast, E. Kremmer, I. Bauer & M. Famulok (2006) Inhibition of cytohesins by SecinH3 leads to hepatic insulin resistance. *Nature,* 444**,** 941-4.

Heuvingh, J., M. Franco, P. Chavrier & C. Sykes (2007) ARF1-mediated actin polymerization produces movement of artificial vesicles. *Proc Natl Acad Sci U S A,* 104**,** 16928-33.

Hodge, R. G. & A. J. Ridley (2016) Regulating Rho GTPases and their regulators. *Nat Rev Mol Cell Biol,* 17**,** 496-510.

Hoebeke, J., G. Van Nijen & M. De Brabander (1976) Interaction of oncodazole (R 17934), a new antitumoral drug, with rat brain tubulin. *Biochem Biophys Res Commun,* 69**,** 319-24.

Humphreys, D., A. Davidson, P. J. Hume & V. Koronakis (2012a) Salmonella virulence effector SopE and Host GEF ARNO cooperate to recruit and activate WAVE to trigger bacterial invasion. *Cell Host Microbe,* 11**,** 129-39.

Humphreys, D., T. Liu, A. C. Davidson, P. J. Hume & V. Koronakis (2012b) The Drosophila Arf1 homologue Arf79F is essential for lamellipodium formation. *J Cell Sci,* 125**,** 5630-5.

Ishizaki, R., H. W. Shin, H. Mitsuhashi & K. Nakayama (2008) Redundant roles of BIG2 and BIG1, guanine-nucleotide exchange factors for ADP-ribosylation factors in membrane traffic between the trans-Golgi network and endosomes. *Mol Biol Cell,* 19**,** 2650-60.

Johannes, L., R. G. Parton, P. Bassereau & S. Mayor (2015) Building endocytic pits without clathrin. *Nat Rev Mol Cell Biol,* 16**,** 311-21.

Jones, G. E., D. Zicha, G. A. Dunn, M. Blundell & A. Thrasher (2002) Restoration of podosomes and chemotaxis in Wiskott-Aldrich syndrome macrophages following induced expression of WASp. *Int J Biochem Cell Biol,* 34**,** 806-15.

Kopp, P., R. Lammers, M. Aepfelbacher, G. Woehlke, T. Rudel, N. Machuy, W. Steffen & S. Linder (2006) The kinesin KIF1C and microtubule plus ends regulate podosome dynamics in macrophages. *Mol Biol Cell,* 17**,** 2811-23.

Koronakis, V., P. J. Hume, D. Humphreys, T. Liu, O. Horning, O. N. Jensen & E. J. McGhie (2011) WAVE regulatory complex activation by cooperating GTPases Arf and Rac1. *Proc Natl Acad Sci U S A,* 108**,** 14449-54.

Kosmalska, A. J., L. Casares, A. Elosegui-Artola, J. J. Thottacherry, R. Moreno-Vicente, V. Gonzalez-Tarrago, M. A. del Pozo, S. Mayor, M. Arroyo, D. Navajas, X. Trepat, N. C.

Gauthier & P. Roca-Cusachs (2015) Physical principles of membrane remodelling during cell mechanoadaptation. *Nat Commun,* 6**,** 7292.

Kozlov, M. M., F. Campelo, N. Liska, L. V. Chernomordik, S. J. Marrink & H. T. McMahon (2014) Mechanisms shaping cell membranes. *Curr Opin Cell Biol,* 29**,** 53-60.

Kozlov, M. M. & L. V. Chernomordik (2015) Membrane tension and membrane fusion. *Curr Opin Struct Biol,* 33**,** 61-7.

Kozlov, M. M., H. T. McMahon & L. V. Chernomordik (2010) Protein-driven membrane stresses in fusion and fission. *Trends Biochem Sci,* 35**,** 699-706.

Krendel, M., F. T. Zenke & G. M. Bokoch (2002) Nucleotide exchange factor GEF-H1 mediates cross-talk between microtubules and the actin cytoskeleton. *Nat Cell Biol,* 4**,** 294-301.

Kumari, S. & S. Mayor (2008) ARF1 is directly involved in dynamin-independent endocytosis. *Nat Cell Biol,* 10**,** 30-41.

Labernadie, A., A. Bouissou, P. Delobelle, S. Balor, R. Voituriez, A. Proag, I. Fourquaux, C. Thibault, C. Vieu, R. Poincloux, G. M. Charriere & I. Maridonneau-Parini (2014) Protrusion force microscopy reveals oscillatory force generation and mechanosensing activity of human macrophage podosomes. *Nat Commun,* 5**,** 5343.

Lieber, A. D., S. Yehudai-Resheff, E. L. Barnhart, J. A. Theriot & K. Keren (2013) Membrane tension in rapidly moving cells is determined by cytoskeletal forces. *Curr Biol,* 23**,** 1409-17.

Linder, S. (2007) The matrix corroded: podosomes and invadopodia in extracellular matrix degradation. *Trends Cell Biol,* 17**,** 107-17.

--- (2009) Invadosomes at a glance. *J Cell Sci,* 122**,** 3009-13.

Linder, S. & M. Aepfelbacher (2003) Podosomes: adhesion hot-spots of invasive cells. *Trends in Cell Biology,* 13**,** 376-385.

Linder, S., K. Hufner, U. Wintergerst & M. Aepfelbacher (2000a) Microtubule-dependent formation of podosomal adhesion structures in primary human macrophages. *J Cell Sci,* 113**,** 4165-4176.

--- (2000b) Microtubule-dependent formation of podosomal adhesion structures in primary human macrophages. *J Cell Sci,* 113 Pt 23**,** 4165-76.

Linder, S. & P. Kopp (2005) Podosomes at a glance. *J Cell Sci,* 118**,** 2079-82.

Linder, S., D. Nelson, M. Weiss & M. Aepfelbacher (1999) Wiskott-Aldrich syndrome protein regulates podosomes in primary human macrophages. *Proc Natl Acad Sci U S A,* 96**,** 9648-53.

Linder, S. & C. Wiesner (2015) Tools of the trade: podosomes as multipurpose organelles of monocytic cells. *Cell Mol Life Sci,* 72**,** 121-35.

Lippincott-Schwartz, J., L. C. Yuan, J. S. Bonifacino & R. D. Klausner (1989) Rapid redistribution of Golgi proteins into the ER in cells treated with brefeldin A: evidence for membrane cycling from Golgi to ER. *Cell,* 56**,** 801-13.

Liu, B. P., M. Chrzanowska-Wodnicka & K. Burridge (1998) Microtubule depolymerization induces stress fibers, focal adhesions, and DNA synthesis via the GTP-binding protein Rho. *Cell Adhes Commun,* 5**,** 249-55.

Liu, Y., J. C. Loijens, K. H. Martin, A. V. Karginov & J. T. Parsons (2002) The association of ASAP1, an ADP ribosylation factor-GTPase activating protein, with

focal adhesion kinase contributes to the process of focal adhesion assembly. *Mol Biol Cell,* 13**,** 2147-56.

Liu, Y., G. M. Yerushalmi, P. R. Grigera & J. T. Parsons (2005) Mislocalization or reduced expression of Arf GTPase-activating protein ASAP1 inhibits cell spreading and migration by influencing Arf1 GTPase cycling. *J Biol Chem,* 280**,** 8884-92.

Luxenburg, C., S. Winograd-Katz, L. Addadi & B. Geiger (2012) Involvement of actin polymerization in podosome dynamics. *J Cell Sci,* 125**,** 1666-72.

Machesky, L. M. & R. H. Insall (1998) Scar1 and the related Wiskott-Aldrich syndrome protein, WASP, regulate the actin cytoskeleton through the Arp2/3 complex. *Curr Biol,* 8**,** 1347-56.

McMahon, H. T. & E. Boucrot (2015) Membrane curvature at a glance. *J Cell Sci,* 128**,** 1065-1070.

Meddens, M. B., K. van den Dries & A. Cambi (2014) Podosomes revealed by advanced bioimaging: what did we learn? *Eur J Cell Biol,* 93**,** 380-7.

Menetrey, J., M. Perderiset, J. Cicolari, T. Dubois, N. Elkhatib, F. El Khadali, M. Franco, P. Chavrier & A. Houdusse (2007) Structural basis for ARF1-mediated recruitment of ARHGAP21 to Golgi membranes. *EMBO J,* 26**,** 1953-62.

Monypenny, J., H. C. Chou, I. Banon-Rodriguez, A. J. Thrasher, I. M. Anton, G. E. Jones & Y. Calle (2011) Role of WASP in cell polarity and podosome dynamics of myeloid cells. *Eur J Cell Biol,* 90**,** 198-204.

Mossessova, E., R. A. Corpina & J. Goldberg (2003) Crystal structure of ARF1*Sec7 complexed with Brefeldin A and its implications for the guanine nucleotide exchange mechanism. *Mol Cell,* 12**,** 1403-11.

Murphy, D. A. & S. A. Courtneidge (2011) The 'ins' and 'outs' of podosomes and invadopodia: characteristics, formation and function. *Nat Rev Mol Cell Biol,* 12**,** 413-26.

Myers, K. R. & J. E. Casanova (2008) Regulation of actin cytoskeleton dynamics by Arf-family GTPases. *Trends Cell Biol,* 18**,** 184-92.

Nakai, W., Y. Kondo, A. Saitoh, T. Naito, K. Nakayama & H. W. Shin (2013) ARF1 and ARF4 regulate recycling endosomal morphology and retrograde transport from endosomes to the Golgi apparatus. *Mol Biol Cell,* 24**,** 2570-81.

Nakamura, I., M. F. Pilkington, P. T. Lakkakorpi, L. Lipfert, S. M. Sims, S. J. Dixon, G. A. Rodan & L. T. Duong (1999) Role of alpha(v)beta(3) integrin in osteoclast migration and formation of the sealing zone. *J Cell Sci,* 112 (Pt 22)**,** 3985-93.

Nalbant, P., Y. C. Chang, J. Birkenfeld, Z. F. Chang & G. M. Bokoch (2009) Guanine nucleotide exchange factor-H1 regulates cell migration via localized activation of RhoA at the leading edge. *Mol Biol Cell,* 20**,** 4070-82.

Niu, T. K., A. C. Pfeifer, J. Lippincott-Schwartz & C. L. Jackson (2005) Dynamics of GBF1, a Brefeldin A-sensitive Arf1 exchange factor at the Golgi. *Mol Biol Cell,* 16**,** 1213-22.

Nogales, E. (2000) Structural insights into microtubule function. *Annu Rev Biochem,* 69**,** 277-302.

Ochoa, G. C., V. I. Slepnev, L. Neff, N. Ringstad, K. Takei, L. Daniell, W. Kim, H. Cao, M. McNiven, R. Baron & P. De Camilli (2000) A functional link between dynamin and the actin cytoskeleton at podosomes. *Journal of Cell Biology,* 150**,** 377-389.

Oser, M., H. Yamaguchi, C. C. Mader, J. J. Bravo-Cordero, M. Arias, X. Chen, V. Desmarais, J. van Rheenen, A. J. Koleske & J. Condeelis (2009) Cortactin regulates cofilin and N-WASp activities to control the stages of invadopodium assembly and maturation. *J Cell Biol,* 186**,** 571-87.

Osiak, A. E., G. Zenner & S. Linder (2005) Subconfluent endothelial cells form podosomes downstream of cytokine and RhoGTPase signaling. *Exp Cell Res,* 307**,** 342-53.

Pan, Y.-R., C.-L. Chen & H.-C. Chen (2011) FAK is required for the assembly of podosome rosettes. *The Journal of Cell Biology,* 195**,** 113-129.

Panzer, L., L. Trube, M. Klose, B. Joosten, J. Slotman, A. Cambi & S. Linder (2016) The formins FHOD1 and INF2 regulate inter- and intra-structural contractility of podosomes. *J Cell Sci,* 129**,** 298-313.

Pepperkok, R., J. A. Whitney, M. Gomez & T. E. Kreis (2000) COPI vesicles accumulating in the presence of a GTP restricted arf1 mutant are depleted of anterograde and retrograde cargo. *J Cell Sci,* 113 (Pt 1)**,** 135-44.

Peyroche, A., B. Antonny, S. Robineau, J. Acker, J. Cherfils & C. L. Jackson (1999) Brefeldin A acts to stabilize an abortive ARF-GDP-Sec7 domain protein complex: involvement of specific residues of the Sec7 domain. *Mol Cell,* 3**,** 275-85.

Poincloux, R., F. Lizarraga & P. Chavrier (2009) Matrix invasion by tumour cells: a focus on MT1-MMP trafficking to invadopodia. *J Cell Sci,* 122**,** 3015-24.

Puertollano, R., P. A. Randazzo, J. F. Presley, L. M. Hartnell & J. S. Bonifacino (2001) The GGAs promote ARF-dependent recruitment of clathrin to the TGN. *Cell,* 105**,** 93-102.

Purev, E., L. Neff, W. C. Horne & R. Baron (2009) c-Cbl and Cbl-b act redundantly to protect osteoclasts from apoptosis and to displace HDAC6 from beta-tubulin, stabilizing microtubules and podosomes. *Mol Biol Cell,* 20**,** 4021-30.

Raucher, D. & M. P. Sheetz (1999) Membrane expansion increases endocytosis rate during mitosis. *J Cell Biol,* 144**,** 497-506.

--- (2000) Cell spreading and lamellipodial extension rate is regulated by membrane tension. *J Cell Biol,* 148**,** 127-36.

Ren, Y., R. Li, Y. Zheng & H. Busch (1998) Cloning and characterization of GEF-H1, a microtubule-associated guanine nucleotide exchange factor for Rac and Rho GTPases. *J Biol Chem,* 273**,** 34954-60.

Ridley, A. J. (2001) Rho GTPases and cell migration. *J Cell Sci,* 114**,** 2713-22.

Ridley, A. J., M. A. Schwartz, K. Burridge, R. A. Firtel, M. H. Ginsberg, G. Borisy, J. T. Parsons & A. R. Horwitz (2003) Cell migration: integrating signals from front to back. *Science,* 302**,** 1704-9.

Riveline, D., E. Zamir, N. Q. Balaban, U. S. Schwarz, T. Ishizaki, S. Narumiya, Z. Kam, B. Geiger & A. D. Bershadsky (2001) Focal contacts as mechanosensors: externally applied local mechanical force induces growth of focal contacts by an mDia1-dependent and ROCK-independent mechanism. *J Cell Biol,* 153**,** 1175-86.

Rocca, D. L., M. Amici, A. Antoniou, E. B. Suarez, N. Halemani, K. Murk, J. McGarvey, N. Jaafari, J. R. Mellor, G. L. Collingridge & J. G. Hanley (2013) The small GTPase Arf1 modulates Arp2/3-mediated actin polymerization via PICK1 to regulate synaptic plasticity. *Neuron,* 79**,** 293-307.

Rooney, C., G. White, A. Nazgiewicz, S. A. Woodcock, K. I. Anderson, C. Ballestrem & A. Malliri (2010) The Rac activator STEF (Tiam2) regulates cell migration by microtubule-mediated focal adhesion disassembly. *EMBO Rep,* 11**,** 292-8.

Rottiers, P., F. Saltel, T. Daubon, B. Chaigne-Delalande, V. Tridon, C. Billottet, E. Reuzeau & E. Genot (2009) TGFbeta-induced endothelial podosomes mediate basement membrane collagen degradation in arterial vessels. *J Cell Sci,* 122**,** 4311-8.

Saenz, J. B., W. J. Sun, J. W. Chang, J. Li, B. Bursulaya, N. S. Gray & D. B. Haslam (2009) Golgicide A reveals essential roles for GBF1 in Golgi assembly and function. *Nat Chem Biol,* 5**,** 157-65.

Santy, L. C., S. R. Frank, J. C. Hatfield & J. E. Casanova (1999) Regulation of ARNO nucleotide exchange by a PH domain electrostatic switch. *Current Biology,* 9**,** 1173-1176.

Schachtner, H., S. D. Calaminus, S. G. Thomas & L. M. Machesky (2013) Podosomes in adhesion, migration, mechanosensing and matrix remodeling. *Cytoskeleton (Hoboken),* 70**,** 572-89.

Schoumacher, M., R. D. Goldman, D. Louvard & D. M. Vignjevic (2010) Actin, microtubules, and vimentin intermediate filaments cooperate for elongation of invadopodia. *J Cell Biol,* 189**,** 541-56.

Sciaky, N., J. Presley, C. Smith, K. J. Zaal, N. Cole, J. E. Moreira, M. Terasaki, E. Siggia & J. Lippincott-Schwartz (1997) Golgi tubule traffic and the effects of brefeldin A visualized in living cells. *J Cell Biol,* 139**,** 1137-55.

Seano, G., G. Chiaverina, P. A. Gagliardi, L. di Blasio, A. Puliafito, C. Bouvard, R. Sessa, G. Tarone, L. Sorokin, D. Helley, R. K. Jain, G. Serini, F. Bussolino & L. Primo (2014)

Endothelial podosome rosettes regulate vascular branching in tumour angiogenesis. *Nat Cell Biol,* 16**,** 931-41, 1-8.

Shattil, S. J., C. Kim & M. H. Ginsberg (2010) The final steps of integrin activation: the end game. *Nat Rev Mol Cell Biol,* 11**,** 288-300.

Shiba, Y. & P. A. Randazzo (2011) GEFH1 binds ASAP1 and regulates podosome formation. *Biochem Biophys Res Commun,* 406**,** 574-9.

Simunovic, M. & G. A. Voth (2015) Membrane tension controls the assembly of curvature-generating proteins. *Nat Commun,* 6**,** 7219.

Sinha, B., D. Koster, R. Ruez, P. Gonnord, M. Bastiani, D. Abankwa, R. V. Stan, G. Butler-Browne, B. Vedie, L. Johannes, N. Morone, R. G. Parton, G. Raposo, P. Sens, C. Lamaze & P. Nassoy (2011) Cells respond to mechanical stress by rapid disassembly of caveolae. *Cell,* 144**,** 402-13.

Soriano, P., C. Montgomery, R. Geske & A. Bradley (1991) Targeted disruption of the c-src proto-oncogene leads to osteopetrosis in mice. *Cell,* 64**,** 693-702.

Szul, T., R. Grabski, S. Lyons, Y. Morohashi, S. Shestopal, M. Lowe & E. Sztul (2007) Dissecting the role of the ARF guanine nucleotide exchange factor GBF1 in Golgi biogenesis and protein trafficking. *J Cell Sci,* 120**,** 3929-40.

Tarone, G., D. Cirillo, F. G. Giancotti, P. M. Comoglio & P. C. Marchisio (1985) Rous sarcoma virus-transformed fibroblasts adhere primarily at discrete protrusions of the ventral membrane called podosomes. *Exp Cell Res,* 159**,** 141-57.

Tatin, F., C. Varon, E. Genot & V. Moreau (2006) A signalling cascade involving PKC, Src and Cdc42 regulates podosome assembly in cultured endothelial cells in response to phorbol ester. *J Cell Sci,* 119**,** 769-81.

Torii, T., Y. Miyamoto, A. Sanbe, K. Nishimura, J. Yamauchi & A. Tanoue (2010) Cytohesin-2/ARNO, through its interaction with focal adhesion adaptor protein paxillin, regulates preadipocyte migration via the downstream activation of Arf6. *J Biol Chem,* 285**,** 24270-81.

Tsuboi, S., H. Takada, T. Hara, N. Mochizuki, T. Funyu, H. Saitoh, Y. Terayama, K. Yamaya, C. Ohyama, S. Nonoyama & H. D. Ochs (2009) FBP17 Mediates a Common Molecular Step in the Formation of Podosomes and Phagocytic Cups in Macrophages. *J Biol Chem,* 284**,** 8548-56.

Tsujita, K., A. Kondo, S. Kurisu, J. Hasegawa, T. Itoh & T. Takenawa (2013) Antagonistic regulation of F-BAR protein assemblies controls actin polymerization during podosome formation. *J Cell Sci,* 126**,** 2267-78.

Tsujita, K., T. Takenawa & T. Itoh (2015) Feedback regulation between plasma membrane tension and membrane-bending proteins organizes cell polarity during leading edge formation. *Nat Cell Biol*.

van den Dries, K., M. B. Meddens, S. de Keijzer, S. Shekhar, V. Subramaniam, C. G. Figdor & A. Cambi (2013a) Interplay between myosin IIA-mediated contractility and actin network integrity orchestrates podosome composition and oscillations. *Nat Commun,* 4**,** 1412.

van den Dries, K., S. L. Schwartz, J. Byars, M. B. Meddens, M. Bolomini-Vittori, D. S. Lidke, C. G. Figdor, K. A. Lidke & A. Cambi (2013b) Dual-color superresolution microscopy reveals nanoscale organization of mechanosensory podosomes. *Mol Biol Cell,* 24**,** 2112-23.

Varon, C., F. Tatin, V. Moreau, E. Van Obberghen-Schilling, S. Fernandez-Sauze, E. Reuzeau, I. Kramer & E. Genot (2006) Transforming growth factor beta induces rosettes of podosomes in primary aortic endothelial cells. *Mol Cell Biol,* 26**,** 3582-94.

Vicente-Manzanares, M., X. Ma, R. S. Adelstein & A. R. Horwitz (2009) Non-muscle myosin II takes centre stage in cell adhesion and migration. *Nat Rev Mol Cell Biol,* 10**,** 778-90.

Vijayakumar, V., J. Monypenny, X. J. Chen, L. M. Machesky, S. Lilla, A. J. Thrasher, I. M. Anton, Y. Calle & G. E. Jones (2015) Tyrosine phosphorylation of WIP releases bound WASP and impairs podosome assembly in macrophages. *J Cell Sci,* 128**,** 251-65.

Vogel, V. & M. Sheetz (2006) Local force and geometry sensing regulate cell functions. *Nature Reviews Molecular Cell Biology,* 7**,** 265-275.

Volkmann, N. & D. Hanein (2000) Actomyosin: law and order in motility. *Curr Opin Cell Biol,* 12**,** 26-34.

Volpicelli-Daley, L. A., Y. Li, C. J. Zhang & R. A. Kahn (2005) Isoform-selective effects of the depletion of ADP-ribosylation factors 1-5 on membrane traffic. *Mol Biol Cell,* 16**,** 4495-508.

Welz, T., J. Wellbourne-Wood & E. Kerkhoff (2014) Orchestration of cell surface proteins by Rab11. *Trends Cell Biol,* 24**,** 407-15.

Wheeler, A. P., C. M. Wells, S. D. Smith, F. M. Vega, R. B. Henderson, V. L. Tybulewicz & A. J. Ridley (2006) Rac1 and Rac2 regulate macrophage morphology but are not essential for migration. *J Cell Sci,* 119**,** 2749-57.

Wiesner, C., K. El Azzouzi & S. Linder (2013) A specific subset of RabGTPases controls cell surface exposure of MT1-MMP, extracellular matrix degradation and three-dimensional invasion of macrophages. *J Cell Sci,* 126**,** 2820-33.

Wiesner, C., J. Faix, M. Himmel, F. Bentzien & S. Linder (2010) KIF5B and KIF3A/KIF3B kinesins drive MT1-MMP surface exposure, CD44 shedding, and extracellular matrix degradation in primary macrophages. *Blood,* 116**,** 1559-69.

Wymann, M. P. & R. Schneiter (2008) Lipid signalling in disease. *Nat Rev Mol Cell Biol,* 9**,** 162-76.

Yamaji, R., R. Adamik, K. Takeda, A. Togawa, G. Pacheco-Rodriguez, V. J. Ferrans, J. Moss & M. Vaughan (2000) Identification and localization of two brefeldin A-inhibited guanine nucleotide-exchange proteins for ADP-ribosylation factors in a macromolecular complex. *Proc Natl Acad Sci U S A,* 97**,** 2567-72.

Yu, C. H., N. B. Rafiq, A. Krishnasamy, K. L. Hartman, G. E. Jones, A. D. Bershadsky & M. P. Sheetz (2013) Integrin-matrix clusters form podosome-like adhesions in the absence of traction forces. *Cell Rep,* 5**,** 1456-68.

Zaidel-Bar, R., S. Itzkovitz, A. Ma'ayan, R. Iyengar & B. Geiger (2007) Functional atlas of the integrin adhesome. *Nat Cell Biol,* 9**,** 858-67.

Zeghouf, M., B. Guibert, J. C. Zeeh & J. Cherfils (2005) Arf, Sec7 and Brefeldin A: a model towards the therapeutic inhibition of guanine nucleotide-exchange factors. *Biochem Soc Trans,* 33**,** 1265-8.